الجمهورية الجزائرية الديمقراطية الشعبية

République Algérienne Démocratique et Populaire
Ministère de L'Enseignement Supérieur et de la Recherche Scientifique

UNIVERSITÉ FERHAT ABBAS - SETIF1
FACULTÉ DE TECHNOLOGIE

THESE

Présenté à la Faculté de Technologie Pour l'Obtention du Diplôme de

Doctorat

Domaine : Science et Technologie
Filière : Electrotechnique
Option : Electrical control

Par

Mr. Billel Kahia

Contribution à la commande des convertisseurs AC/DC à Absorption Sinusoidale de Courant

Soutenue le : 12 / 03 / 2020 devant un jury composé de :

M. RAHMANI Lazhar	Professeur	Univ. Ferhat Abbas Sétif 1	Président
M. BOUAFIA Abdelouahab	Professeur	Univ. Ferhat Abbas Sétif 1	Directeur de thèse
M. CHAOUI Abdelmadjid	M.C.A	Univ. Ferhat Abbas Sétif 1	Co-Directeur
M. REKIOUA Toufik	Professeur	Univ. A. Mira Béjaia	Examinateur
M. CHOUDER Aissa	M.C.A	Univ. M. Boudiaf M'sila	Examinateur

To my Mother
To my Father
To my Brother and Sister
To all my Family

Billel Kahia

Keywords

- Power Electronics
- Direct power control (DPC)
- Space vector modulation (SVM)
- Unbalanced grid voltage
- Unit power factor
- Three-level active-front end neutral-point-clamped
- Model predictive control (MPC)
- Total harmonic distortion (THD)
- Sinusoidal input current

Abstract

Recently, researchers have shown an increased interest in using of multilevel converter in wide range of application such as: AC adjustable speed drives, industry, transportation, renewable energies and so on. Unfortunately, using the line-side diode rectifiers in such application as, AC adjustable speed drives, provoke harmonic pollution, which required using the active and passive filters, or PWM rectifiers. The use of a three-phase PWM rectifier as a front-end stage represents an interesting solution for equipment which frequently works in regenerative operation, like adjustable speed drives (ASDs) and distributed power generation system. This PWM ac–dc converter offers several advanced features such as sinusoidal input currents at unity power factor, bidirectional power flow, small filter circuit, and high-quality dc output voltage. It is the new alternative technique for ac–dc power conversion which draws a continuous sinusoidal current from the ac supply under all load conditions. In this dissertation, the three-level active-front end neutral-point-clamped (3L AFE-NPC) is utilized.

Preface

In the name of **Allah**, the Most Gracious and the Most Merciful. I would like to say "**Alhamdulillah**", all praises to Allah for the strengths and His guidance in completing this dissertation.

I express my deep sense of gratitude and heart-felt thanks to my supervisor and co-supervisor, Prof. Abdelouahab BOUAFIA and Prof. Abdelmadjid CHAOUI at Laboratoire Qualité d'Energie dans les Réseaux Electriques (QUERE) and to my co-supervisors Prof. Ralph Kennel, Prof. Zhenbin Zhang, und Mr. Mohamed Abdelrahem at Institute for Electrical Drive Systems and Power Electronics, Technical University of Munich (TUM) for all their support during my time at their institutes for his invaluable guidance, patience, kindness and consistent encouragement throughout the course of this work. I am very glad that I have pursued my doctoral studies under their excellent supervision.
I would like to express my appreciation to my thesis committee members: Prof. Lazhar RAHMANI, Prof. Toufik REKIOUA and Prof. Aissa CHOUDER.

I cannot forget to mention all my friends, Talbi Billel, Laib Abdelbasset, Amrane Faycel, and the other for their great friendship, help and support.

Setif, Algeria, in

Kahia Billel

List of symbols

Superscript

Reference of x	x^*
Absolute value of x	$\|\|x\|\|$
New definition of x	x^{nov}
Lagging value of x	$x^{'}$
Unity value of x	$\bar{x}$
$\odot$	Dot product
$\otimes$	Cross product

Subscripts

General symbols

$\boldsymbol{x}$	State vector
$\boldsymbol{u}$	Input vector
$\boldsymbol{y}$	Output vector
$\boldsymbol{A}$	State matrix
$\boldsymbol{B}$	Input matrix
$\boldsymbol{C}$	Output matrix
$\boldsymbol{D}$	Feedthrough matrix
t	Time (continuous)
k	Time (discrete, current sample)
$k+1$	Time (discrete, next sample)
g	Cost function
$\frac{\mathrm{d}}{\mathrm{d}t}$	Time derivation
T_s	Sampling time
Δ	Difference
H_P , H_Q	Hysteresis widths of hysteresis controllers
n	Sector number
θ_g	Angle position of space voltage vector

General electrical variables

a, b, c	Phases
α, β	Equivalent two-phase coordinates
j	$\sqrt{-1}$
e_g^{abc}	Phase grid voltage in reference frame
$e_g^{\alpha\beta}$	Phase grid voltage in stationary reference frame
e_g^{dq}	Phase grid voltage in synchronous reference frame
i_g^{abc}	Phase grid current in reference frame
$i_g^{\alpha\beta}$	Phase grid current in stationary reference frame
i_g^{dq}	Phase grid voltage in synchronous reference frame
V_d	DC link voltage
V_o	Different DC-link voltage
V_{dc1}, V_{dc2}	DC link voltage of upper, lower capacitors
$v_g^{a,b,c}$	Line-to-line voltage
I_d	DC link current
I_d^p	Positive DC link current
I_d^o	Neutral DC link current
I_d^n	Negative DC link current
$\vec{u}_g^{abc}$	Switching states of three legs of converter
$\vec{v}_g$	Grid voltage vector
$G_g^{(a,b,c),(1,2)}$	Gate signal vector
$\bar{G}_g^{(a,b,c),(1,2)}$	Complementary gate signal vector
R_g	Resistor of input filter
L_g	Inductance of input filter
C	DC-Link Capacitor
$\vec{S}$	Apparent power
P	Active power
Q	Reactive power
P_o	Average value of active power
P_{c2}, P_{s2}	harmonic peak of cosine and sine phase of active power
Q_o	Average value of reactive power
Q_{c2}, Q_{s2}	harmonic peak of cosine and sine phase of reactive power

Abbreviations

2L	Two-Level
3L	Three-Level
AC	Alternating Current
DA	Digital to Analog (converter)
DTC	Direct Torque Control
FOC	Field Oriented Control
FPGA	Field Programmable Gate Array
FS	Finite-Set
FS-MPC	Finite-Set Model Predictive Control
IGBT	Insulated Gate Bipolar Transistor
LTI	Linear Time-Invariant
MPC	Model Predictive Control
MPDTC	Model Predictive Direct Torque Control
MSC	Machine-side Converter
NPC	Neutral Point Clamped
PCC	Predictive Current Control
PWM	Pulse Width Modulation
RMS	Root Mean Square
SVM	Space Vector Modulation
THD	Total Harmonic Distortion
UPF	Unity Power Factor
VOC	Voltage Oriented Control
VSI	Voltage Source Inverter

List of Figures

List of Tables

Contents

CHAPTER 1

Introduction

Three-level neutral-point-clamped (3L-NPC) power converter and its control techniques is the major objective of this study. The organization of this Chapter is as follow: the overview of power electronics and control techniques for renewable energy systems in section 1.1. Control technique for 3L-AFE is outlined in Section 1.2. Problem description in section 1.3, motivation and objectives for the Dissertation research in Section 1.4. Finally, in Section 1.5, the outline of the dissertation is summarized.

1.1 Power electronics, renewable energy systems and control strategies

Every day life, technology and development is impacted for far-reaching by *Energy*. Energy production from two resources, the first one called *primary energy resource*, which is extracted/captured directly from the *environment*. The second one called *secondary energy resource*, which is derived from the primary energy source. Primary energy source can be listed in three distinctive groups [2]:
Nonrenewable energy (fossil fuels): coal, crude oil, natural gas and nuclear fuel.
Waste: petroleum, coal, natural gas, and nuclear
Renewable energy: solar energy, wind, hydropower, geothermal, biomass and ocean energy. Due to huge increase of energy demand, limited fossil fuel resources, and environmental concerns, renewable energy sources have remarkably increased world wide in recent years. Among all the renewable energy sources, solar photovoltaic (PV) energy and wind energy is increasingly becoming mainstream and competitive with conventional sources of energy. The

reasons of this success are the technological developments in solar PV and wind systems as well as the encouragement of governments incentive programs. In terms of sufficient energy product, power quality and efficiency, conversion and control of electrical energy using power electronics becomes a very important topic today. Therefore, new semiconductor devices, topologies, and control schemes are being developed.

A major breakthrough in power electronics, which started a revolution in the control of power, was the thyristor, introduced by General Electric in 1957 [3]. The introduction of thyristor (First controlled semiconductor device) was a soft starter of modern power electronics as we know it. Currently, for low and medium power applications, the metal-oxide-semiconductor field-effect transistor (MOSFET) and insulated-gate bipolar transistor (IGBT) are dominated; for high power applications, the high-voltage IGBT, integrated gate-commutated thyristor, and thyristors are dominated [4]. Three main research areas play a fateful role in the efficient energy conversion are: (1) semi-conductor devices, (2) power converter configuration (arrangement of the electronics devices), and (3) control scheme (proper turn on/off of electronic devices). Since the 1980s, commercial wind turbines has seen developed various combination of wind generators and power electronics converters, in the aim of achieving a fixed speed, semi-variable and full-variable-speed operation. At the beginning of 1980s, wind energy system was constructed using squirrel-cage induction generator with power grid and power electronics with *thyristor* components [5], there was no requirement to carry the power continuously [6]. In the 1990s, in order to reduce the mechanical stress and load especially at the nominal power operation points, advanced diode bridges with a chopper were [7] used in the application of the power electronics for controlling the rotor resistance of the wound-rotor induction generator. After that, the regulation of the electrical power transferred from the wind turbines is considered in the double fed induction generator (DFIG) with partial-scale power capacity of the system and asynchronous/synchronous generators using more advanced *back-to-back (BTB) power converter*.

Back-to-back (BTB) power converter is identical on both the generator and grid side, and linked through a dc-link. This power converter has many advantages such as, ability to perform a conversion of variable voltage/frequency output of the generator ac to dc, and then dc to ac, with fixed voltage/frequency for the grid connection, possibility to reverse the active power flow at any time (bidirectional power flow). This topology can be used with the squirrel-cage induction generator (SCIG), wound rotor induction generator (WRIG), doubly-fed induction generator (DFIG), permanent magnet synchronous generator (PMSG) and wound rotor synchronous generator (WRSG). According to the voltage rating and IEC 60038 standard, the back-to-back (BTB) power converter can be classified as low voltage ($<$1 kV) and medium voltage (1-35 kV) converters, as shown in Figure 1.1. for more details, see [8].

Among the low voltage converter, the most known topology, which is voltage source converters (VSCs), is utilized with a low switching frequency (1-3 kHz)

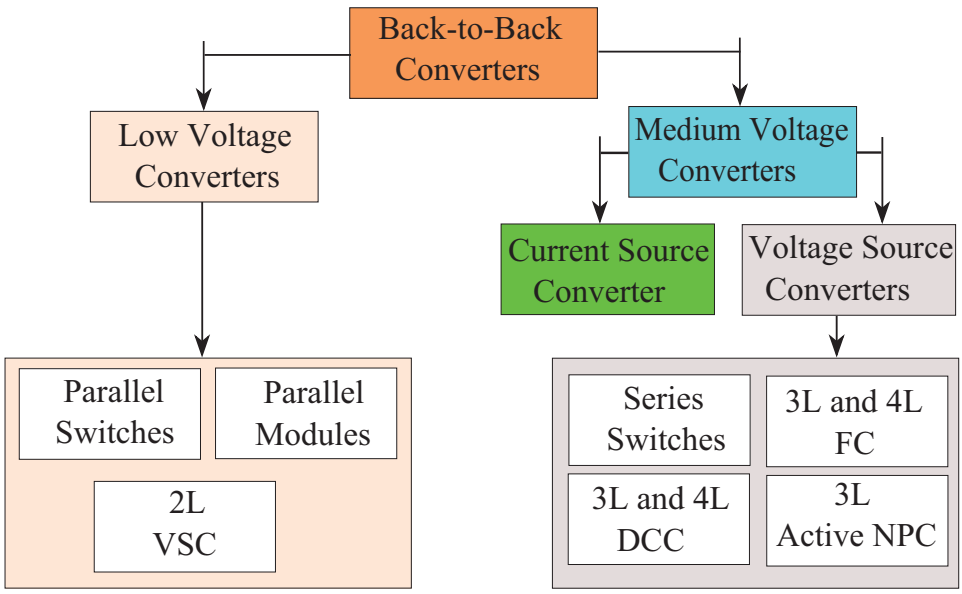

Figure 1.1: Classification of back-to-back converters

to achieve lower switching losses, due to the higher total harmonic distortion in the grid current, the LCL filters are connected to grid side to decrease the harmonics in grid currents.
Among the medium voltage converters (MV), neutral-point-clamped (NPC) back-to-back converter plays an important role in the high power applications, the using of this topology in commercial wind turbines with power rating 6 MW without connecting switching devices in series or parallel [9] is possible. High power applications, low harmonic distortion of input currents, low switching voltage stress and less amount of components (compared to another high power converters) are the advantage of 3L-NPC converter. A detail comparison of multilevel power converter is listed in [8] (Table 2.2, page 33).

In this work, the grid side of back-to-back three-level neutral-point-clamped (3L-NPC) and their control techniques are investigated. This converter is a 3L NPC Active Front End (3L NPC-AFE) rectifier with choke ((R)L-filter).

1.2 Control technique for 3L-AFE

A topology of a 3L NPC-AFE with choke RL Filter is illustrated in Figure 1.2. The control objectives (primary objectives) for this power converter can be broadly listed as:
(po1): *Grid side power (current) control*: The control techniques assure grid-side active and reactive power (current) control. According to the grid codes, a

certain power (current) quality should be guarantied by the control techniques.
(po2): *DC-link voltage control*: With a finite value for C_{dc1} and C_{dc2}, the capacitors can be charged or discharged by neutral current I_g^o, causing neutral-point voltage deviation and fluctuations, these may leads to damage the switching devices and capacitors, and increase additional harmonics in output voltage of the converter [10]. Therefore, assuring the balancing of upper and lower DC-link capacitors is necessary to maintaining a constant DC-link voltage and to allow for low-voltage ride through (LVRT) capabilities [11].
As we mentioned above, one of the main research area in efficient energy conversion is the control scheme, which will be considered in the next step.

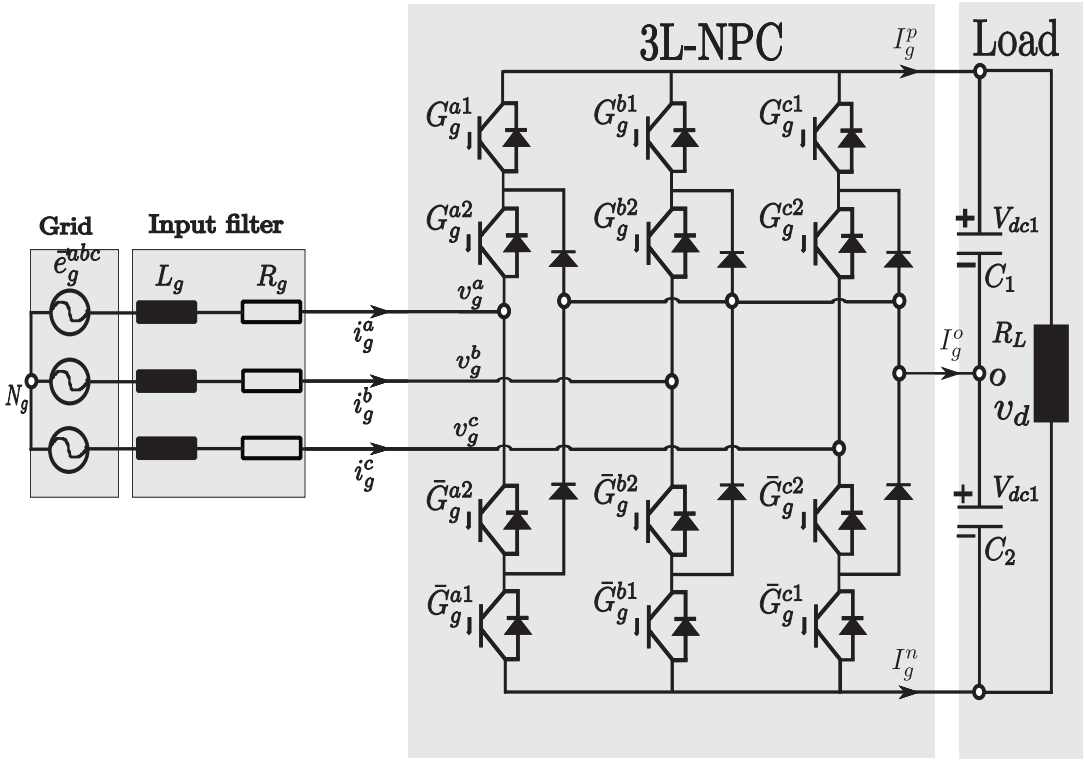

Figure 1.2: Scheme for the topology of a 3L NPC Active Front End (3L-AFE) with RL Filter

1.2.1 Nonlinear Hysteresis control scheme

The measured variables are compared to their reference values and the output data (error in references tracking) connected to hysteresis (bang-bang) controllers, these ones generate the gating signal. The error in reference tracking is proportional related to the hysteresis band width. The reference values in power control technique generate from PI controller (multiplied by DC value to get P_{ref}) and constant value for Q_{ref}. One of the major drawbacks of this method is the uncontrollable switching frequency, which varies according to the hysteresis width, load parameters, and operating conditions.

Direct power control (DPC) (reported by Nouguchi in 1996 [12]), which is based on the instantaneous active and reactive power theory, is developed analogously with the direct torque control (DTC). In DPC, the switching states are selected via a switching table. Therefore, no internal current loops or modulator blocks are required. The switching table is synthesizing based on the sign and magnitude of the control variables (active and reactive power). For the multilevel power converters, the design and implementation of switching table are more difficult and the switching losses are higher. Many works have been presented in a effort to improve this controller, new works are proposed from us and will be presented in this dissertation.

1.2.2 Intelligent Control techniques

Intelligent control techniques or artificial intelligence (AI) considers as an important branch of computer engineering. In the last years, the researches started to use the AI in the electrical engineering area, specifically in the application in power electronics and motion control. The fuzzy logic (FL), artificial neutral network (ANN), genetic algorithms (GA) and expert system (ES) belongs to the family of intelligent control techniques. Fuzzy logic is developed based on Boolean logic and the argument that the human thinking do not always follow the crisp yes/no logic (it can be vague, qualitative, uncertain, imprecise or fuzzy in logic). Generally, all the input information is defined in the input space, then is processed though fuzzy logic system (a fuzzy inference process), and the solutions are appeared in the output space. A fuzzy inference process consists of the following steps:
Fuzzification of input variables, application of fuzzy operator (AND, OR, NOT) in the IF (antecedent) part of the rule, implication from the antecedent to the consequent (THEN part of the rule), aggregation of the consequents across the rules, and defuzzification [13]. A conference paper about FLC-DPC is already prepared and will be submitted as soon as possible. Therefore, no more discussion will be added.

1.2.3 Linear control using modulation scheme

In order to solve the major drawbacks of the hysteresis controller (i.e., variable switching frequency), some control techniques are developed and combined with nonlinear controller, as modulation stage and cascaded linear regulators have been investigated. Space vector modulation (SVM), pulse width modulation (PWM) and selective harmonic elimination (SHE) are the most utilized modulation schemes [14–18]. For the application in the drivers industry and energy systems, the linear control scheme covers a very wide class of controllers. The field oriented control (FOC) is utilized to control the motor; voltage oriented control (VOC) and DPC-SVM to control the grid-connected converter. With the DPC-SVM control, small ripples in active and reactive power, a constant switching frequency and a lower current harmonic are achieved [19].

Also, the PI controllers in power loops can be further eliminated if the predictive deadbeat power control is used [20]. The principle of SVM is based on selecting the closest vectors to the reference voltage vectors based on switching scheme design and dwell time calculation. For more detail about SVM, please see my master thesis [21].

1.2.4 Sliding Mode Control Technique

The sliding mode control technique considers as nonlinear in nature with possibility to be applied to linear/nonlinear systems [22–25]. This technique is an advanced control technique and can achieve robust and stable response under normal operations, system parameter variations and load disturbances [26]. Compared to the non-linear hysteresis power control, and linear power control scheme using SVM, the sliding mode control technique is very robust.

1.2.5 Predictive Control Techniques

In the recent years, *Predictive control* covers a very wide class of controllers for the application in power converters. Different predictive control methods are available, for more details, see [27]. With the predictive control (PC), the system model is used to predict the future response of a plant, and used it by the controller to obtain the optimal control action, according to a predefined optimization criterion. The logical and intuitive procedure of MPC in power electronics converter makes it easy to understand as concept and simple to implement. The main key element required in MPC concept is the model of the system (it should be precise): This model depends directly on which application and power converter are used. In drives, induction, synchronous, permanents magnets, switched reluctance, etc., are the physical models, which have been widely studied. Also, another elements such as loads, sources, and filters can be modeled in a combination of resistive, inductive, and capacitive components. The interaction of mechanical systems with electrical systems can be modeled and included in the MPC algorithm. In power electronics, the control objectives (mandatory and additional terms) are usually designated to follow reference of voltages, currents, torque, power, flux, common-mode voltage, switching frequency, losses, total harmonic distortion (THD), etc. In MPC, the cost function evaluates the error between the control objectives and their correspond references.
One of the predictive control techniques called *Finite control set* is widely used by the scholarly among the other predictive control methods. FCS-MPC shows strong ability to treating the properties, conditions and requirement of a power electronic converter, for example, faster response for the electric control variables, achieve safe and reliable operation, etc, more details in [8]. Simple concept and easy to understand it, possibility to apply to a wide wide variety of systems, compensation of system perturbations, an intuitive approach for real-time implementation, etc can be assured with FCS-MPC. Therefore, chapter 5

is spent in this work to exclusively examine FCS-MPC technique.

1.3 Description of the Problem

In this section, the problems of the state-of-the-art direct power control based on look-up-table (DPC-LUT), DC-link control, unbalanced and distorted grid voltage conditions, FPGA realizations are formulated.

❣ **Uncontrollable switching frequency/ large power ripples**

Direct power control (DPC) has several obvious advantages, such as, simple structure, rapid dynamic response, no PWM blocks/current-control loops are required. Based on predefined switching table, the desired voltage vector is selected for active and reactive power regulation. However, switching table-based DPC produces *large power ripples* and the *switching frequency* is *variable*, the last problem is due to the use of heuristic switching table and hysteresis comparators. Therefore,
(Pr1): *how to reduce the power ripples and fix the switching frequency, without complicating the structure and conserving the advantage of rapid dynamic response.*

❣ **Unbalanced and distorted grid voltages**

Unbalanced and harmonically grid voltage has already been a very common phenomenon, which can caused by, eg, non-ideal three-phase load, asymmetry faults, large capacity single-phase load, asymmetry of power transmission system, etc. The unbalanced and harmonically voltage conditions occur frequently in the input supply (presence of negative sequence and harmonically voltage component), particularly in a weak ac system. Therefore, the *performance of the PWM converters deteriorates*, i,e, harmonics appearing at the output dc-link voltage and in the ac currents. Extensive studies are carried out the influence of non-real grid voltage on the power system. In this work, DPC strategy will be investigated under no-real grid voltage conditions. Therefore,
(Pr2): *how to improve the steady-state performance of the DPC, with keeping the structure simple and less computation burden.*

1.4 Motivation and Objectives for Dissertation Research

1.4.1 Motivation from the Power Converters Perspective

At higher power levels, the use of medium voltage (MV) converters (3-4 kV) proves their advantages over low voltage converters, such as, the switching rat-

ing is reduced, higher efficiency and better grid code compliance [28, 29]. The most popular MV power converters are neutral-point clamped (NPC) converters. Compared to the useful two level converter, the main features of the NPC converter can be mentioned as, reduced dv/dt and THD of ac output voltages, less switching devices (compared to another MV converters), ability to reach a certain voltage level without switching devices in series and uncomplicated dc-link voltage balancing methods (compared to multilevel NPC converters). Currently, for the drives rated at 4160 V, 6000 V devices are used in NPC converter. The points mentioned above have been taken as starting point for motivation to use the 3L NPC-AFE converter among all the other converters in this dissertation. Also, the drawbacks of this power converter such as, neutral point voltage balancing (unbalanced neutral point voltage will lead to produce low order harmonics, and to shorten the lifetime of electrolytic capacitors) will be discussed and solutions are proposed to solve them.

1.4.2 Motivation and objectives from the control techniques Perspective

This dissertation is investigated to increase the efficiency of power converter through using classical and advanced control techniques, which are widely accepted by power electronics and energy systems. The performance of the classical and advanced control techniques have been improved by the development of new improved classical and advanced control techniques which are numerically evaluated through Matlab-simulink environment and experimentally through FPGA based Hil simulation concept.
Some of several issues of classical control technique (exactly DPC-LUT technique) and model predictive control (MPC) technique (exactly, FSC-MPC technique) have been motivations to investigate the performance of DPC-LUT and FCS-MPC techniques, these issues are summarized as yielding [8],
• The grid voltage harmonics degrades the performance of system (FCS-MPC, DPC-LUT).
• Poor power quality and conflict to the grid codes due to significant harmonic (FCS-MPC, DPC-LUT).
• Coupling of control variables such as d- and q-axis grid currents.
• Accurate modeling of multilevel converters.
• Enhancement of robustness.
• The characteristics of performance is non-symmetrical due to nonlinear nature of power converters.

1.5 Outline of Dissertation

In this part, the outline of the dissertation research is summarized. The dissertation is divided to five chapters. The content of each one is

❣ **Chapter 1**

In this first chapter, a general introduction is formulated. The section 1.1 is concerned to discuss one of the very important theme in day life, which is *Energy*, and what has to do with production and conversion of the energy, which are resource of energy, power electronics (for the conversion part), and control strategies for the systems. Then, a second section 1.2 is added, content details about the control techniques for the power converter (3L NPC-AFE), that are used in this dissertation. Before the end, the energy system suffers from different problems, these problems are collected in 1.3. Finally, motivations and objectives of the dissertation research is resumed in 1.4, and the outline of dissertation in 1.5.

❣ **Chapter 2**

The energy system contents three level neutral point clamped active front-end (3L NPC-AFE), three phase grid voltage, RL filter, and resistance load is presented in this Chapter, in modeling and description terms. At the end, the lab-constructed test-benches and real-time controller is presented.

❣ **Chapter 3**

An introduction about classical control techniques of power converter is formulated. Then, a description of nonlinear direct power control with conventional switching table (DPC-LUT) is added.

❣ **Chapter 4**

This chapter is concerned to discuss the advanced classical control techniques that proposed by us. First of all, a small introduction about the challenges of classical direct power control with conventional switching table (DPC-LUT) is presented. Then, a detail explication of the two proposed switching tables is discussed. After that, the challenge of unbalanced grid voltage is taken into consideration, and new definition of active power is proposed in this work, to solve the weakness of direct power control with look up table (DPC-LUT) under unbalanced grid voltage. Finally, the performance evaluation of the three proposed strategies with extensive simulation data is validated.

❣ **Chapter 5**

The advanced direct model predictive control is putted under the microscope, the general principle of model predictive control (MPC) technique is summarized. Following, the choose finite control-set model predictive control (FCS-MPC) is explicated in term of operation principle and design procedure. Finally, the performance evaluation of FCS-MPC in implementation is dis-

cussed.

❣ **Chapter 6**

This dissertation is finished with a global conclusion, which included work's goal, resume of the achieved works and the future plans.

CHAPTER 2

System description and modeling

First of all, the nomenclature (symbols and abbreviations) used in this dissertation are listed, see Table 2.1. The correspondence of each symbols and abbreviations are listed in the table. The mathematical models of 3L NPC-AFE rectifier are detailed in this chapter. Finally, the lab-constructed three-level power converter test-bench for experimentally verification is briefly presented.

2.1 3L NPC-AFE rectifier

Figure 1.2 shows the topology of 3L NPC-AFE rectifier. The rectifier is composed of: three legs, each leg has four active switches, with four anti-parallel diodes. The IGBT devices are used in practice. On the DC-link side of the rectifier, two equal capacitors C_1 and C_2 (upper and lower capacitors) are used, dc bus capacitor is split into two, and **neutral point** o is provided. The diodes connected to the neutral point, D^a_{z1} and D^a_{z2}, are named **clamping diodes**. Take a leg a as example, when inner two switches (G^{a2}_g / $\overline{G}^{a2}_g$), are turned on the converter output terminals (a) connected to the neutral point through one of the clamping diodes.
Table 2.2 represents the operating status of the switches in the 3L NPC-AFE rectifier. Taking for example leg a, the switching state 'P' means that the upper two switches (G^{a1}_g, G^{a2}_g) are on, and the voltage between terminals a and the neutral point o, called **rectifier terminal voltage** V_{ao}, is equal to +E. And the opposite of switching state 'P' is 'N', in this case, the lower two switches ($\overline{G}^{a2}_g$ / $\overline{G}^{a1}_g$) are on, and V_{ao}= -E. Finally, the switching state 'O' signifies that the inner two switches (G^{a2}_g / $\overline{G}^{a2}_g$) are on, and V_{ao}=0. The direction of grid current determine which one of two clamping diodes is turned on. The

Table 2.1: The nomenclature for this dissertation.

Name	Nomenclature/Unit
N, R, C	Natural, real and complex numbers
$\mathrm{R}^n(n\in\mathrm{N})$, ^{T},†	Column vector, transpose of column vector and its conjugate
R_g, L_g, C	Resistance [Ω], Inductance [H], Capacitance [F]
ω, ϕ_g	Frequency [Hz], position of voltage
t, T_s, k	Time [s], Sampling time [s], sampling instant [1]
$\vec{X}^{dq}$, $\vec{X}^{\alpha\beta}$, $\vec{X}^{abc}$	Vectors in dq, $\alpha\beta$, abc reference frame
$\vec{u}$, $\vec{G}$	Switching state, gate signal vector
$\vec{S}$, P, Q	Apparent power [VA], active [W], reactive power [V A]

Table 2.2: Switching state' definition

States	G_g^{y1}	G_g^{y2}	$\overline{G}_g^{y1}$	$\overline{G}_g^{y2}$	terminal voltage
P	1	1	0	0	+E
O	0	1	1	0	0
N	0	0	1	1	-E

switches (G_g^{a1} and $\overline{G}_g^{a2}$), (G_g^{a2} and $\overline{G}_g^{a1}$) operate in a complementary manner, as shown in Table 2.2. For more details, about the commutation of switching devices in the NPC converter, when the current line is positive or negative, see [30], chapter 8.

The phase voltages of the converter can be obtained as

$$\vec{v}_g^{abc} = \frac{V_{c1}+V_{c2}}{6}\begin{bmatrix}2 & -1 & -1\\ -1 & 2 & -1\\ -1 & -1 & 2\end{bmatrix}\vec{u}_g + \frac{V_{c1}-V_{c2}}{6}\begin{bmatrix}2 & -1 & -1\\ -1 & 2 & -1\\ -1 & -1 & 2\end{bmatrix}|\vec{u}_g| \tag{2.1}$$

Where $|\vec{u}_g|=(|u_g^a|,|u_g^b|,|u_g^c|)^T$, $\vec{u}_g$ represents the switching state vectors, $\vec{u}_g=(\vec{u}_g^a,\vec{u}_g^b,\vec{u}_g^c)\ \in \mathrm{U}_{27}$:=NNN, NNO,..., PPO, PPP of 27 possible switching states, and $V_{c1}=V_{c2}=E$.
The line-to-line voltage $\vec{v}_g^{|t|}$ can be determined by

$$\vec{v}_g^{abc} = \begin{bmatrix}v_g^a - v_g^b\\ v_g^b - v_g^c\\ v_g^c - v_g^a\end{bmatrix} = \frac{V_{c1}}{2}\begin{bmatrix}1 & -1 & 0\\ 0 & 1 & -1\\ -1 & 0 & 1\end{bmatrix}(|\vec{u}_g|+\vec{u}_g) - \frac{V_{c2}}{2}\begin{bmatrix}1 & -1 & 0\\ 0 & 1 & -1\\ -1 & 0 & 1\end{bmatrix}(|\vec{u}_g|-\vec{u}_g) \tag{2.2}$$

Where $|\vec{u}_g|$ represents the absolute values of vector $\vec{u}_g$.

2.2 DC-link of 3L NPC-AFE

With a finite value for upper and lower capacitors (C_1, C_2), charging and discharging process is inevitable. In additional, the difference voltages between the two capacitors should be concerned to achieve voltage balancing in DC-link side. Therefore, two subsections about charging and discharging of both capacitors and their difference voltage will be discussed in the next step.

2.2.1 Charging and discharging of DC-link capacitors

The relation between the voltage of dc-link capacitor and the current flow of the converter can be written as

$$\frac{dV_d(t)}{dt} = \frac{1}{C} I_d(t) = \frac{1}{C} I_g(t) = \frac{1}{C} \vec{I}_g^{abc}(t) \,.\, \vec{u}_g^{abc}(t) \tag{2.3}$$

Based on the forward Euler approximation, the equation 2.3 is rewritten in discrete form as

$$V_{d[k+1]} = V_{d[k]} + \frac{T_s}{C} I_{g[k]} = V_{d[k]} + \frac{T_s}{C} \vec{I}_{g[k]}^{abc} \,.\, \vec{u}_{g[k]}^{abcT} \tag{2.4}$$

2.2.2 DC-link capacitor voltage difference

As we mentioned above, the balancing of neutral point voltage in 3L NPC-AFE is an essential issue for reliability and efficiency. Therefore, the difference voltage between the upper capacitor voltage and lower capacitor voltage shall be zero, i.e., $V_o(t)=V_{c1}(t)-V_{c2}(t) = 0$. The variation in neutral point voltage is fundamentally caused by the non-zero current of the neutral point. The neutral point current can be expressed in terms of positive and negative currents at the DC-link part yielding

$$I_g^o = I_g^p - I_g^n \tag{2.5}$$

The positive and negative currents at the DC-link side can be calculated as

$$I_g^p = \frac{1}{2}(|\vec{u}_g| + \vec{u_g})\, \vec{i}_g^{abc} = \frac{1}{2}\left((|\vec{u}_g^a| + \vec{u}_g^a), (|\vec{u}_g^b| + \vec{u}_g^b), (|\vec{u}_g^c| + \vec{u}_g^c)\right) \vec{i}_g^{abcT} \tag{2.6}$$

$$I_g^n = \frac{1}{2}(|\vec{u}_g| - \vec{u}_g)\, \vec{i}_g^{abc} = \frac{1}{2}\left((|\vec{u}_g^a| - \vec{u}_g^a), (|\vec{u_g^b}| - \vec{u}_g^b), (|\vec{u_g^c}| - \vec{u_g^c})\right) \vec{i_g^{abc}}^T \tag{2.7}$$

The difference voltage V_o depends on charging/discharging state of the upper and lower capacitors (V_{c1} and V_{c2}). The dynamic of V_o is given by

$$\frac{dV_o}{dt} = \frac{dV_{c1}}{dt} - \frac{dV_{c2}}{dt} = \frac{1}{C}(I_g^p - I_g^n) = \frac{1}{C}\left(|\vec{u}_g^{abc}|\, \vec{i}_g^{abcT}\right) \tag{2.8}$$

Finally, the discrete equation for the DC-link capacity voltage difference can be determined by applying the forward Euler approximation as

$$V_{o[k+1]} = V_{o[k]} + \frac{T_s}{C}\left(|\vec{u}_{g[k]}^{abc}|\, \vec{i}_{g[k]}^{abcT}\right) \tag{2.9}$$

2.3 System's Dynamic: Grid, Filter and power

Grid connected rectifiers have evolved for the past years for interconnection of electrical load demand with the grid. However, grid-load rectifier systems suffers from the major drawbacks of switching harmonics caused by the rectifier switches. Therefore, a filter is necessary to reduce the harmonic components from the power converter. LCL or L filters are mainly inserted between the grid and the power converter, LCL filters are more attractive as L filter, compared to the L filters, LCL filters (with same size as L filters) has high attenuation of high frequency harmonics and better decoupling between filter and grid impedance. However, dynamics and steady state current distortion may caused due to resonance. Therefore, in this work, a R-L filter is connected between grid and power converter, due to its advantages such as, simple structure, and requires just basic control technique.
The modeling of 3L NPC-AFE with RL choke filter in $\alpha\beta$ and dq frame and grid side power dynamics will be investigated in the next step.

2.3.1 3L NPC-AFE with RL choke filter modeling

With a balanced three-phase system, according to Kirchhoff's voltage law, the mathematical model of 3L NPC-AFE composed by RL filter, voltage and current grid can be represented in static abc coordinates as:

$$\frac{d\vec{i}_g^{abc}}{dt} = \frac{1}{L_g}(\vec{e}_g^{abc} - R_g\vec{i}_g^{abc} - \vec{v}_g^{abc}), \tag{2.10}$$

where i_g^{abc} is the three phase grid line current vector in abc, e_g^{abc} is the the three phase grid voltage vector in abc frame, and v_g^{abc} is the switching state vector in abc frame.

So, the equation 2.10 is rewriting in $\alpha\beta$ frames as:

$$\frac{d\vec{i}_g^{\alpha\beta}}{dt} = \frac{1}{L_g}(\vec{e}_g^{\alpha\beta} - R_g\vec{i}_g^{\alpha\beta} - \vec{v}_g^{\alpha\beta}) \tag{2.11}$$

where $i_g^{\alpha\beta}$ is the three phase grid line current vector in $\alpha\beta$, $e_g^{\alpha\beta}$ is the three phase grid voltage vector in $\alpha\beta$ frame, and $v_g^{\alpha\beta}$ is output voltage vector of the AFE in $\alpha\beta$ frame.
The discrete format of equation 2.11 is

$$\vec{i}_{g[k+1]}^{\alpha\beta} = \left(1 - T_s\frac{R_g}{L_g}\right)\vec{i}_{g[k]}^{\alpha\beta} + \frac{T_s}{L_g}\left(\vec{v}_{g[k]}^{\alpha\beta} - \vec{e}_{g[k]}^{\alpha\beta}\right), \tag{2.12}$$

where $R_g\,[\Omega]$ and L_g [H] are the resistance and inductance of input filter, respectively, T_s [s] is the sampling time, $\vec{i}_g^{\alpha\beta} = (i_g^{\alpha},\ \ i_g^{\beta})^{\top}$[A] is the grid current vector, $\vec{v}_g^{\alpha\beta} = (v_g^{\alpha},\ \ v_g^{\beta})^{\top}$ [V] is the output voltage vector of the AFE, and $\vec{e}_g^{\alpha\beta} = (e_g^{\alpha},\ \ e_g^{\beta})^{\top}$ [V] is the grid voltage vector.

In dq reference frame, the equation 2.10 can be written in continuous and discrete format as yielding

$$\frac{d\vec{i}_g^{dq}}{dt} = \underbrace{\begin{bmatrix} \frac{-R_g}{L_g} & \omega_g \\ -\omega_g & \frac{-R_g}{L_g} \end{bmatrix}}_{A} \vec{i}_g^{dq\,T} + \underbrace{\begin{bmatrix} \frac{1}{L_g} & 0 \\ 0 & \frac{1}{L_g} \end{bmatrix}}_{B} \vec{v}^{dq\,T} + \underbrace{\begin{bmatrix} -\frac{1}{L_g} & 0 \\ 0 & -\frac{1}{L_g} \end{bmatrix}}_{C} \vec{e}_g^{dq\,T} \tag{2.13}$$

$$\vec{i}_{g[k+1]}^{dq} = T_s\, A\, \vec{i}_{g[k]}^{dq\,T} + T_s\, B\, \vec{v}_{[k]}^{dq\,T} + T_s\, C\, \vec{e}_{g[k]}^{dq\,T} \tag{2.14}$$

where $\vec{i}_g^{dq} = (i_g^d,\, i_g^q)^\top$ [A] is the grid current vector in dq frame, $\vec{v}_g^{dq} = (v_g^d,\, v_g^q)^\top$ [V] is the output voltage vector of the AFE in dq frame, and $\vec{e}_g^{dq} = (e_g^d,\, e_g^q)^\top$ [V] is the (symmetrical) grid voltage vector.
Direct power control (DPC) and predictive direct power control (P-DPC) are used in this work. Therefore, the relevant equations of the grid side power dynamics will be presented in this part. Based on the instantaneous power theory, the active and reactive power can be calculated in terms of grid voltage and current in static *abc* coordinates as:

$$\begin{aligned} \vec{S} = e_g\, \bar{i}_g = P + jQ = e_g^a\, i_g^a + e_g^b\, i_g^b + e_g^c\, i_g^c + \\ j\,\frac{1}{\sqrt{3}}\big[(e_g^b - e_g^c)\, i_g^a + (e_g^c - e_g^a)\, i_g^b + (e_g^a - e_g^b)\, i_g^c\,\big], \end{aligned} \tag{2.15}$$

where $\overline{i_g}$ represent the complex conjugate of a vector i_g.

In stationary $\alpha\beta$ coordinates and rotational dq coordinates, the equation 2.15 can be written as

$$\vec{S} = P + jQ = e_\alpha i_\alpha + e_\beta i_\beta + j\big(e_\beta i_\alpha - e_\alpha i_\beta\big) \tag{2.16}$$

$$\vec{S} = P + jQ = e_d i_d + e_q i_q + j\big(e_q i_d - e_d i_q\big) \tag{2.17}$$

The dynamics of powers (active and reactive power) in stationary $\alpha\beta$ coordinates, and rotational dq coordinates can be expressed respectively as follows

$$\frac{dP}{dt} = \frac{1}{L_g}\left({e_g}^2 - \Re(\vec{e}_g^{\alpha\beta}\vec{v}_g^{\alpha\beta}) - R_g P - \omega_g\, Q\right), \tag{2.18}$$

$$\frac{dQ}{dt} = \frac{1}{L_g}\left(\Im(\vec{e}_g^{\alpha\beta}\vec{v}_g^{\alpha\beta}) - R_g Q_+ \omega_g\, P\right), \tag{2.19}$$

$$\frac{dP}{dt} = \frac{1}{L_g}\left(e_g^{d2} - R_g P - \omega_g\, L_g\, Q + v_g^d\, e_g^d\right), \tag{2.20}$$

$$\frac{dQ}{dt} = \frac{1}{L_g}\left(-R_g Q + \omega_g\, L_g\, P - v_g^q\, e_g^d\right), \tag{2.21}$$

where $e_g{=}(e_g^d, 0) \Rightarrow e_g{=}e_g^d$.

As it is known, the grid side source voltage has a sinusoidal format $\vec{e}_g^{\alpha\beta}$=A$e^{jw_g t}$, where A and ω_g are the magnitude and frequency, respectively. Therefore, $\frac{d\vec{e}_g^{\beta}}{dt}$=$j\omega_g \vec{e}_g^{\alpha\beta}$. Based on that and on the forward Euler approximation, the discrete format of the dynamics of active and reactive power in the $\alpha\beta$ can be expressed as

$$\vec{G}_{S[k]} = \frac{d\vec{S_{[k]}}}{dt} = [g_{P[k]}, g_{Q[k]}]^T = \frac{1}{L}\begin{bmatrix} e^{\alpha}_{g[k]} & e^{\beta}_{g[k]} \\ e^{\beta}_{g[k]} & -e^{\alpha}_{g[k]} \end{bmatrix}\begin{bmatrix} e^{\alpha}_{g[k]} - v^{\alpha}_{g[k]} \\ e^{\beta}_{g[k]} - v^{\beta}_{g[k]} \end{bmatrix} - \begin{bmatrix} \frac{R_g}{L_g} P_{[k]} + \omega_g Q_{[k]} \\ \frac{R_g}{L_g} Q_{[k]} - \omega_g P_{[k]} \end{bmatrix} \tag{2.22}$$

And the predicted value of grid power dynamic at instant time k+1 can be calculated as

$$\vec{S}_{[k+1]} = \frac{d\vec{S[k]}}{dt} = (P_{[k+1]},\, Q_{[k+1]})^T = (P_{[k]}, Q_{[k]})^T + T_s.\vec{G}_{S[k]} \tag{2.23}$$

2.4 FPGA based HiL simulation system configuration

Figure 2.1 shows the FPGA based signal level Hardware-in-the-Loop (HiL) system. Additionally, Figure 2.1 illustrates a detailed instruction of each controller chassis. The PMSG (2MW) wind turbine system parameters for using such HiL system to evaluate its refreshing rate evicts are listed in [1].

2.4.1 Real-Time System - Design and Analysis -

The LabVIEW for FPGA-Hardware technology (Real-Time system) used in this dissertation are divided into three main levels with regarding to their implementation environments, namely, the personal computer (PC), the real-time processor (RT) and the field-programmable gate array (FPGA). More detail about this test-bench is given in [1].
A so-called single-cycle-time-loop (SCTL) NI-FPGA technique is used for FPGA realizations of the control algorithms. With a slightly higher implementation evicts, the technique introduces two considerable benefits, which called, reduced resource usage and improved code execution speed. By taking SCTL as the key word, more detail of such techniques can be founded online. Noticeably, the execution time of each sub-routines can be easily measured with an accuracy of 25[ns].
For more clarification, Figure 2.3 [1] shows the realization overview of a classical direct model predictive control scheme for the 3L back-to-back power converter PMSG system, where time durations represent by different colors.

2.4.2 Three-level back-to-back power converter system

Figure 2.2 [1] illustrates the three-level NPC back-to-back power converter and its inside configuration. The switches are with a power rating of 30kVA,

the heat-sink and the measurement board are designed to work within 5 kVA to reduce cost and ease its design and realization for laboratory use.

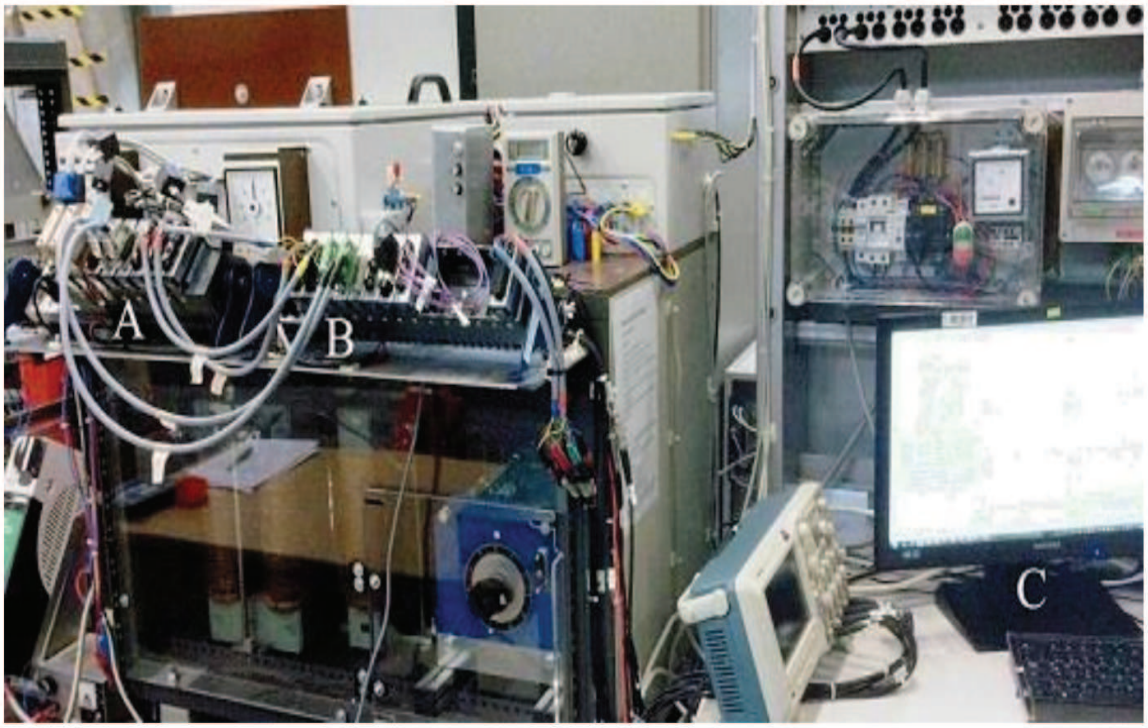

Figure 2.1: FPGA HiL platform of a back-to-back power converter PMSG wind turbine system. A: FPGA platform (NI-cRIO-9082), for implementing the ECU; B: FPGA platform (NI-9159), for implementing the back-to-back converter PMSG wind turbine emulator; C: User interface, programmed using Labview running in a PC. [1]

In the PC, LabVIEW or Matlab environments are utilized to realize the simulation, which can be coded with Labview graphical coding (VIs), Matlab (m.files), C, generated .dll and math-scripts. Meanwhile the data/result processing procedure, user interface and communication host to the real-time controller are also done here. The real-time controller is in charge of the real-time debugging, (real-time) data logging (as the host) and communication with the host PC. It can be coded with VIs, C, mathscripts and incorporating ḋll" files generated from certain third-part software (e.g., Visual Studio, Matlab/Simulink, etc.).

The main controller is the FPGA and coded with LV-FPGA (it can also incorporate hardware description languages such as VHDL, Verilog, etc.). The mains functions of the FPGA are real-time host of the controllers, real-time data-logging slaver, etc. In non-real-time, TCP/IP are utilized in between the PC and RT ; at the same time DMA-FIFO and PCI-e are utilized as the real-time communication solution in between the FPGA and real time (RT) [1].

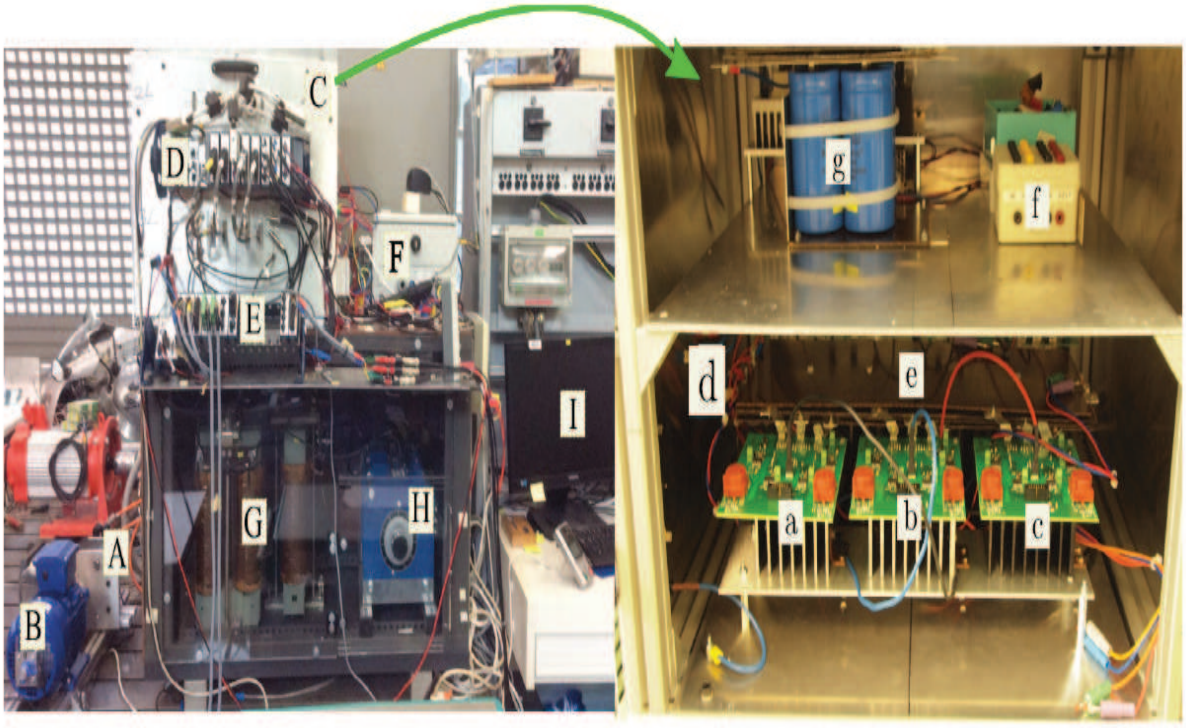

Figure 2.2: Three-level NPC back-to-back power converter system with PMSG. A and B are the PMSG and an asynchronous motor -controlled by a commercial drive- emulating the turbine; -inside of- C is a self-designed three-level NPC back-to-back power converter using Infineon switching modules; D is a fully configurable FPGA based real-time controller (NI-cRIO-9082) for deploying the control algorithms; G is the grid side L(R) filter, H is the grid side variac and F is the protection devices against short circuit and input inrush current. The detailed depictions of in side C are shown in the right side: a, b, c are the machine/load side three-phase three-level NPC power converter and its heat-sink, beyond e (not visible due to its position is a four/three-leg three-level NPC power converter serving as the grid side AFE); d is the DC-link voltage measurement interface; e is the layered DC-bus (its bellow are the capacitors), g (and its behind) is a DC-bus with a two-level voltage source power inverter serving as a SVG for extension and f is the power source for the gate driver, the current and voltage measurements boards. [1]

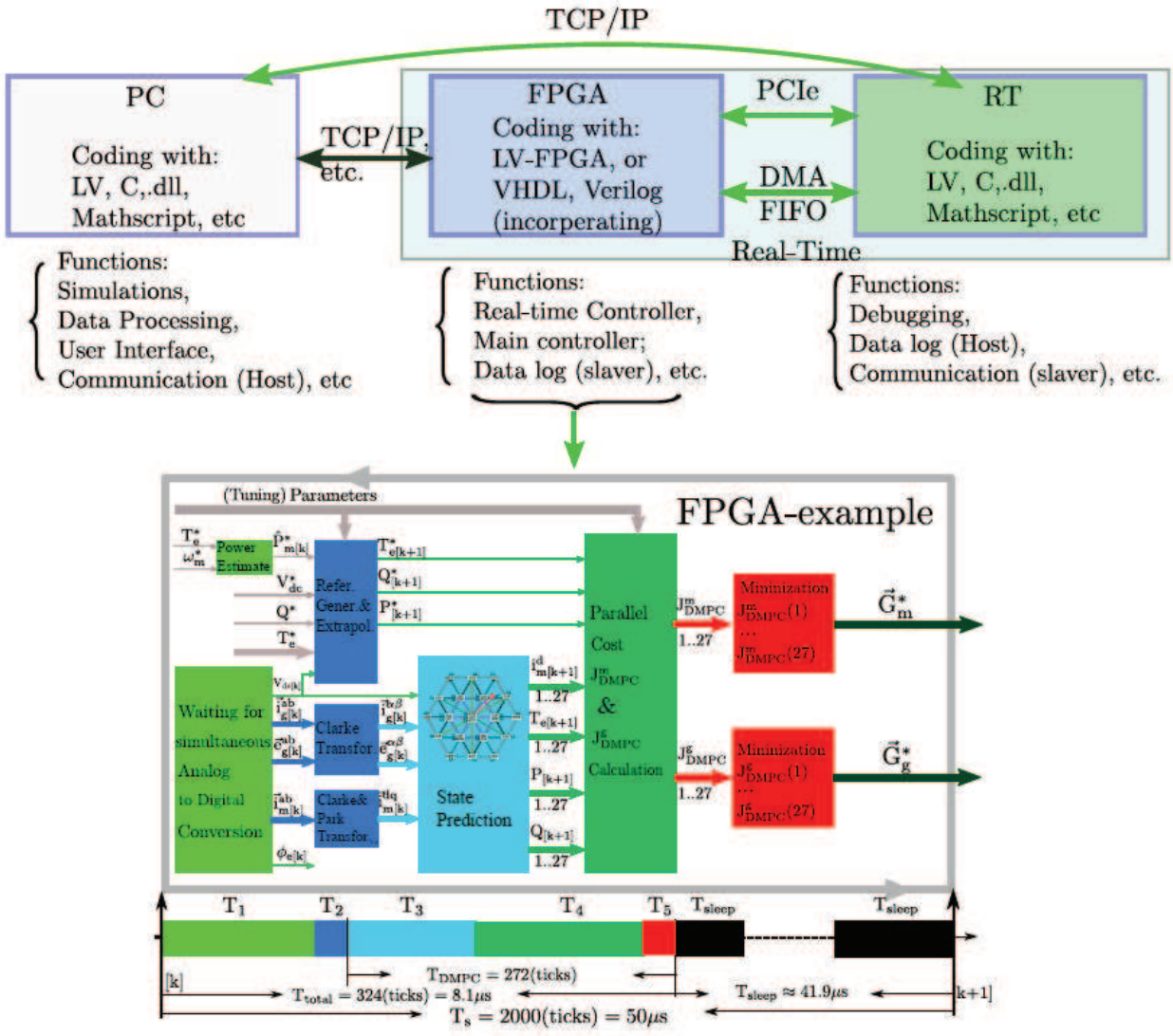

Figure 2.3: Real-time deploying system structure. [1]

CHAPTER 3

Classical Control Techniques of 3L NPC-AFE

In this chapter, the classical control techniques, which are used in this work to control the power converter (3L NPC-AFE) will be discussed in details. Therefore, the following points are concerned:
• Nonlinear direct power control with conventional switching table (DPC-LUT) (see section 3.2).
First of all, a general introduction about classical control techniques is included. Then, the mentioned point will be discussed.

3.1 Introduction

Regarding to the history of control systems for power converters, the control technique based on linear cascaded control loops was the first control technique in 1950, the modulations stages and coordinates transformations are used to linear the power converter as much as possible. The nonlinear control techniques are also develop for the power electronics, the practical applications are possible for some of them. A hysteresis DTC strategy is one of the nonlinear control strategies that shows a good successful. Based on the principle of DTC [31], direct power control (DPC) is proposed by Togushi in (1990). In term of implementation, these nonlinear control techniques implemented with analog electronics, later digitized and programmed in microprocessors. The huge increase of computational power and revolutionary development of microprocessing technology in the last decade cause to think more about exploration of new and more advanced approach of control techniques for power electronics, i.e., fuzzy logic control [32], sliding mode control [33], model predictive control [34], ..etc.

3.2 Nonlinear direct power control with conventional switching table (DPC-LUT)

As we mentioned above, nonlinear direct power control with look up table reported by Nouguchi in 1996, is based on the instantaneous power theory. The idea of DPC-LUT technique is easy to understand, and can be summarized as follow, the errors between the measured and reference values of active P and reactive Q power (S_p and S_q, respectively), are used as input of hysteresis controllers (2 elements). The reference value of active power is obtained from the signal generated by proportional integral (PI) controller multiplied by constant reference value of DC voltage, and reactive power reference is constant and null in order to achieve unity power factor. The grid voltage signal is used to calculate the angular position of space voltage vector θ_g. The digitized error between the upper and lower capacitor voltages (V_{c1} and V_{c2}, respectively) represents in sign S. Finally, based on these inputs: S_p, S_q, ω, S, and i_g^{abc}, the gate signal can be generated to the switches of power converter through the switching table. Figure 3.3 illustrated the scheme of direct power control-look up table (DPC-LUT) of 3L NPC-AFE. In the classical DPC-LUT, the hysteresis controllers are two level comparators [12]. Therefore, the active and reactive power digital hysteresis controllers can be expressed as follow:

$$H_p^{3L} = \begin{cases} 1, \ \Delta P \in (BD_p, +\infty) \\ 0, \ \Delta P \in (-\infty, 0) \end{cases} \tag{3.1}$$

$$H_Q^{3L} = \begin{cases} 1, \ \Delta Q \in (BD_Q, +\infty) \\ 0, \ \Delta P \in (-\infty, 0), \end{cases} \tag{3.2}$$

where H_P^{3L} and H_Q^{3L} represents the hysteresis widths of hysteresis controllers. Using $\alpha\beta$ plane, and divide it into twelve sectors (more accurate voltage vector selection is provided compared to 6 sectors) as shown in Figure 3.1. The relation between the sectors and angular position of space voltage vector can be described as

$$Sector_n = \theta_g \in (n\frac{\pi}{6}; \ (n+1)\frac{\pi}{6}) \tag{3.3}$$

where n represent the sector number, and θ_g is angular position of space voltage vector, which can determined as

$$\theta_g = arc2tan\,(\frac{e_g^{\beta}}{e_g^{\alpha}}) \tag{3.4}$$

To allow a control of instantaneous active and reactive power with errors limited to the hysteresis controller band, sampling frequency has to be about

ten times higher than average switching frequency. Also, the harmonic current distortion, the average converter switching frequency, the power pulsation and losses are affected (strongly) by the hysteresis wide. With the 3L NPC-AFE, 27 switching state vectors are possible, it is very important to known the influence of each vector on powers, then the switching table can be constructed, that what we will see at the next step.

3.2.1 Design of the switching table

Under balanced grid voltage, the switching voltage vector can be expressed as

$$v = |v_i|_{max}\, e^{j(\frac{\pi}{3})(i-1)} \tag{3.5}$$

where i=1,...12, and $|v_i|_{max}$ is the amplitude of small or medium or large voltage vectors.
Applying some hypothesizes as ignoring the line resistance R_g and the coupling terms, the equations 2.11 of line current can be rewritten in terms of changing based on a discrete first-order approximation as

$$\begin{cases} \Delta i_g^{\alpha} = i_{g[k+1]}^{\alpha} - i_{g[k]}^{\alpha} = \frac{T_s}{L_g}\left(e_{g[k]}^{\alpha} - v_{g[k]}^{\alpha}\right) \\ \Delta i_g^{\beta} = i_{g[k+1]}^{\beta} - i_{g[k]}^{\beta} = \frac{T_s}{L_g}\left(e_{g[k]}^{\beta} - v_{g[k]}^{\beta}\right) \end{cases} \tag{3.6}$$

Due to the high switching frequency, the change in power-source voltage is neglected. Using equation 2.16, the dynamic change of active and reactive power can be calculated as

$$\begin{cases} \Delta P = e_{g[k]}^{\alpha}.\Delta i_{g[k]}^{\alpha} + e_{g[k]}^{\beta}.\Delta i_{g[k]}^{\beta} \\ \Delta Q = e_{g[k]}^{\beta}.\Delta i_{g[k]}^{\alpha} - e_{g[k]}^{\alpha}.\Delta i_{g[k]}^{\beta} \end{cases} \tag{3.7}$$

Replacing equation 3.6 in equation 3.7 yielding

$$\begin{cases} \Delta P = \frac{T_s}{L_g}\left((e_{g[k]}^{\alpha})^2 + (e_{g[k]}^{\beta})^2\right) - \frac{T_s}{L_g}(e_{g[k]}^{\alpha}.v_{g[k]}^{\alpha} + e_{g[k]}^{\beta}.v_{g[k]}^{\beta}) \\ \Delta Q = \frac{T_s}{L_g}(e_{g[k]}^{\alpha}.v_{g[k]}^{\beta} - e_{g[k]}^{\beta}.v_{g[k]}^{\alpha}) \end{cases} \tag{3.8}$$

The active and reactive power changing depend on rectifier voltage vector that is applied. Twenty-seven rectifier voltage vectors produce twenty-seven possible values of change in active and reactive power. To select the corresponding switching state that controls the evaluation in active and reactive power, two equations are formulated, which are

$$\begin{cases} \Delta P_i = \frac{T_s}{L_g}\left((e_{g[k]}^{\alpha})^2 + (e_{g[k]}^{\beta})^2\right) - \frac{T_s}{L_g}(e_{g[k]}^{\alpha}.v_{gi}^{\alpha} + e_{g[k]}^{\beta}.v_{gi}^{\beta}) \\ \Delta Q_i = \frac{T_s}{L_g}(e_{g[k]}^{\alpha}.v_{gi[k]}^{\beta} - e_{g[k]}^{\beta}.v_{gi[k]}^{\alpha}) \end{cases} \tag{3.9}$$

Under ideal grid voltage, the grid voltage in stationary reference frame $\alpha - \beta$ can be expressed as

$$\begin{bmatrix} e_g^{\alpha} \\ e_g^{\beta} \end{bmatrix} = \sqrt{\frac{2}{3}} \begin{bmatrix} 1 & -\frac{1}{2} & -\frac{1}{2} \\ 0 & \frac{\sqrt{3}}{2} & -\frac{\sqrt{3}}{2} \end{bmatrix} \begin{bmatrix} e_g^{a} \\ e_g^{b} \\ e_g^{c} \end{bmatrix}, \tag{3.10}$$

Replacing equation 3.10 in equation 3.9, yielding

$$\begin{cases} \Delta P_i = \frac{T_s}{L_g} ||e_g^{\alpha\beta}||^2 - \frac{T_s}{L_g} ||e_g^{\alpha\beta}||.(cos(\theta).v_{gi}^{\alpha} + sin(\theta).v_{gi}^{\beta}) \\ \Delta Q_i = \frac{T_s}{L_g} ||e_g^{\alpha\beta}||.(cos(\theta).v_{gi}^{\beta} + sin(\theta).v_{gi}^{\alpha}) \end{cases} \tag{3.11}$$

Finally, the normalized value of change in active and reactive power can be expressed after divided equation 3.11 by $\frac{T_s}{L_g} ||e_g^{\alpha\beta}||.||v_g^{\alpha\beta}||$ as

$$\overline{\Delta P_i} = \frac{||e_g^{\alpha\beta}||}{||v_g^{\alpha\beta}||} - (cos(\theta).\bar{v}_{gi}^{\alpha} + sin(\theta).\bar{v}_{gi}^{\beta}) \tag{3.12}$$

$$\overline{\Delta Q_i} = cos(\theta).\bar{v}_{gi}^{\beta} - sin(\theta).\bar{v}_{gi}^{\alpha}, \tag{3.13}$$

where $||v_g^{\alpha\beta}||$ represents the max amplitude value of $v_g^{\alpha\beta}$ for small or medium or large space voltage vector, $\bar{v}_{gi}^{\alpha} = \frac{v_{gi}^{\alpha}}{||v_g^{\alpha\beta}||}$ and $\bar{v}_{gi}^{\beta} = \frac{v_{gi}^{\beta}}{||v_g^{\alpha\beta}||}$.
For a safety operation of rectifier, these condition $(||e_g^{\alpha\beta}||/||v_g^{\alpha\beta}|| \leq sin(\frac{\pi}{3}))$ shall took on consideration.
From the equation 3.11 and 3.13, the influence of each switching space vector on active and reactive power can be easily determined, which are illustrated in Figure 3.2.
According to the magnitude of each space vector, the vectors can be classified into four groups, as shown in Figure 3.1: zero voltage vector (ZVV) v_0, which produces null output voltage and it corresponds to three different configurations, small voltage vectors (SVVs) $v_1, v_4, v_7, v_{10}, v_{13}$ and v_{16} with has an amplitude equal to $V_{dc}/\sqrt{6}$, medium voltage vectors (MVV) $v_3, v_6, v_9, v_{12}, v_{15}$ and v_{18} with amplitude of $V_{dc}/\sqrt{2}$ and the large voltage vectors (LVVs) $v_2, v_5, v_8, v_{11}, v_{14}$ and v_{17} that generate a space vector with amplitude equal to $\sqrt{2/3}V_{dc}$.
For example, the influence of voltage vectors provided by the rectifier on the active and reactive power is shown in Table 1 considering the first sector θ_1, the table is classified according to the LVV, MVV, SVV and ZVV. The vectors of the same type are listed in an ascending order according to the impact degree on the power. As an example, firstly, the influence of LVVs on the active power, v_{11} can increase the active power more than v_{14}, and v_{14} can increase the active power more than v_8. v_2 can decrease the active power more than v_5, and v_5 can decrease the active power more than v_{17}. Secondly, the influence of LVVs on the reactive power, v_8 can increase the reactive power more than v_5, and v_5 can increase the reactive power more than v_{11}. v_{17} can decrease the reactive power more than v_{14}, and v_{14} can decrease the reactive power more

Table 3.1: Variations of active power and reactive power in sector θ_1.

	$\overline{\Delta p_i}$		$\overline{\Delta q_i}$		
	> 0	< 0	> 0	$= 0$	< 0
LVV	$v_8\ v_{14}\ v_{11}$	$v_{17}\ v_5\ v_2$	$v_{11}\ v_5\ v_8$		$v_2\ v_{14}\ v_{17}$
MVV	$v_6\ v_{15}\ v_9\ v_{12}$	$v_{18}\ v_3$	$v_3\ v_9\ v_6$		$v_{12}\ v_{18}\ v_{15}$
SVV	$v_1\ v_4\ v_{16}\ v_7\ v_{13}\ v_{10}$		$v_{10}\ v_4\ v_7$		$v_1\ v_{13}\ v_{16}$
ZVV	v_0			v_0	

Table 3.2: Switching table relative to the conventional DPC.

P	Q	θ_1	θ_2	θ_3	θ_4	θ_5	θ_6	θ_7	θ_8	θ_9	θ_{10}	θ_{11}	θ_{12}
↑	↓	v_{16}	v_{16}	v_1	v_1	v_4	v_4	v_7	v_7	v_{10}	v_{10}	v_{13}	v_{13}
↑	↑	v_4	v_4	v_7	v_7	v_{10}	v_{10}	v_{13}	v_{13}	v_{16}	v_{16}	v_1	v_1
↓	↓	v_2	v_3	v_5	v_6	v_8	v_9	v_{11}	v_{12}	v_{14}	v_{15}	v_{17}	v_{18}
↓	↑	v_3	v_5	v_6	v_8	v_9	v_{11}	v_{12}	v_{14}	v_{15}	v_{17}	v_{18}	v_2

than v_2. The same principal for the other voltage vectors.
Therefore, From this analysis and from Table 3.1, it appears that all voltage vectors have influences on active power and reactive power, but the effected extent was diverse. Thus, the conventional switching table has been constructed based on this analysis, in order to achieve simultaneous control of both P and Q, see Table 3.2. A detail scheme of direct power control with switching

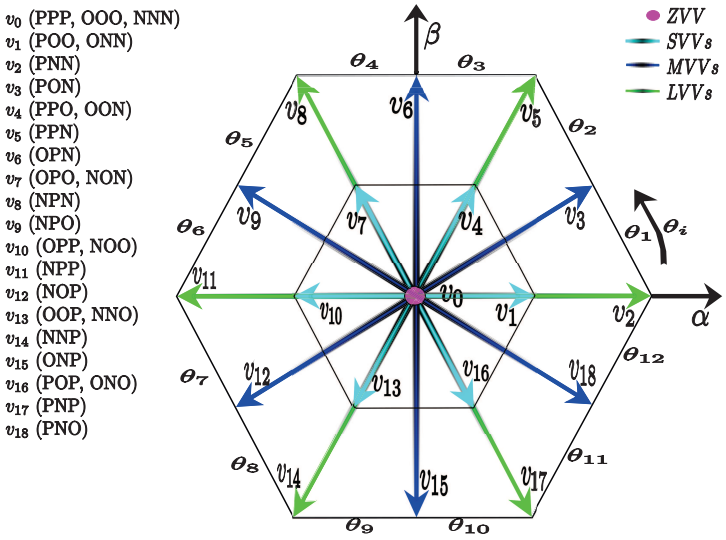

Figure 3.1: Space voltage vector of 3L NPC-AFE

table for 3L NPC-AFE is added (see Figure 3.3) in order to make the principle of this technique more clear.

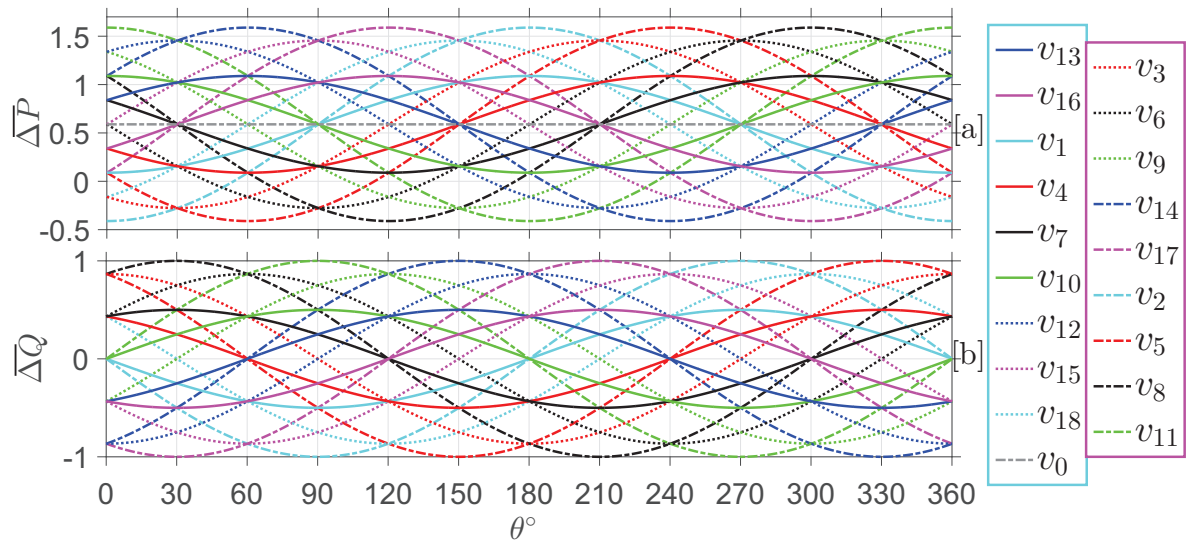

Figure 3.2: Variation of instantaneous active power and reactive power for various rectifier voltage vectors

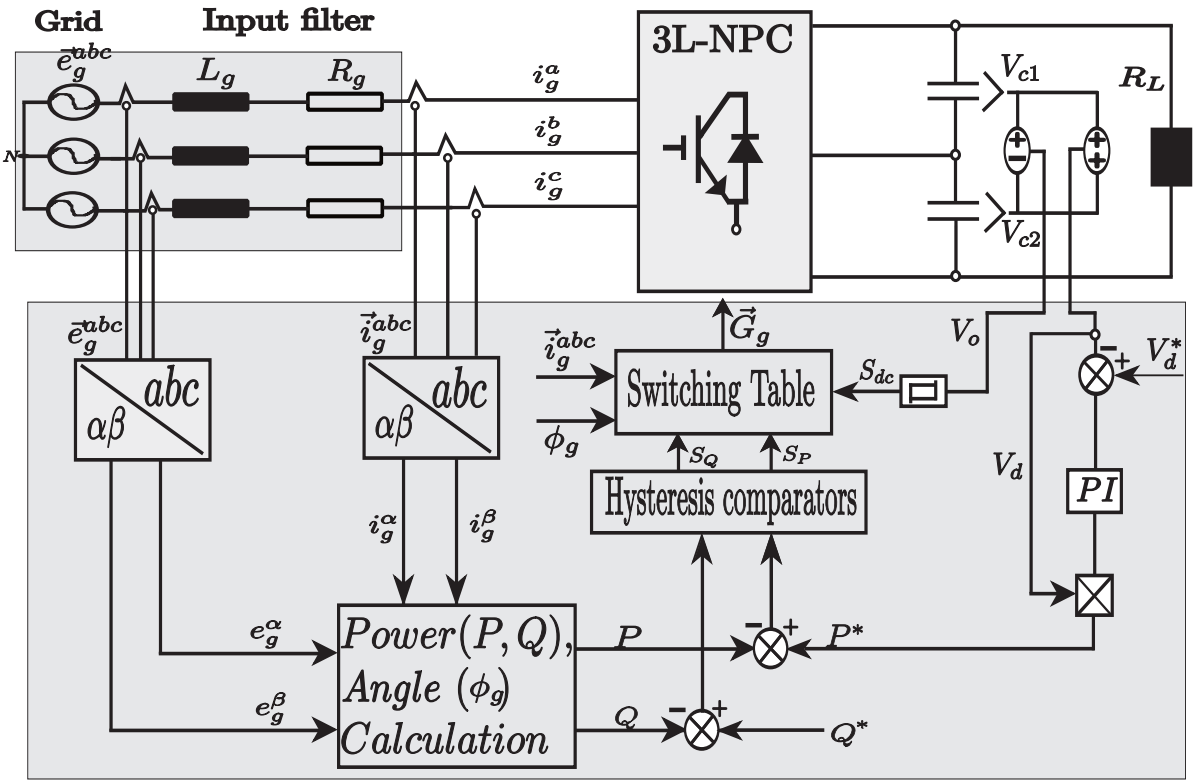

Figure 3.3: Scheme of LUT-DPC strategy for 3L NPC-AFE

CHAPTER 4

Advanced classical control techniques

4.1 Introduction

Despite the many features of the direct power control with switching table (DPC-LUT), as a simple structure, low switching frequency, no requirement of current loop/ PWM block. DPC with switching table suffers from some problems, which are, variable switching frequency, large power ripples, and weak performance under non-ideal grid voltage. The space voltage vector (SVM) is used as one of the solutions to fix the switching frequency, this point is discussed in details in the previous chapter. Many works with DPC-LUT technique have been proposed in this work and applied in order to reduce the power ripples, and conserving the advantages of simple structure and rapid dynamic response. The classical switching table of direct power control (DPC) for 3L AFE-NPC is constructed based on the adjacent vectors strategy according to the dynamics of active and reactive power in $\alpha-\beta$ frame. Various new methods have been introduced to further improve the steady-state performance of the conventional LUT-DPC strategy by using hysteresis comparators with more than two level [35], [36]. In [37], an optimization method for voltage vector in LUT-DPC strategy is proposed to avoid the selection of voltage vectors which produce large reactive power variations. However, extra calculation of source virtual-flux position is required to subdivide each 60 sector into unequal 3 sub sectors. In [38], a novel three level LUT-DPC strategy is proposed by adding transitional sectors and their corresponding voltage vector to each 60 sector to eliminate the abnormal reactive power fluctuations, but this method required calculations of the width of the additional sectors. Furthermore, the switching loss increases than with the conventional LUT-DPC strategy. In [39], DPC based on space vector modulation (SVM) is applied, constant switching frequency is achieved, but using the PI controllers and dq reference frame lead

to lose the advantages of LUT-DPC strategy.
In this work, two new switching table under ideal grid voltage, and a new definition of active power under unbalanced grid voltage are proposed and will be discussed separately in the next step.

4.2 An Improved Look-up Table

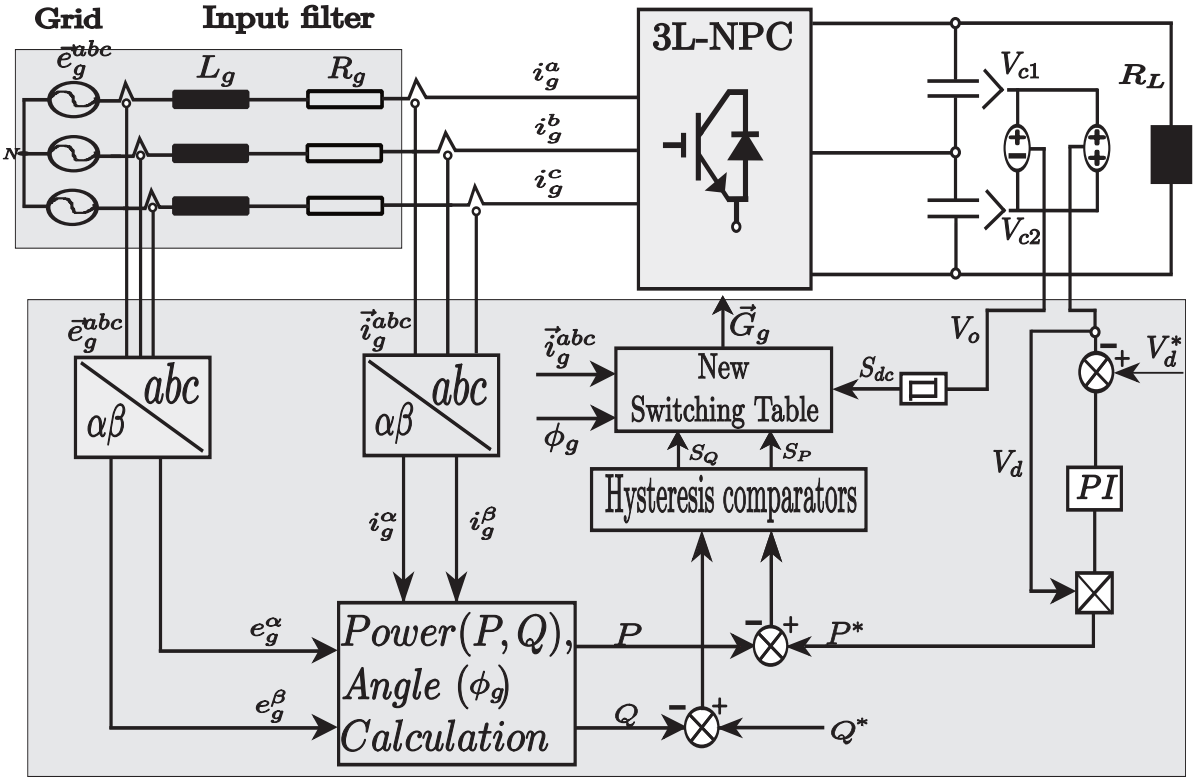

Figure 4.1: Scheme of improved LUT-DPC strategy for 3L NPC-AFE

While the conventional switching table is applied, positive fluctuations are produced in the waveform of reactive power in the beginning part of odd sectors, which will lead to increase the THD of grid currents and depress the power factor in steady state. The fluctuations are appeared because the vectors that applied during each odd sector cannot cause tracking of the reactive power reference. In view of this, a new switching table is constructed and proposed in this work to solve this problem and to assure small switching losses as can as possible. Three different voltage vectors are applied equally during each odd sector instead of one vector when the active power needs to be increased and reactive power needs to be decreased. The three voltage vectors are applied in descending order (the first one can reduce the reactive power more than the third one). The control diagram of the improved LUT-DPC strategy is

Table 4.1: Improved switching table for LUT-DPC strategy.

P	Q	θ_1	θ_2	θ_3	θ_4	θ_5	θ_6	θ_7	θ_8	θ_9	θ_{10}	θ_{11}	θ_{12}
↑	↓	v_{16}-v_{13}-v_1	v_1	v_1-v_{16}-v_4	v_4	v_4-v_1-v_7	v_7	v_7-v_4-v_{10}	v_{10}	v_{10}-v_7-v_{13}	v_{13}	v_{13}-v_{10}-v_{16}	v_{16}
↑	↑	v_4	v_4	v_7	v_7	v_{10}	v_{10}	v_{13}	v_{13}	v_{16}	v_{16}	v_1	v_1
↓	↓	v_2	v_3	v_5	v_6	v_8	v_9	v_{11}	v_{12}	v_{14}	v_{15}	v_{17}	v_{18}
↓	↑	v_3	v_5	v_6	v_8	v_9	v_{11}	v_{12}	v_{14}	v_{15}	v_{17}	v_{18}	v_2

Table 4.2: New switching table with 3 level hysteresis controller for LUT-DPC strategy.

P	Q	θ_1	θ_2	θ_3	θ_4	θ_5	θ_6	θ_7	θ_8	θ_9	θ_{10}	θ_{11}	θ_{12}
↑↑	↑	v_{10}	v_{10}	v_{13}	v_{13}	v_{16}	v_{16}	v_1	v_1	v_4	v_4	v_7	v_7
↑↑	↓	v_{13}	v_{16}	v_{16}	v_1	v_1	v_4	v_4	v_7	v_7	v_{10}	v_{10}	v_{13}
↑↑	↓↓	v_{13}	v_{16}	v_{16}	v_1	v_1	v_4	v_4	v_7	v_7	v_{10}	v_{10}	v_{13}
↑	↑	v_4	v_4	v_7	v_7	v_{10}	v_{10}	v_{13}	v_{13}	v_{16}	v_{16}	v_1	v_1
↑	↓	v_1	v_1	v_4	v_4	v_7	v_7	v_{10}	v_{10}	v_{13}	v_{13}	v_{16}	v_{16}
↑	↓↓	v_{16}	v_{16}	v_1	v_1	v_4	v_4	v_7	v_7	v_{10}	v_{10}	v_{13}	v_{13}
↓↓	↑	v_3	v_5	v_6	v_8	v_9	v_{11}	v_{12}	v_{14}	v_{15}	v_{17}	v_{18}	v_2
↓↓	↓	v_2	v_3	v_5	v_6	v_8	v_9	v_{11}	v_{12}	v_{14}	v_{15}	v_{17}	v_{18}
↓↓	↓↓	v_2	v_3	v_5	v_6	v_8	v_9	v_{11}	v_{12}	v_{14}	v_{15}	v_{17}	v_{18}

represented in Figure 4.1 and its switching table is given in Table 4.1.
As a clarification, the proposed switching table is constructed after determine the impact of each space voltage vector on both powers (active and reactive power) in each sector by using the instantaneous power theory. These determination steps is already explained in subsection 3.2.1.

4.3 New look-Up-Table

The use of two level hysteresis comparators and conventional switching table in the conventional LUT-DPC strategy causes many problems (poor regulation of reactive power, non-sinusoidal input currents with a little high THD and depressed power factor). Thus, three level hysteresis comparators are used instead of two level one, and a new switching table is constructed through following the same steps as in subsection 3.2.1. The main reason for synthesizing the new LUT-DPC switching table is to select the best rectifier voltage vector among all the possible vectors in order to restrict the instantaneous active and reactive power tracking errors, simultaneously. The new switching table and the block scheme of the proposed LUT-DPC strategy are shown respectively in Table 4.2 and Figure 4.2.

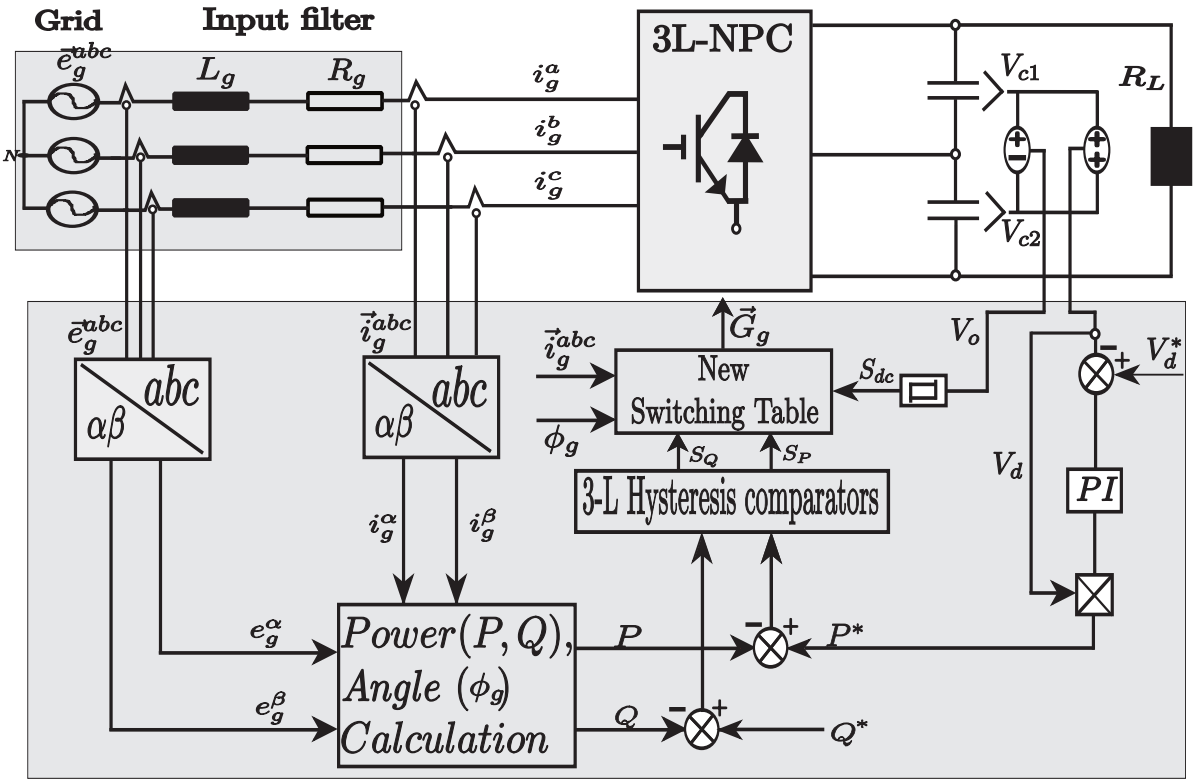

Figure 4.2: Control scheme of the new LUT-DPC strategy for 3L NPC-AFE

4.4 Direct Power Control with Switching Table under Unbalanced Grid Voltage

As high-performance classical control strategies for PWM ac/dc converters, direct power control (DPC) [39–42] and voltage oriented control (VOC) [43–45] are considered. The former (VOC) was developed based on the well-known *field oriented control* (FOC); whilst the latter has the similar properties of *direct torque control* (DTC) [46] for AC drives. In VOC, both active and reactive components of input currents in synchronous frame are obtained by decomposing the grid currents. Through inner current loops using PI controller, the active and reactive current components can be regulated. Several VOC strategies have been introduced in the literature to cope with the voltage unbalanced [35, 47–54]. In [47], by deriving and regulating the positive- and negative-sequence components of grid currents in the synchronous reference frame [48, 49], constant active power is achieved. However, the computational burden and tuning efforts are significantly increased due to the use of several PI controllers and the extraction of positive- and negative-sequence components. In [50], a dual-frequency resonant compensator and PI regulator were employed to enhance the performance of the control system under unbalanced

and distorted grid voltages for doubly-fed induction generators (DFIGs) in variable-speed wind turbine applications. However, due to the sequence decomposition of voltage and current, the time delay and control error in VOC are inevitable. Additionally, the reference current computation for different control targets is also complicated. Hence, to reduce the control complexity of dual current controller, a number of improved methods have been presented in the literature using PI plus resonant and vector PI controller (see e.g., [35, 51–53]). Although, the extraction of positive- and negative-sequence components of grid voltages is still needed. In [54], a new definition of reactive power (proposed in [55]) is proposed and investigated in VOC strategy, sinusoidal input current with low THD and accurate regulation of DC-voltage are achieved. However, the computational burden is reduced and the control structure is simplified, as long as the positive- and negative-sequence extraction of both grid voltage/currents and complicated calculations of current reference are not required anymore [56].

Different new methods have been presented in the literature to further improve the steady-state performance of the DPC [20, 36, 57–63], as utilized multi-level hysteresis instead of the conventional two-level one (see e.g., [36, 57–59]); using of a modulation stage (see e.g., [20, 60]); employing of *predictive algorithm* instead of the switching table (see e.g., [61–63]). Nevertheless, only a few publications consider the operation under unbalanced grid voltages [64, 65]. Unbalanced grid voltage has already been a very common phenomenon, which can be caused by, e.g., non-ideal three-phase load, asymmetry faults, large capacity single-phase load, asymmetry of power transmission system, etc. In [64], the distorted terms are added into the power references, three different specialized control targets under unbalanced grid conditions can be achieved with LUT-DPC. No negative sequence current, smooth active power, and smooth reactive power are the control targets. However, synchronous transformation, extraction of both positive/ negative components of grid voltage and current are required. In [65], a simplified power compensation block is proposed, where the negative sequence current is not required and three different targets are implemented. Nevertheless, the extraction of the positive- and negative-sequence components of grid voltages and the positive-sequence component of grid currents are still required, which increases the control complexity and computational burden. To entirely eliminate the sequence decomposition and keep the simplicity of DPC scheme as far as possible, the authors in [66] combines the merits of DPC and the new definition of instantaneous reactive power, taking the active power and new reactive power as control variables, which is more suitable for unbalanced grid voltages than the conventional reactive power definition. To simplify the calculation process, DPC with this new definition of the reactive power for two-level voltage source converter based on $\alpha\beta$ frame instead of dq frame was presented in [67]. However, here is the room for further improvement.

In the following section, a proposed DPC strategy with *a new definition* of instantaneous active power (DPC-NP) expressed in the dq reference frame

for three-level NPC rectifier under unbalanced grid voltages will be discussed. Through the utilization of the new definition of active power, instead of conventional one under unbalanced grid voltage, good performance of the DPC scheme is achieved and the decoupling process of positive and negative sequences are not required. As a result, reducing the computational burden and simplifying the control structure. The proposed DPC strategy is much simpler in structure, in comparison with the conventional DPC (CDPC) solutions and the DPC scheme with the new definition of the reactive power (DPC-NQ) that presented in [67]. Furthermore, no compensation block or calculations of the current references are required. Extensive simulation data in different scenarios are provided to validate the effectiveness of proposed DPC. Its performance is compared with that of *both* CDPC *and* DPC-NQ schemes. The results illustrate the superior performance of proposed DPC-NP in comparison with CDPD and DPC-NQ, see 4.5.4.

4.5 DPC of 3L NPC-AFE

In this section, the system description and modeling of the underlying 3L NPC-AFE is presented.

4.5.1 Topology and mathematical modeling of 3L NPC-AFE

According to the instantaneous power theory [68], the complex power, active power, and reactive power of the NPC rectifier can be calculated respectively as

$$S = \frac{3}{2}\left(i_g^* e_g\right) \tag{4.1}$$

$$P = Re(S) = \frac{3}{2}\Re(i_g^* e_g) = \frac{3}{2}\left(i_g \odot e_g\right) \tag{4.2}$$

$$Q = Im(S) = \frac{3}{2}\Im(i_g^* e_g) = \frac{3}{2}\left(i_g \otimes e_g\right) \tag{4.3}$$

where * signifies the conjugate of a complex vector, $\odot$ is dot product and $\otimes$ is cross product.
An improved definition of reactive power from the extended *pq* theory is utilized in [66, 67], which is writing as

$$Q^{nov} = \frac{3}{2}\Re(i_g^* e_g^{'}) = \frac{3}{2}\left(i \odot e^{'}\right) \tag{4.4}$$

where $e^{'}$ signifies the variable that lags e by 90 electrical degrees in the time domain [68].

In this work, a *new definition* of active power is proposed, which is expressed as

$$P^{nov} = \frac{3}{2}\Im(i_g^* e_g^{'}) = \frac{3}{2}\left(i_g \otimes e_g^{'}\right) \tag{4.5}$$

Under unbalanced grid voltage condition, the sum of positive- and negative-sequence vectors represents respectively the grid voltage and grid current as [66]:

$$e_g = e_g^+ + e_g^- = e_g^{dq^+}\, e^{+jwt} + e_g^{dq^-}\, e^{-jwt} \tag{4.6}$$

$$i_g = i_g^+ + i_g^- = i^{dq^+}\, i^{+jwt} + i_g^{dq-}\, i^{-jwt} \tag{4.7}$$

where $e_g^{dq^+} = e_g^{d^+} + je_g^{q^+}$, $e_g^{dq^-} = e_g^{d^-} + je_g^{q^-}$, $i_g^{dq^+} = i_g^{d^+} + ji_g^{q^+}$, $i_g^{dq^-} = i_g^{d^-} + ji_g^{q^-}$, and ω is the grid frequency in [rad/s].
The lagging vector $e_g^{'}$ of unbalanced grid voltage can be expressed as

$$e_g^{'} = e_g^{dq^+}\, e^{+j(wt-\frac{\pi}{2})} + e_g^{dq^-}\, e^{-j(wt-\frac{\pi}{2})} = -je_g^{dq^+}\, e^{+j(wt)} + je_g^{dq^-}\, e^{-j(wt)} \tag{4.8}$$

Taking into consideration the grid voltages and currents in equations (4.6), (4.7) and (4.8); (4.2), (4.3) and (4.5) can be rewriting as

$$\begin{cases} P = \frac{3}{2}\, Re(i_g^* e) = \frac{3}{2}\, \Re(i_g^{dq^+}\, e^{+j(wt)} + i_g^{dq^-}\, e^{-j(wt)})^*(e_g^{dq^+}\, e^{+j(wt)} + e_g^{dq^-}\, e^{-j(wt)}) \\ = P_o + P_{c2} cos(2\omega t) + P_{s2} sin(2\omega t) \end{cases} \tag{4.9}$$

$$\begin{cases} P^{nov} = \frac{3}{2}\, \Im(i_g^* e_g^{'}) = \frac{3}{2}\, \Im(i_g^{dq^+}\, e^{+j(wt)} + i_g^{dq^-}\, e^{-j(wt)})^*(-je_g^{dq^+}\, e^{+j(wt)} + je_g^{dq^-}\, e^{-j(wt)}) \\ = P_o^{nov} + P_{c2}^{nov} cos(2\omega t) + P_{s2}^{nov} sin(2\omega t) \end{cases} \tag{4.10}$$

$$\begin{cases} Q = \frac{3}{2}\, Im(i_g^* e_g) = \frac{3}{2}\, \Im(i_g^{dq^+}\, e^{+j(wt)} + i_g^{dq^-}\, e^{-j(wt)})^*(e_g^{dq^+}\, e^{+j(wt)} + e_g^{dq^-}\, e^{-j(wt)}) \\ = Q_o + Q_{c2} cos(2\omega t) + Q_{s2} sin(2\omega t) \end{cases} \tag{4.11}$$

with

$$\begin{cases} P_o = \frac{3}{2}\, (i_g^{dq^+} \odot e_g^{dq^+} + i_g^{dq^-} \odot e_g^{dq^-}) \\ P_{c2} = \frac{3}{2}\, (i_g^{dq^+} \odot e_g^{dq^-} + i_g^{dq^-} \odot e_g^{dq^+}) \\ P_{s2} = \frac{3}{2}\, (i_g^{dq+} \otimes e_g^{dq^-} - i_g^{dq^-} \otimes e_g^{dq^+}) \end{cases} \tag{4.12}$$

$$\begin{cases} P_o^{nov} = \frac{3}{2}\, (-i_g^{dq^+} \odot e_g^{dq^+} + i_g^{dq^-} \odot e_g^{dq^-}) \\ P_{c2}^{nov} = \frac{3}{2}\, (i_g^{dq^+} \odot e_{dq}^- - i_{dq}^- \odot e_{dq}^+) \\ P_{s2}^{nov} = \frac{3}{2}\, (i_{dq}^+ \otimes e_g^{dq^-} + i_g^{dq^-} \otimes e_g^{dq^+}) \end{cases} \tag{4.13}$$

$$\begin{cases} Q_o = \frac{3}{2}\, (i_g^{dq^+} \otimes e_g^{dq^+} + i_g^{dq^-} \otimes e_g^{dq^-}) \\ Q_{c2} = \frac{3}{2}\, (i_g^{dq^+} \otimes e_g^{dq^-} + i_g^{dq^-} \otimes e_g^{dq^+}) \\ Q_{s2} = \frac{3}{2}\, (-i_g^{dq^+} \odot e_g^{dq^-} + i_g^{dq^-} \odot e_g^{dq^+}) \end{cases} \tag{4.14}$$

where (P_o, Q_o), (P_{c2}, Q_{c2}), and (P_{s2}, Q_{s2}) are respectively the average value of active and reactive power, the harmonics peak of active and reactive power cosine phase, and the harmonics peak of active and reactive power sine phase, respectively.

From equations (4.13) and (4.14), it is appeared that $P_{c2}^{nov} = -Q_{s2}$ and $P_{s2}^{nov} = Q_{c2}$. The active power and reactive power in equations (4.10) and (4.11) can be rewritten, respectively, as

$$\begin{cases} P^{nov} = P_o^{nov} + P_{c2}^{nov} cos(2\omega t) + P_{s2}^{nov} sin(2\omega t) \\ = P_o^{nov} - Q_{s2} cos(2\omega t) + Q_{c2} sin(2\omega t) \\ = P_o^{nov} + \sqrt{(Q_{c2}^2 + Q_{s2}^2)} sin(2\omega t + \theta - \frac{\pi}{2}) \end{cases} \tag{4.15}$$

$$\begin{cases} Q = Q_o^{nov} + Q_{c2} cos(2\omega t) + Q_{s2} sin(2\omega t) \\ = Q_o + \sqrt{(Q_{c2}^2 + Q_{s2}^2)} sin(2\omega t + \theta) \end{cases} \tag{4.16}$$

According to $(\sqrt{(Q_{c2}^2 + Q_{s2}^2)} sin(2\omega t + \theta - \frac{\pi}{2}))$ and $(\sqrt{(Q_{c2}^2 + Q_{s2}^2)} sin(2\omega t + \theta))$, the ripple amplitude of active power is the same as that of reactive power, where $\theta = \arctan(Q_{c2}/Q_{s2})$. Thus, if the oscillation in the active power is nullified (i.e, the ripple amplitude of the active power is null), the oscillation in reactive power should be null. Thus, the active and reactive power will be constant and without oscillations, which make both the active and reactive power track their respective references.

4.5.2 Comparison between conventional and new active power

Under the assumption that the grid currents contain only both positive- and negative-sequence components (i.e. no zero-sequence component is exist), the use of the extended *pq* theory to compute the active power under unbalanced grid voltage allows getting constant active and reactive power. According to equations (4.15) and (4.16), constant active and reactive power means that

$$\begin{cases} P_o^{nov} & = P^{ref} \\ P_{c2}^{nov} & = -Q_{s2} \\ P_{s2}^{nov} & = Q_{c2} \\ Q_0 & = 0 \end{cases} \tag{4.17}$$

where P^{ref} is the reference value of active power.

The four values of the reference currents $(i_d^+ \; i_q^+ \; i_d^- \; i_q^-)$ can be determined through solving the four equations of (4.17). Therefore, the injection of negative-sequence current is sufficient and necessary to obtain constant active and reactive power, in case of unbalanced grid voltage. The harmonics in grid current would be eliminate, as far as both active and reactive power track accurately their respective reference values. Hence, by using the new active power definition instead of the conventional one, the grid current will be sinusoidal but still unbalanced. Thus, the new active power in the extended *pq* theory is more suitable under unbalanced grid voltage, compared to the conventional active power definition.

In contrast, if conventional active power is employed, constant active and reactive power requires that

$$\begin{cases} P_o &= P^{ref} \\ P_{c2} &= 0 \\ P_{s2} &= 0 \\ Q_0 &= 0 \\ Q_{c2} &= 0 \\ Q_{s2} &= 0 \end{cases} \tag{4.18}$$

From equation (4.18), the four values of the reference currents ($i_d^+\ i_q^+\ i_d^-\ i_q^-$) cannot be obtained by solving the six equations of (4.18). In this case, harmonics components shall be added to the grid to obtain constant active and reactive power [66]. The grid current amplitude can be determined from equations (4.2) and (4.3) as

$$|i_g| = \frac{P + jQ}{1.5 e_g} \tag{4.19}$$

Constant values of P and Q result in variable amplitude of grid current with time. consequently, the harmonics would appear.

4.5.3 Design of the new switching table

A more *suitable look up table* is proposed and will be discussed here. It is *newly* established to achieve simultaneous control of both new active power and reactive power under unbalanced grid voltage, which is the key aspect of DPC. To the best of the authors knowledge, the new active power has not been reported in the frame of DPC with 3L AFE-NPC.

The lagging value of grid voltage vector and its differentiation can be written from equations (4.6) and (4.8) as

$$\frac{de_g}{dt} = j\omega e_g^+ - j\omega e_g^- = -\omega e_g^{'} \tag{4.20}$$

$$\frac{de_g^{'}}{dt} = \omega e_g^+ + \omega e_g^- = \omega e_g \tag{4.21}$$

And the differentiations of new active power is obtained from equations (2.11), (4.2),(4.5), and (4.21)as

$$\frac{dP^{nov}}{dt} = \frac{1}{L_g} \Im[(e^* - v^*)e^{'}] - \frac{R}{L_g} P^{nov} - \omega\, Q. \tag{4.22}$$

Similarly, the differentiation of reactive power can be determined from equations (2.11), (4.3) and (4.20) as

$$\frac{dQ}{dt} = \frac{1}{L_g} \left(\Im[(e^* - (v^*)e)] - R_g Q_+ \omega_g\, P^{nov}\right), \tag{4.23}$$

To simplify the equations, the resistance R and the coupling terms are ignored. Therefore, equations (4.22) and (4.23) are rewritten as

$$\frac{dP^{nov}}{dt} = -\frac{1}{L_g} E^2 - \frac{1}{L_g} ||v_i||_{max} E.sin(\omega t - \frac{\pi}{2} - \frac{\pi}{3}(n-1)) \tag{4.24}$$

$$\frac{dQ}{dt} = -\frac{1}{L_g} ||v_i||_{max} E\, sin(\omega t - \frac{\pi}{3}(n-1)) \tag{4.25}$$

where E is the RMS value of line to line grid voltage and (n = 1, . . .,12), and $||v_i||_{max}$ is the amplitude of small or medium or large voltage vectors.

The influence of each switching space vector on active and reactive power at each sampling period can be expressed as

$$\Delta P^{nov} = -\frac{T_s}{L_g} E^2 - \frac{T_s}{L} ||v_i||_{max} E\, sin(\omega t - \frac{\pi}{2} - \frac{\pi}{3}(n-1)), \tag{4.26}$$

$$\Delta Q = -\frac{T_s}{L_g} ||v_i||_{max} E\, sin(\omega t - \frac{\pi}{3}(n-1)), \tag{4.27}$$

To normalize the power variation, both sides of equations (4.26) and (4.27) are divided by the constant $\frac{T_s}{L_g}.E.|v_i|_{max}$, yielding

$$\overline{\Delta P}_i^{nov} = -\sqrt{\frac{3}{2}} \frac{E}{V_{dc}} - sin(\omega t - \frac{\pi}{2} - \frac{\pi}{3}(n-1)) \tag{4.28}$$

$$\overline{\Delta Q}_i = -sin(\omega t - \frac{\pi}{3}(n-1)) \tag{4.29}$$

From the equations in (3.13), and (4.28), we can draw that: $\overline{\Delta P}_i = -\overline{\Delta P}_i^{nov}$.

The influence of each switching space vector on the normalized value of variation of the instantaneous new active power and reactive power under unbalanced grid voltage can be determined from equations (4.28) and (4.29), which are illustrated in Figure 4.3. According to the magnitude of each space vector, the switching space vectors are classified to four groups: zero voltage vector (ZVV), small voltage vectors (SVVs), medium voltage vectors (MVV) and large voltage vectors (LVVs). For more details, please see 3.2.1.

The unbalance of grid voltage is initially set to 15% to consider more rigorous grid unbalance condition. As shown in Figure 4.3, the variation of instantaneous active and reactive power are symmetrical with the same peak value when the grid voltage is balanced, and are also symmetrical but with different peak value when the grid voltage is unbalanced. Therefore, the classification of the impact of each voltage vectors on active and reactive power is the same under both balanced and unbalanced grid voltages. As a results, the new switching table is the same under balanced or unbalanced grid voltages. The basic idea for synthesizing the new DPC switching table is to select the best rectifier voltage vector among all the possible vectors in order to restrict the instantaneous active and reactive power tracking errors, simultaneously. The new switching table synthesis is based on the sign and magnitude of variation of instantaneous active and reactive power for each sector as shown in Figure 4.3.

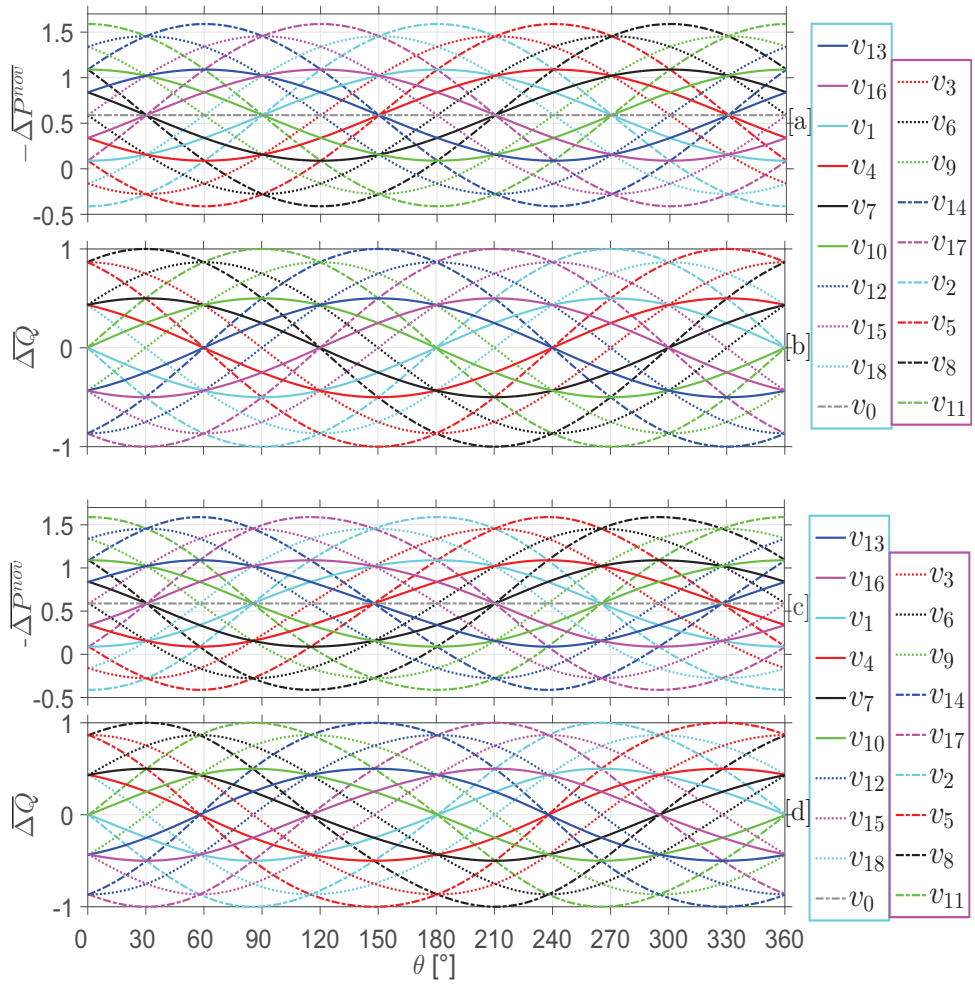

Figure 4.3: Variation of instantaneous active power and reactive power for various rectifier voltage vectors under [a], [b] balanced grid voltages, [c], [d] unbalanced grid voltages.

For example, the influence of voltage vectors provided by the rectifier on the active and reactive power is shown in Table 1 considering the first sector θ_1, the table is classified according to the LVV, MVV, SVV and ZVV. The vectors of the same type are listed in an ascending order according to the impact degree on the power. Therefore, From this analysis and from Table 4.3, it appears that all voltage vectors have influence on active power and reactive power, but the effected extent was diverse. Thus, the switching table suitable for accuracy simultaneous control of both P_{nov} and Q can be obtained in Table 2. It is clear from Table 4.4 that the switching table derived under balanced grid voltage is the same as that under unbalanced grid voltage. The Figure 4.4 shows the new DPC and the simulation block of the conventional and new DPC for three-level NPC rectifier, respectively.

Table 4.3: Variations of active power and reactive power in sector θ_1.

	$-\overline{\Delta p_i^{nov}}$		$\overline{\Delta q_i}$		
	> 0	< 0	> 0	$= 0$	< 0
LVV	$v_8\ v_{14}\ v_{11}$	$v_{17}\ v_5\ v_2$	$v_{11}\ v_5\ v_8$		$v_2\ v_{14}\ v_{17}$
MVV	$v_6\ v_{15}\ v_9\ v_{12}$	$v_{18}\ v_3$	$v_3\ v_9\ v_6$		$v_{12}\ v_{18}\ v_{15}$
SVV	$v_1\ v_4\ v_{16}\ v_7\ v_{13}\ v_{10}$		$v_{10}\ v_4\ v_7$		$v_1\ v_{13}\ v_{16}$
ZVV	v_0			v_0	

Table 4.4: Switching table relative to the proposed DPC under balanced or unbalanced grid voltages.

P/P^{nov}	Q	θ_1	θ_2	θ_3	θ_4	θ_5	θ_6	θ_7	θ_8	θ_9	θ_{10}	θ_{11}	θ_{12}
↑	↓	v_{16}	v_{16}	v_1	v_1	v_4	v_4	v_7	v_7	v_{10}	v_{10}	v_{13}	v_{13}
↑	↑	v_4	v_4	v_4	v_7	v_{10}	v_{10}	v_{13}	v_{13}	v_{16}	v_{16}	v_1	v_1
↓	↓	v_2	v_3	v_5	v_6	v_8	v_9	v_{11}	v_{12}	v_{14}	v_{15}	v_{17}	v_{18}
↓	↑	v_3	v_5	v_6	v_8	v_9	v_{11}	v_{12}	v_{14}	v_{15}	v_{17}	v_{18}	v_2

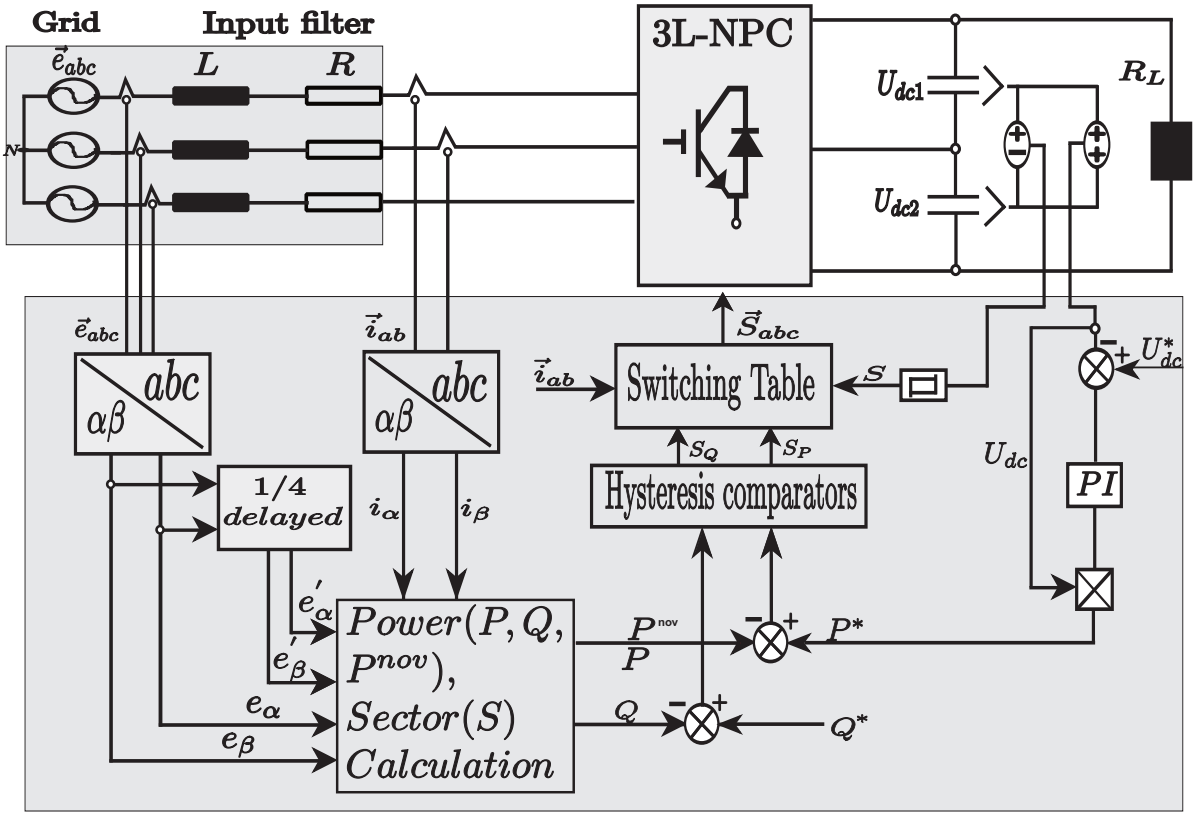

Figure 4.4: Block scheme of the new DPC for three-level NPC rectifier.

Table 4.5: Parameters of the three-level NPC rectifier.

Name	Nomenclature/Unit	Value
AC line voltage	e_a [V]	$170.\sqrt{2}$
Line resistance	R [Ω]	0.3
Load resistance	R_L [Ω]	80
Frequency	f [Hz]	50
AC-side inductance	L [H]	0.01
DC-bus capacitors	C_1, C_2 [F]	680.10^{-6}
DC-bus voltage	U_{dc} [V]	500

4.5.4 Performance evaluation with simulation data

The validity of the advanced classical control techniques for the 3L NPC-AFE is proved by simulation results using Matlab/simulink environment. Each technique is evaluated through comparative simulation tests, and under the same condition for each testing scenario. The DC-link voltage reference remains at 500 [V], the reactive power reference is set at 0 [Var] for unity power factor, $50e^{-6}$ [s] is the value of the sampling period T_s, and the bandwidths of upper and lower capacitors are set to a small value for an acceptable switching frequency (bellow 5kHz). All the techniques operate at variable switching frequency. The simulation results represent the overall and steady-state operation of each control technique, included the measured and reference values of active power, reactive power and DC-voltage, the DC-voltage of upper and lower capacitors, and grid current. The simulation was done with a DC-load of a different step change. Table 4.5 shows the data of the system.

4.5.4.1 Performance evaluation of an improved look-up table

Figure 4.5, Figure 4.6, Figure 4.7 and Figure 4.8 illustrate the overall and steady state performance of conventional and improved LUT-DPC techniques, respectively. A comparative simulation results between conventional LUT-DPC technique and improved LUT-DPC technique are summarized in this part.

❣ Steady steady performance

As can be seen, the improved LUT-DPC technique show a good performance, the reactive power fluctuations are eliminated effectively (which appear with conventional LUT-DPC technique during each odd sectors) and the power factor is improved. The grid current is closer to sinusoidal wave (distorted current with conventional LUT-DPC), the THD of current is lower compared to with conventional LUT-DPC. In the DC-side, the dc voltage has a small ripple and the upper and lower capacitors voltages are around half of DC-voltage value

with small ripples. In opposite of that, no accuracy controlled of V_{dc1} and V_{dc2} with large ripple, in case of utilizing the conventional LUT-DPC.

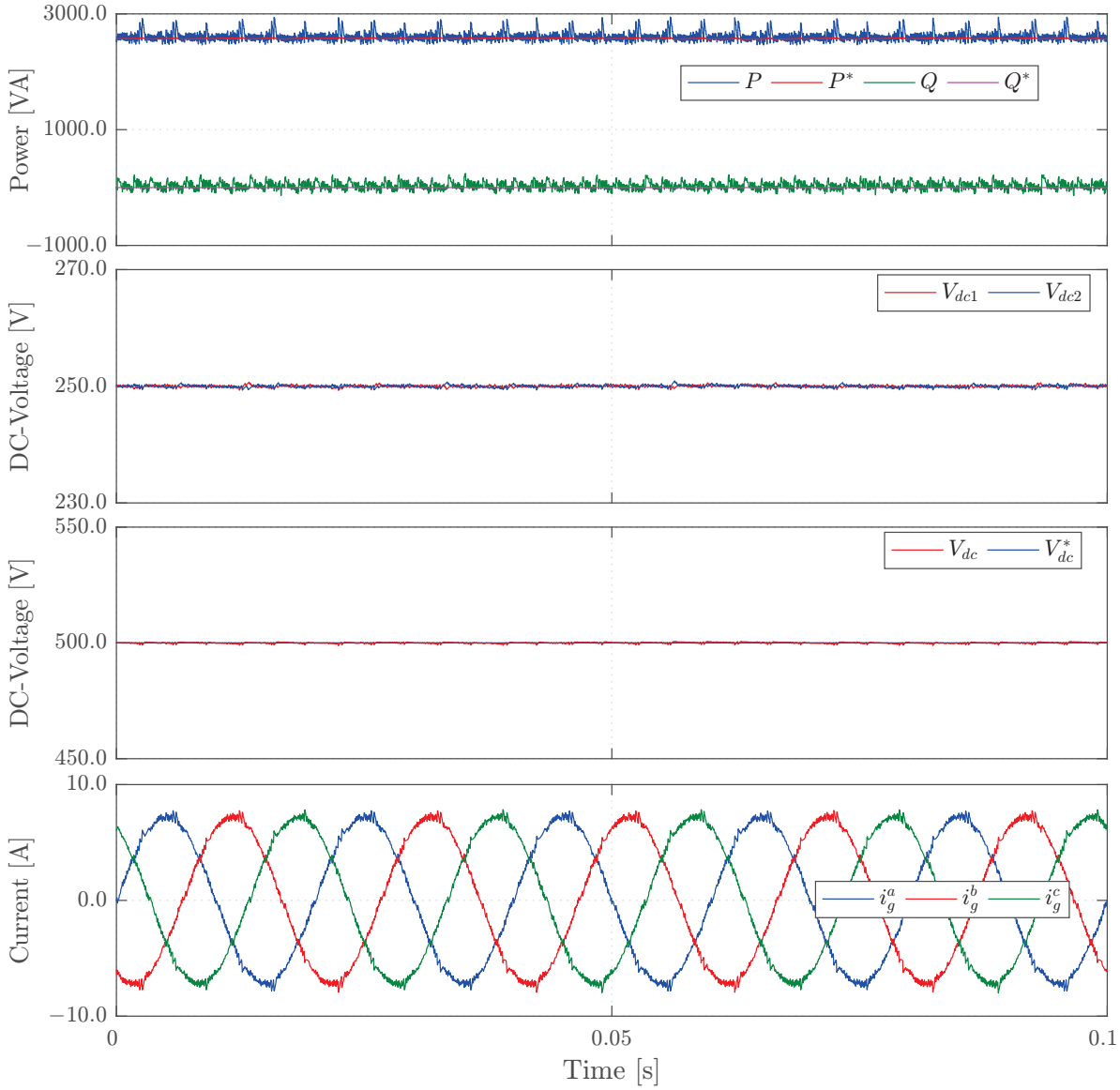

Figure 4.5: Steady-state results of improved LUT-DPC for 3L NPC-AFE

❣ Transient-Steady Performance

The load power was increased and decreased during the transient-steady of conventional and improved LUT-DPC strategy. It can be seen from the results of improved LUT-DPC technique that the system operates successfully under unity power factor (depressed power factor with conventional LUT-DPC). Additionally, the dc-bus voltage is maintained closer to its reference value after a short transient (the same performance with conventional LUT-DPC technique), and upper and lower capacitor voltages are well controlled (weak controlled with large ripple in upper and lower capacitor voltages, with the

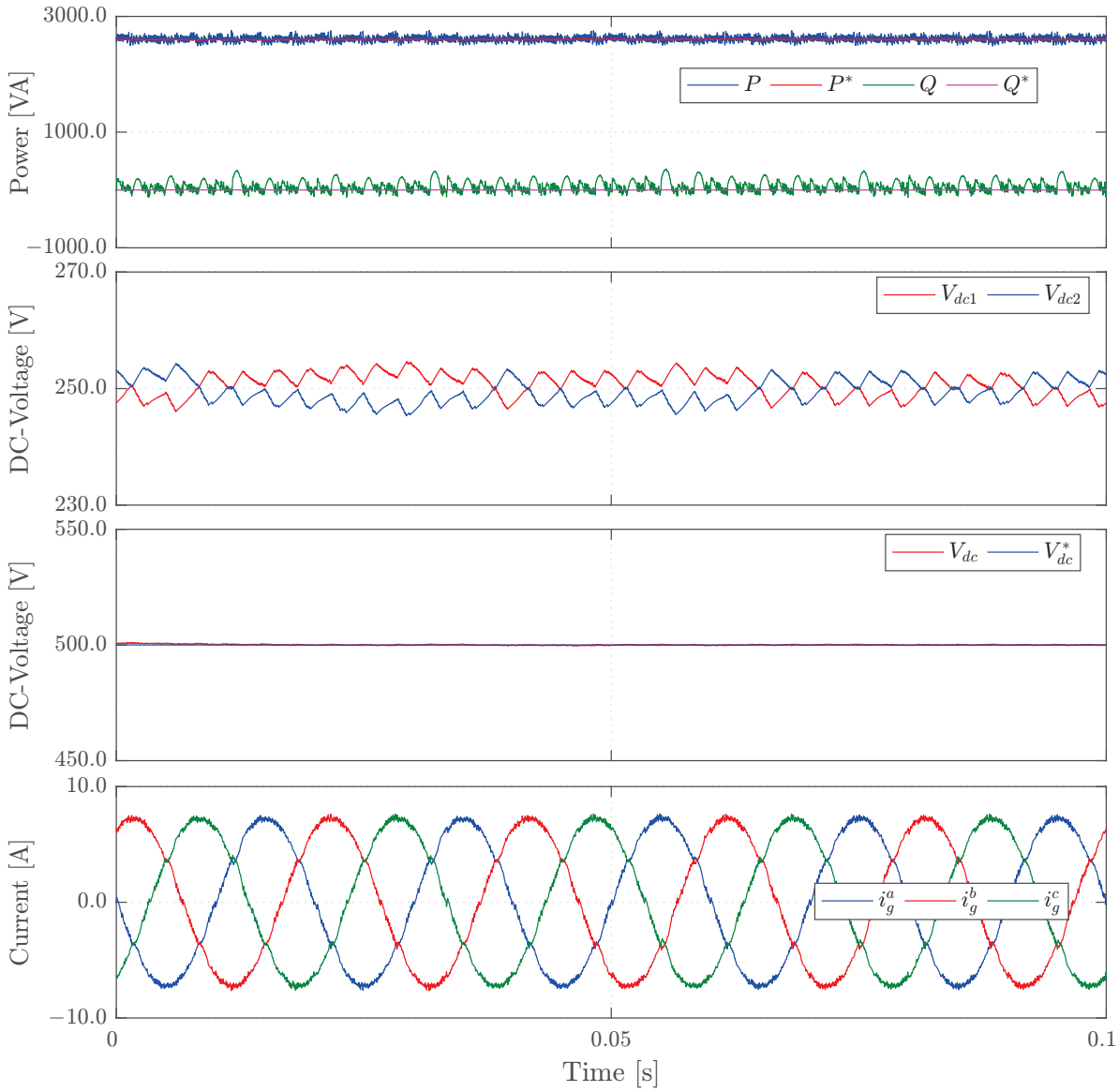

Figure 4.6: Steady-state results of conventional LUT-DPC for 3L NPC-AFE

conventional LUT-DPC technique). The results prove that active and reactive control are independent of each other (the same with conventional LUT-DPC technique). As we can note that the active power has some peak values due to applying three voltage vector in each odd sector instead one vector. However, the improved LUT-DPC technique gives good dynamic performance in comparison to the conventional LUT-DPC strategy.

4.5.4.2 Performance evaluation of new look-up table

The comparison results of new LUT-DPC technique with conventional LUT-DPC will be discussed in this subsection. The Figure 4.11, Figure 4.12, Figure 4.9 and Figure 4.10 show respectively steady and overall state performance

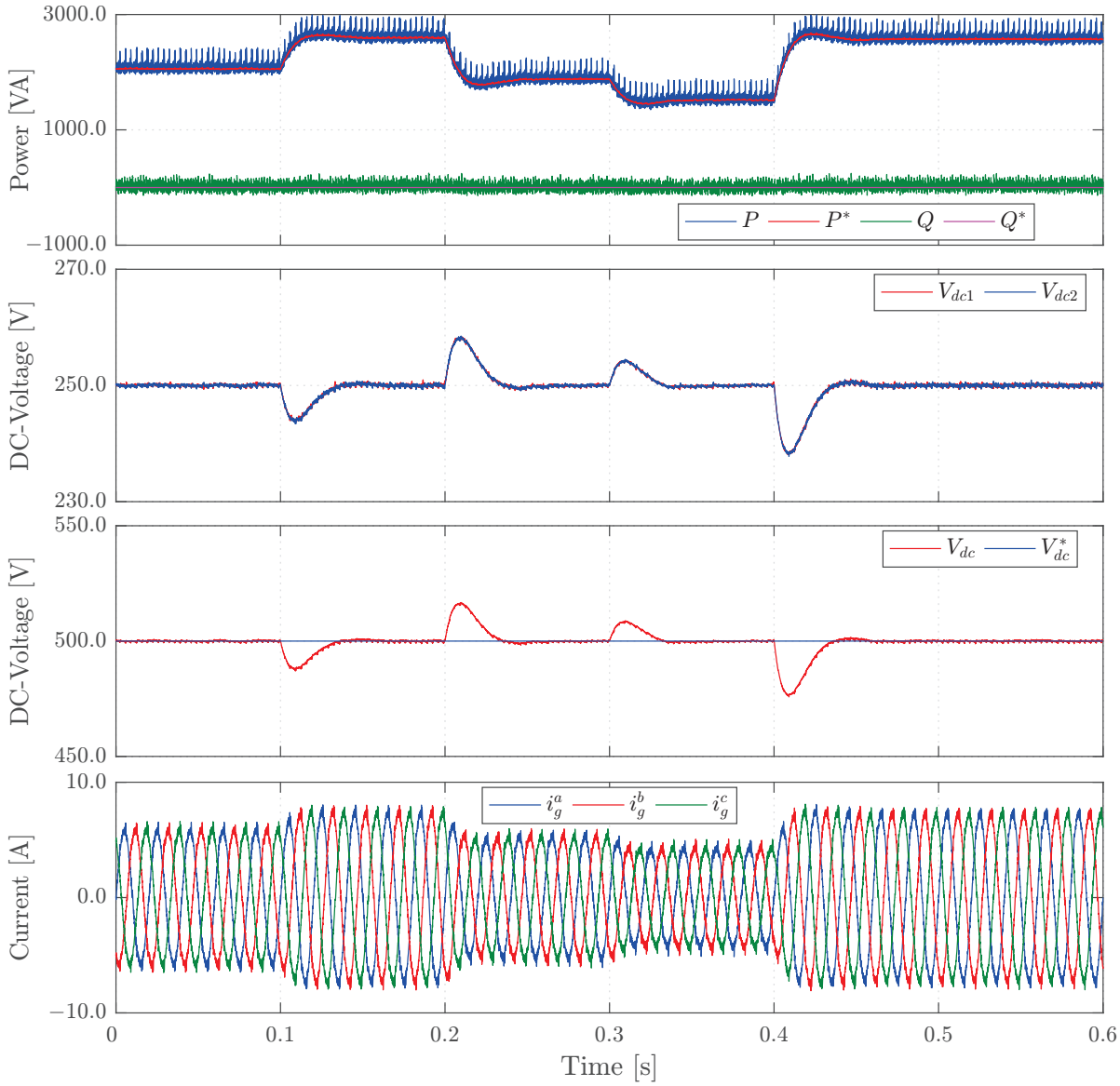

Figure 4.7: Overall results of improved LUT-DPC for 3L NPC-AFE

of conventional LUT-DPC technique and proposed LUT-DPC technique with new switching table.

❣ Steady steady performance

From the data in the Figure 4.12, it apparent that using the conventional LUT-DPC strategy causes some inherent problems, which are poor regulation of reactive power, no-sinusoidal input currents with little high THD and depressed power factor. Turning now into the simulation results of the system with the new LUT-DPC strategy (see. Figure 4.11), it can be seen from these figures that sinusoidal input currents with low THD, good regulation

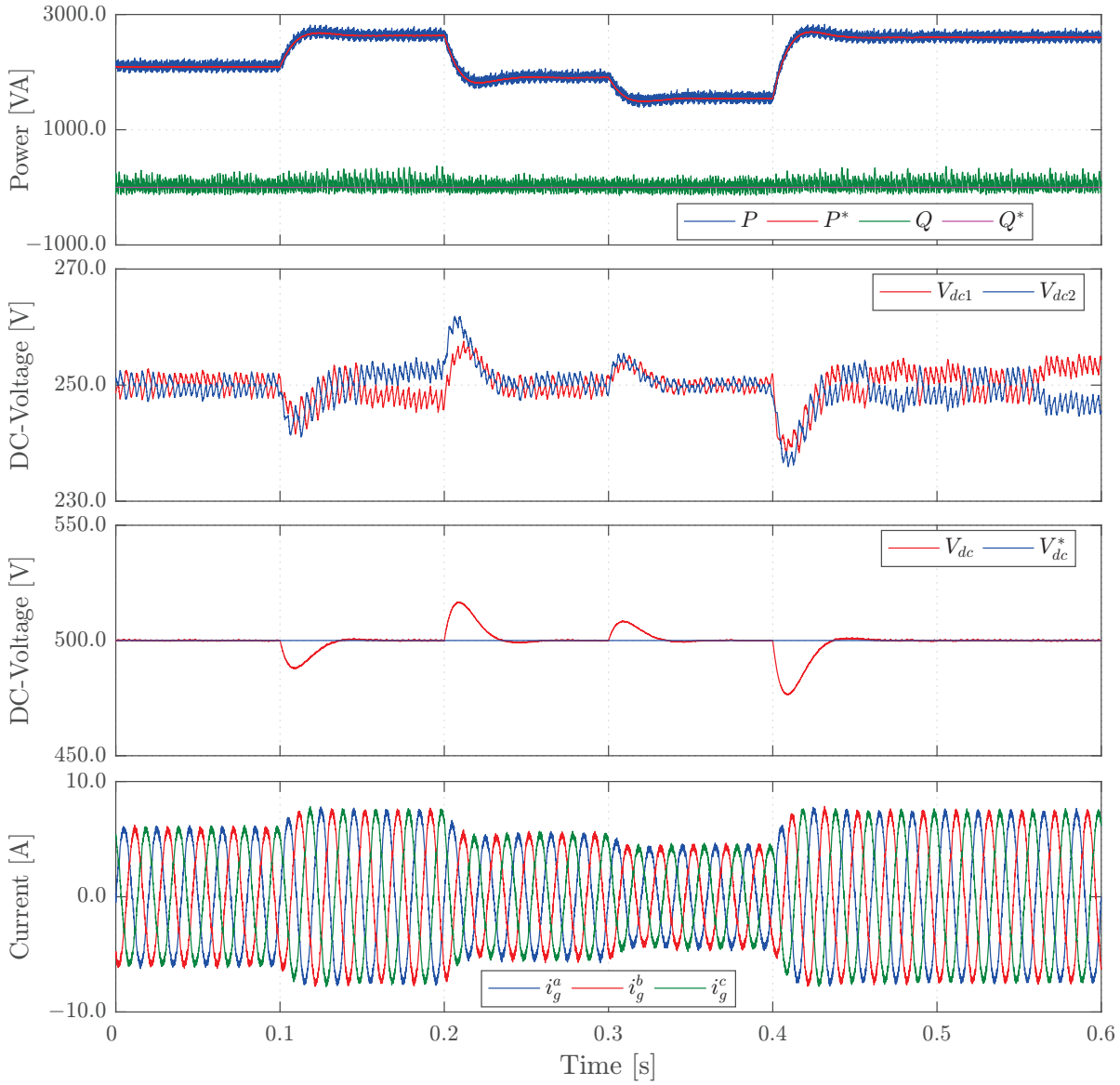

Figure 4.8: Overall results of conventional LUT-DPC for 3L NPC-AFE

of powers and high power factor are obtained with the new LUT-DPC strategy.

❣ **Transient-Steady Performance**

In this part, step changes in the R-load are applied to test and validate the effectiveness of the new LUT-DPC technique (see. Figure 4.9) and compared it with the conventional LUT-DPC strategy (see. Figure 4.10), the input currents are sinusoidal and its THD is lower (3.74%). The active power has some peak values due to the using of the three level hysteresis comparators and more switching voltage vectors are applied. However, the new LUT-DPC technique gives good dynamic performance in comparison to the conventional

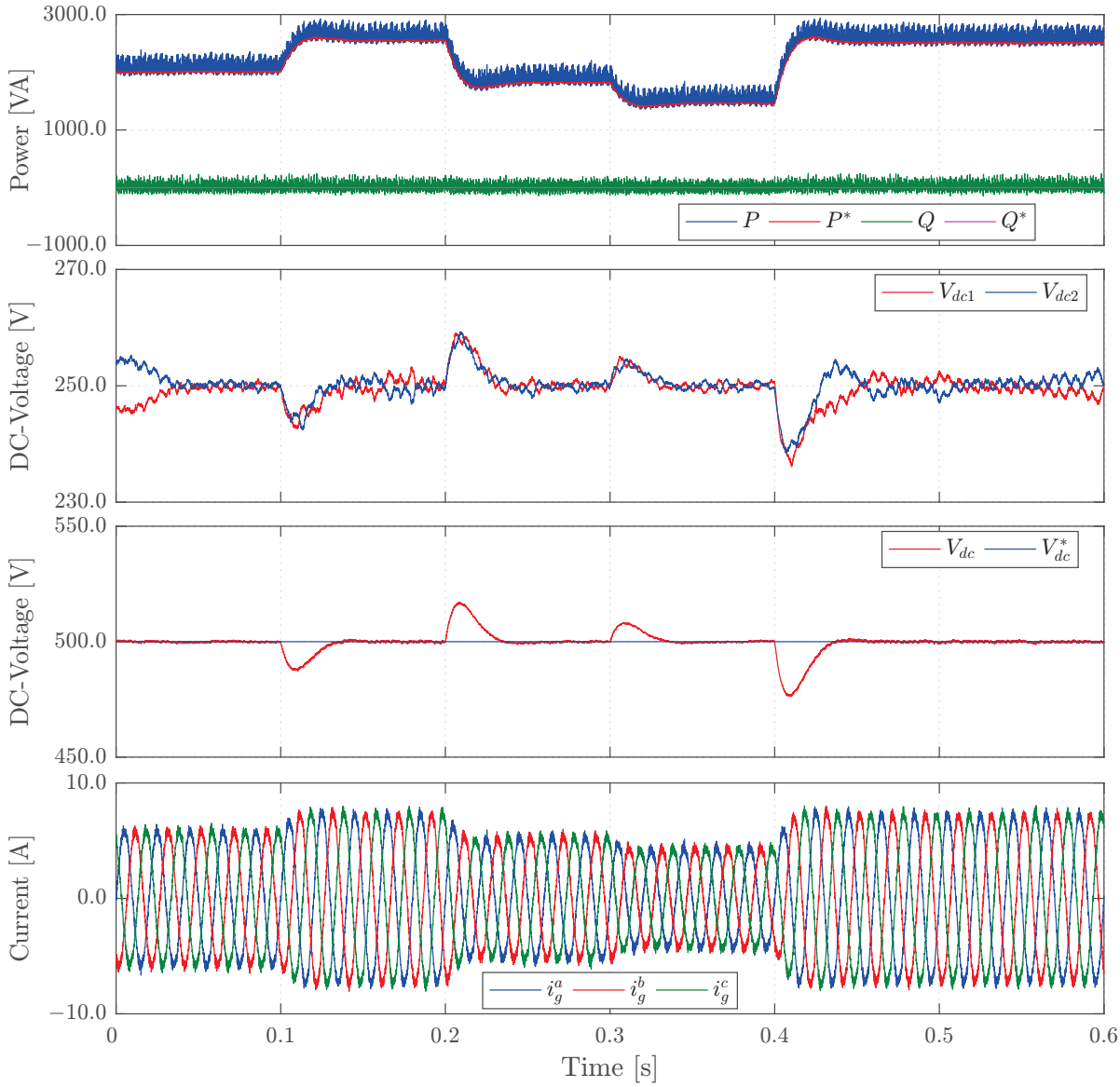

Figure 4.9: Overall results of new LUT-DPC for 3L NPC-AFE

LUT-DPC strategy.

4.5.4.3 Performance evaluation of proposed LUT-DPC under unbalanced grid voltage

The simulation evaluations of the proposed LUT-DPC under unbalanced grid voltage and other two conventional LUT-DPC strategies are performed. The grid voltage is unbalanced with an amplitude of the negative sequence grid voltage equal to 15%. The two utilized techniques are: 1) the conventional DPC (CDPC) method with the traditional definition of the active and reactive power, 2) the DPC scheme with the new definition of the reactive power (DPC-NQ) that presented in [66]. With the CDPC strategy, the control tar-

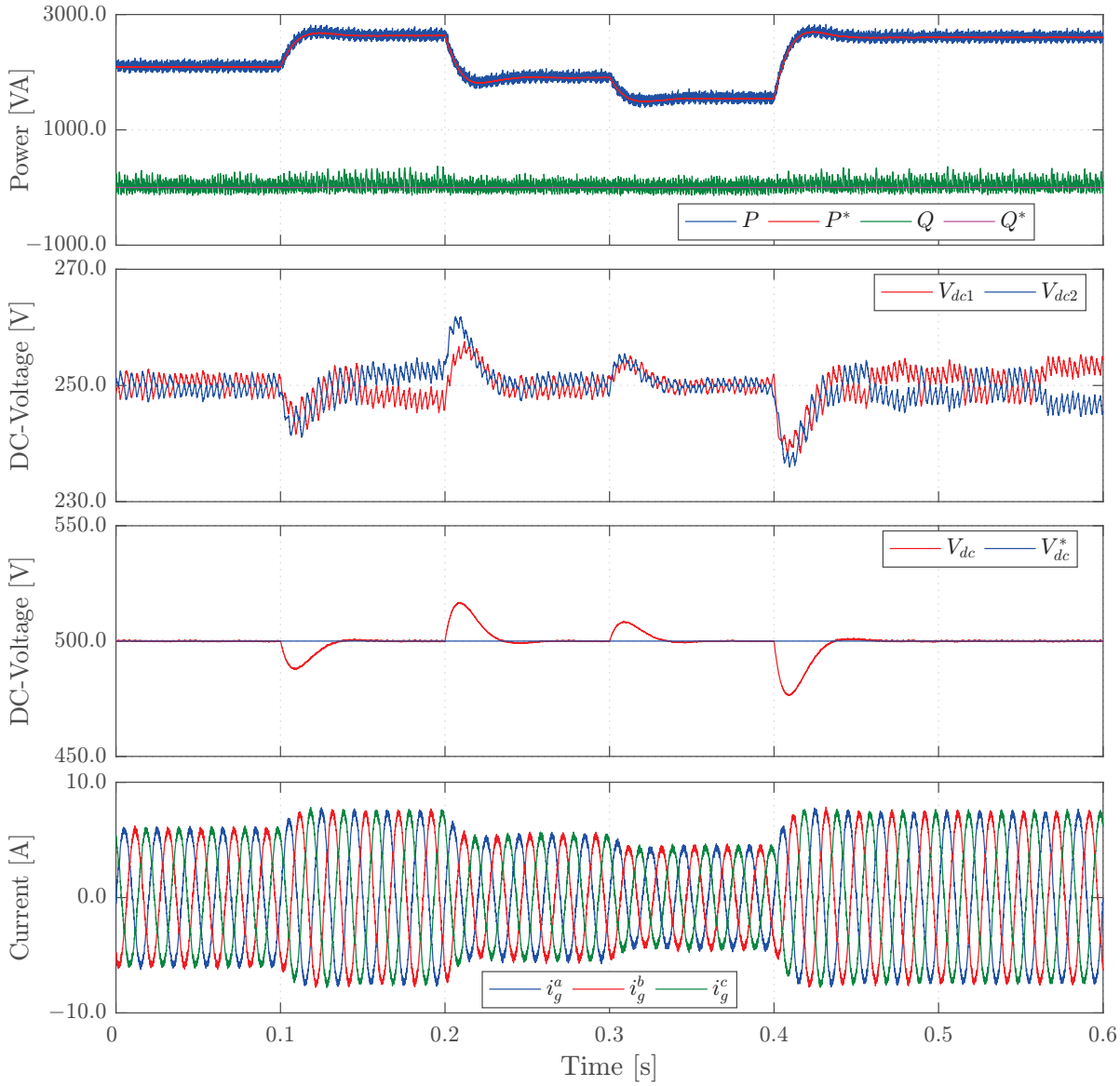

Figure 4.10: Overall results of conventional LUT-DPC for 3L NPC-AFE

gets are the conventional active power and conventional reactive power. With the DPC-NQ strategy, the control targets are the conventional active power and new reactive power. With the DPC-NP strategy, the control targets are the new active power and conventional reactive power.

❣ **Steady steady performance**

The simulation results of those three control schemes (i.e. CDPC, DPC-NQ, and proposed DPC-NP) under balanced and unbalanced grid voltages are shown in Figures 4.13, 4.14, and 4.15 . At the time instant $t = 0.1\,\mathrm{s}$, a 15%

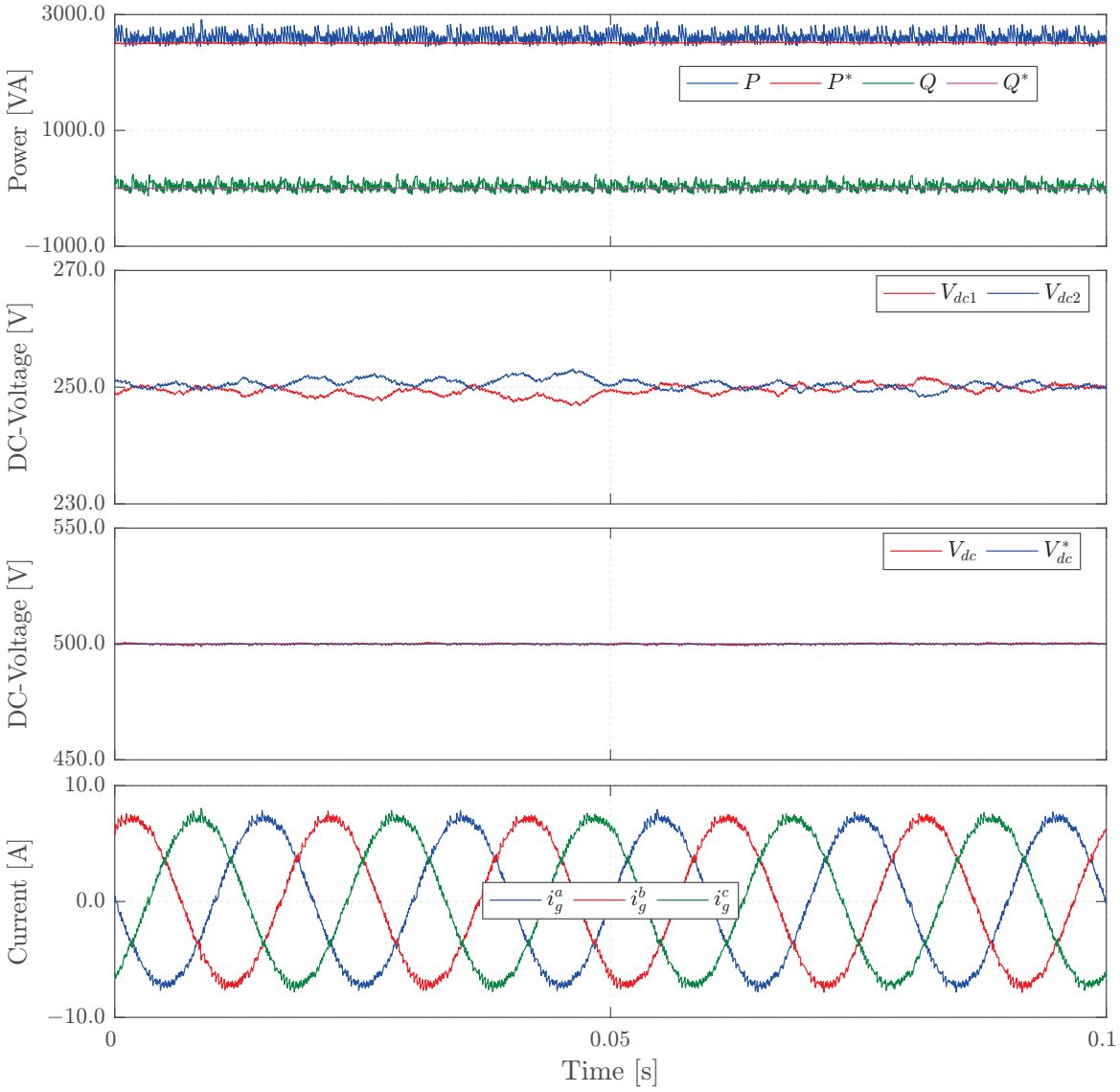

Figure 4.11: Steady-state results of new LUT-DPC for 3L NPC-AFE

negative-sequence voltage is imposed on the grid. The response of the CDPC scheme is illustrated in Figure 4.13, this figure shows that the grid currents are highly distorted when the grid voltages become unbalanced and the new active and new reactive power, computed according to the new definition, start to oscillate. The DC-link voltage U_{dc} tracks its reference value $U_{dc}^{*} = 500V$, with achieving the balancing of the upper and lower capacitors. The THD of the grid currents using the conventional DPC is 5.44%, see Figure 4.16.a. Following, regarding to the performance of the DPC-NQ (see Figure 4.14), the active power and the new reactive power are constant without oscillations and the grid currents are almost sinusoidal. The DC-link voltage U_{dc} follows its reference value $U_{dc}^{*} = 500V$, and the balancing of capacitor voltages U_{dc1} and U_{dc2} is fulfilled. The THD of the grid currents using DPC-NQ is 1.23%, see

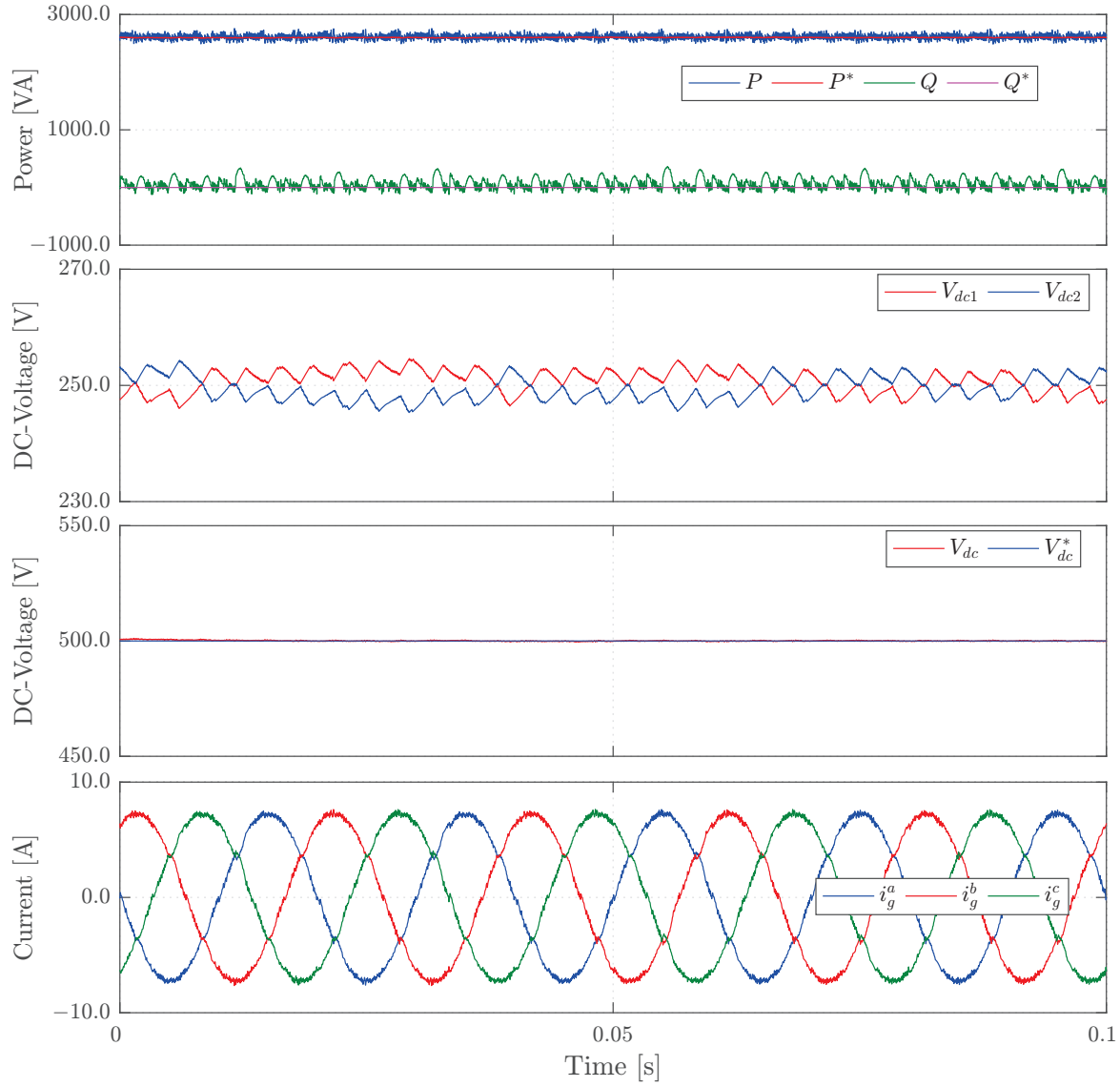

Figure 4.12: Steady-state results of conventional LUT-DPC for 3L NPC-AFE

Figure 4.16.b. Finally, Figure 4.15 shows the response of the proposed DPC-NP. It can be noticed that both the new active power and the reactive power are constant without any oscillations. Also, the tracking of the DC-bus voltage U_{dc} to its reference value $U^*_{dc} = 500V$ and the balancing of upper and lower capacitor voltages (i.e, U_{dc1} and U_{dc2}, respectively) are achieved. Additionally, the grid currents are almost sinusoidal and its THD is 1.14%, see Figure 4.16.c.

❣ Transient-Steady Performance

To further investigate the performance of the proposed DPC-NP under unbalanced grid voltage, a step change at the time instant $t = 0.1\,\mathrm{s}$ in the DC load R_L from $120\,\Omega$ to $89.36\,\Omega$. It can be seen from Figure 4.17 that the proposed

DPC-NP achieves good dynamic performance. Furthermore, the THD of the grid currents is low (0.99%), see Figure 4.20.a.

Furthermore, the following scenarios are set: a step change in the reactive power from 0 Var to 1000 Var at time instant $t = 0.1\,\mathrm{s}$ (see Figure 4.18). The result proves the good dynamic performance of DPC-NP (the input current is almost sinusoidal with THD equal to 1.17%, see Figure 4.20.b) and both new active power and reactive power follow respectively their reference values.

At the end, 20% negative sequence voltage is utilized at the time instant $t = 0.1\,\mathrm{s}$. From Figure 4.19, we can see that: the performance of the proposed DPC-NP is still good. Only, very small oscillations in the new active power appeared. However, the input current waveforms are almost sinusoidal with a THD of 1.07%, see Figure 4.20.c.

As a conclusions, the proposed LUT-DPC under unbalanced grid voltage is investigated to solve the drawbacks of the conventional direct power control (CDPC) while the grid voltage is unbalanced. Therefore, a new definition of active power based on the extend *pq* theory is proposed, and discussed in detail. With the new definition of active power and based on theory of the instantaneous power, a novel table-based DPC suitable to operate a 3L NPC-AFE under unbalanced grid voltage condition is proposed, the construction process of new switching table is also discussed. The new switching table is suitable in both cases of balanced and unbalanced grid voltage. A comparison simulation results between three control schemes are done. The three control schemes are: CDPC, the proposed DPC-NP, and DPC scheme with new definition of reactive power (DPC-NQ). The results have validated that the proposed DPC-NP considerably outperformed the CDPC and DPC-NQ methods, in terms of better dynamic and steady-state performance. Furthermore, the waveforms of the grid side currents are almost sinusoidal with very low THDs under both balanced and/or unbalanced grid voltages. The following comments represent the important features of the proposed DPC-NP strategy under unbalanced grid voltage.

1) No need to the extraction of the positive and/or negative components of grid voltage and current to achieve a sinusoidal input currents with low total harmonic distortion (THD).

2) No need to the extraction of the positive and/or negative components of grid voltage and current to achieve smooth active and reactive power waveforms.

3) Its model is much simpler than the improved methods that proposed to solve the drawbacks of the conventional DPC (CDPC) under unbalanced grid voltage.

4) Compared to DPC scheme with new definition of reactive power (DPC-NQ), the proposed DPC-NP strategy shows good performance with very low THDs of input currents under different step changes in the DC-bus load, reactive power reference and grid voltage unbalanced value.

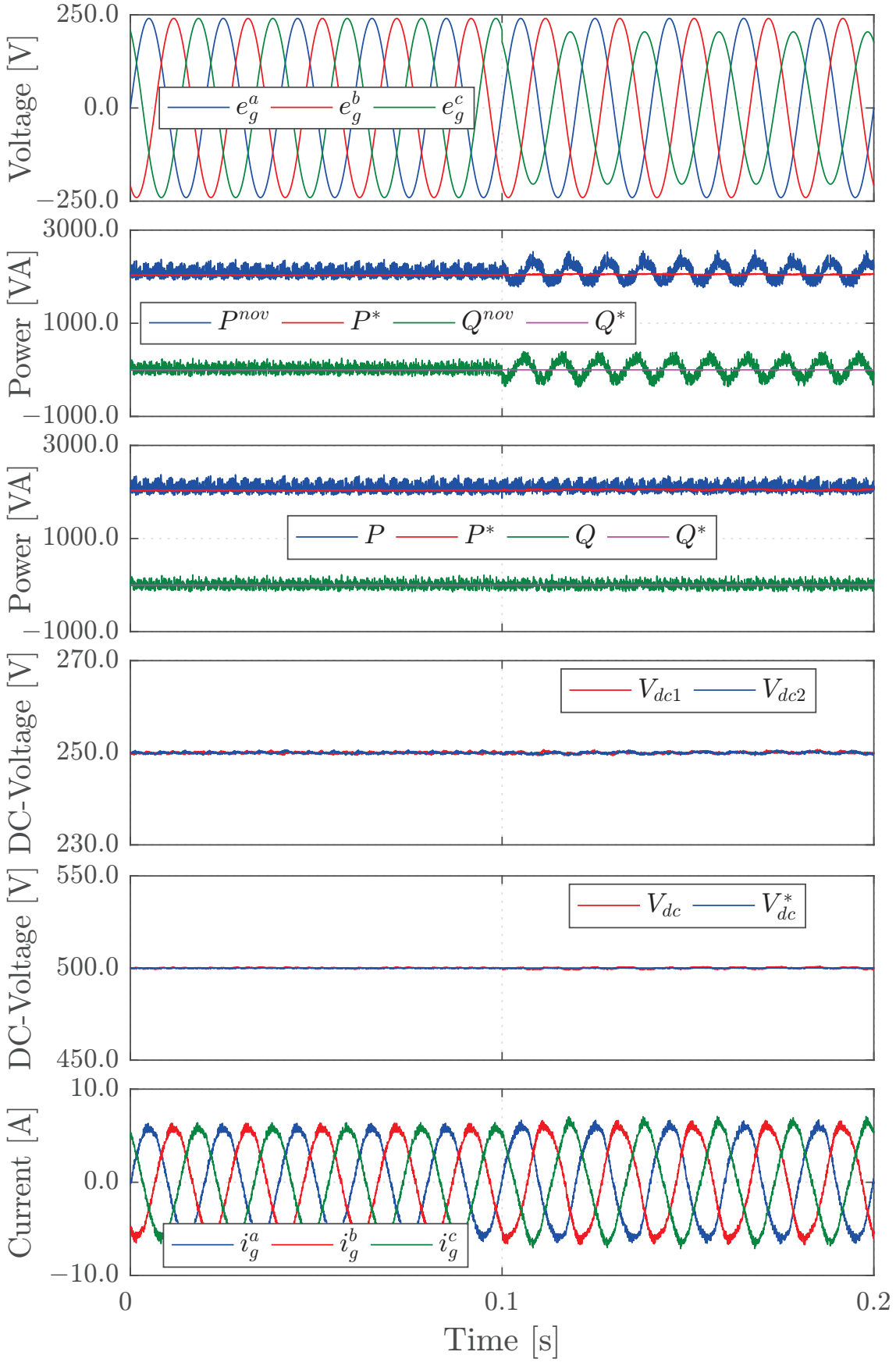

Figure 4.13: Simulation results of the CDPC strategy under balanced and unbalanced grid voltages

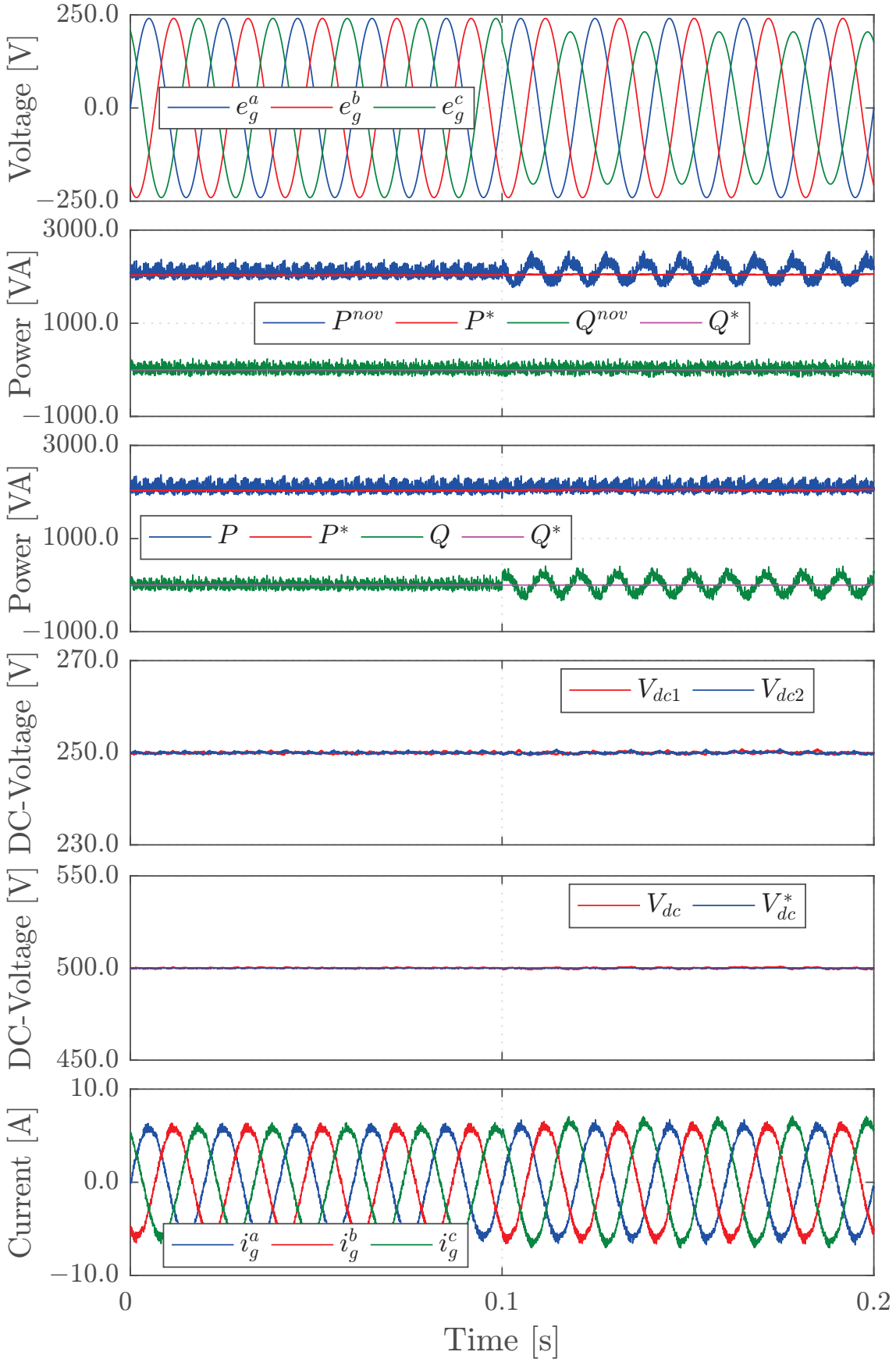

Figure 4.14: Simulation results of the DPC-NQ strategy under balanced and unbalanced grid voltages

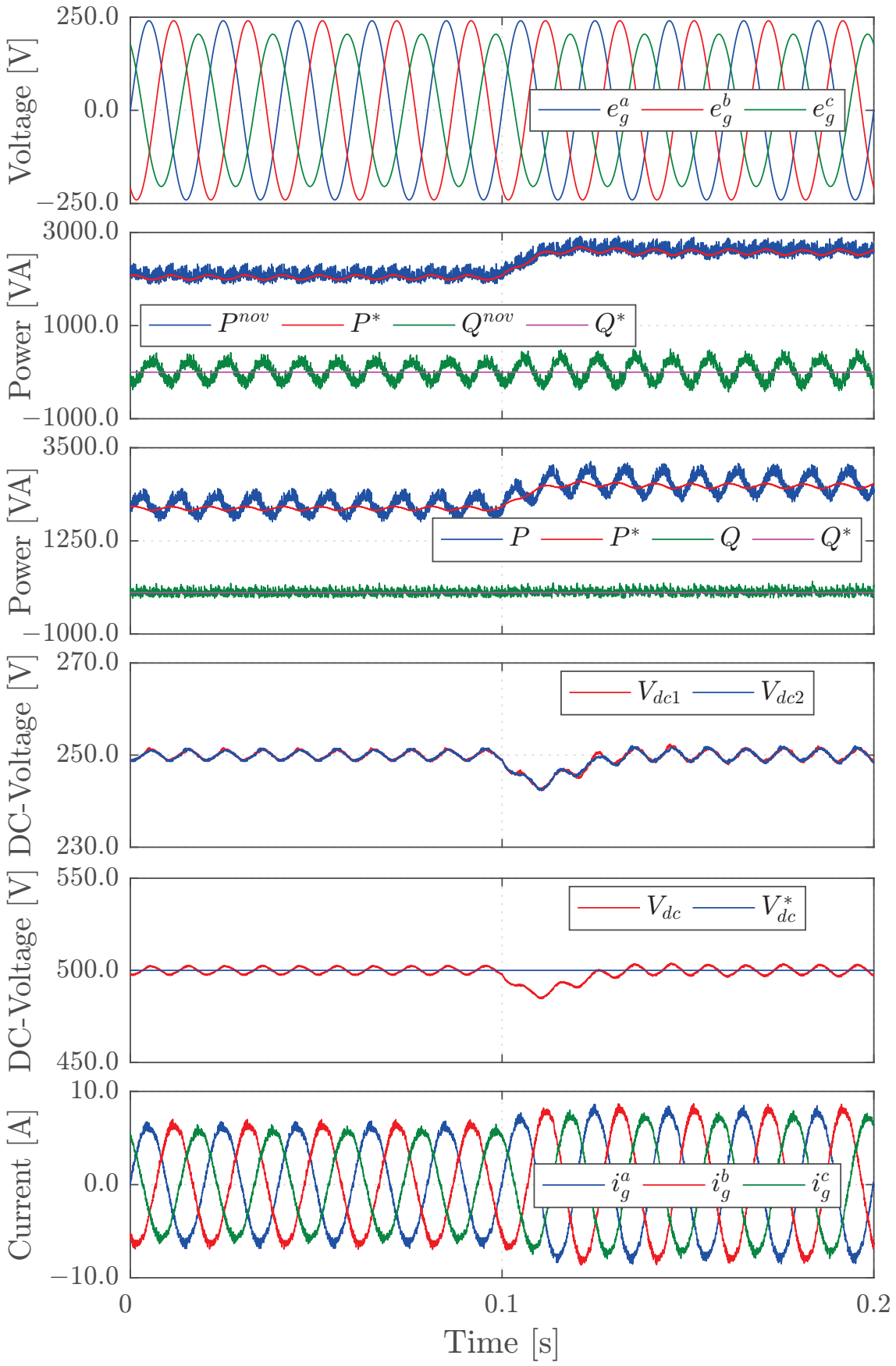

Figure 4.15: Simulation results of the DPC-NP strategy under balanced and unbalanced grid voltages

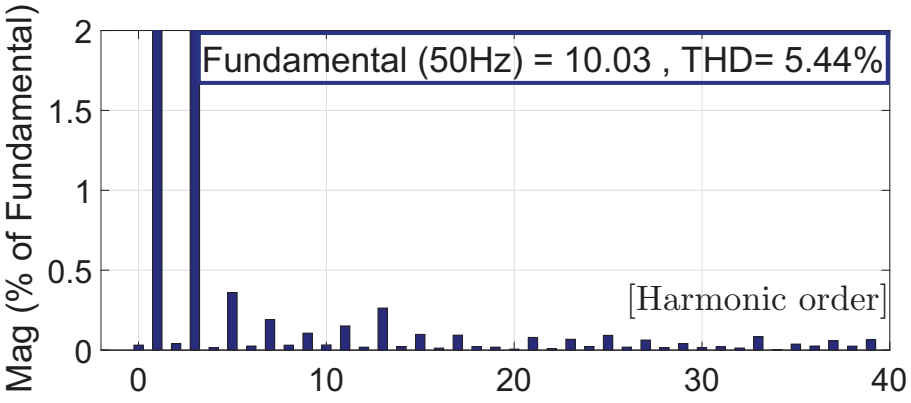

(a) CDPC strategy.

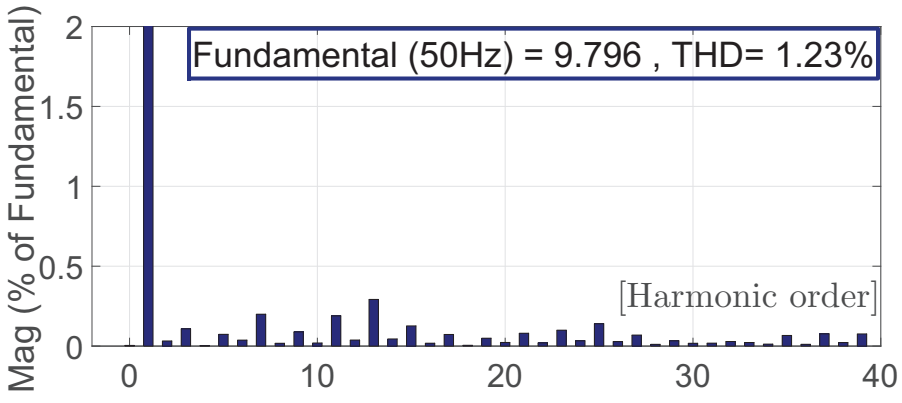

(b) DPC-NQ strategy.

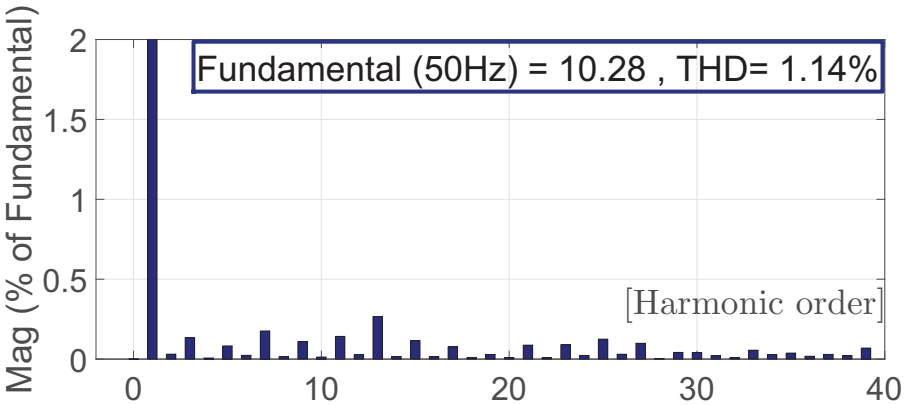

(c) DPC-NP strategy.

Figure 4.16: Harmonic spectrum and THD of input currents for three-level NPC rectifier, with the aforementioned control methods.

Absolutely, the proposed DPC-NP strategy is also attractive for three phase PWM converter applications, and it can be applied into wind converter systems.

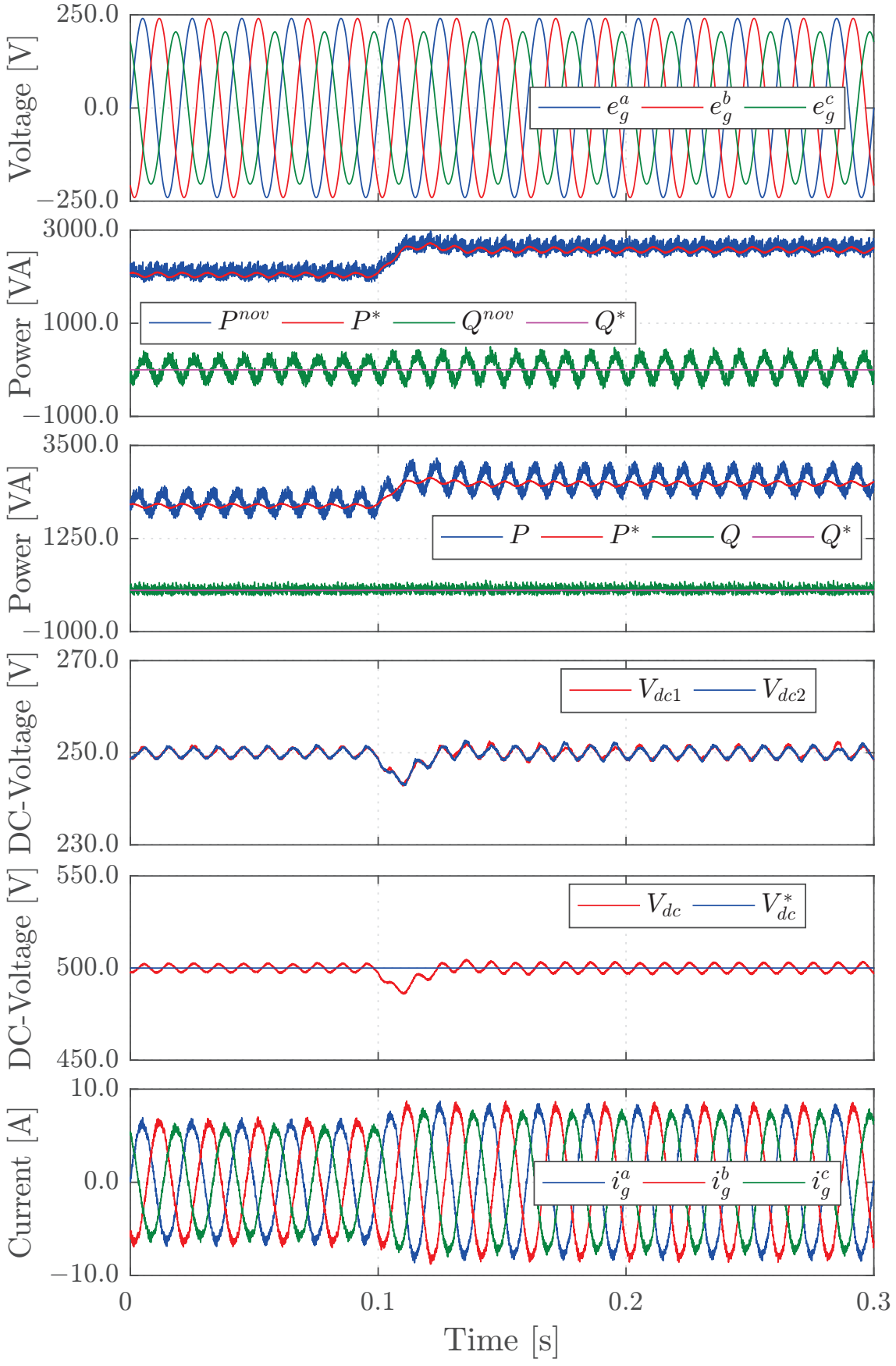

Figure 4.17: Simulation results of the DPC-NP strategy under step change in the DC Load RL

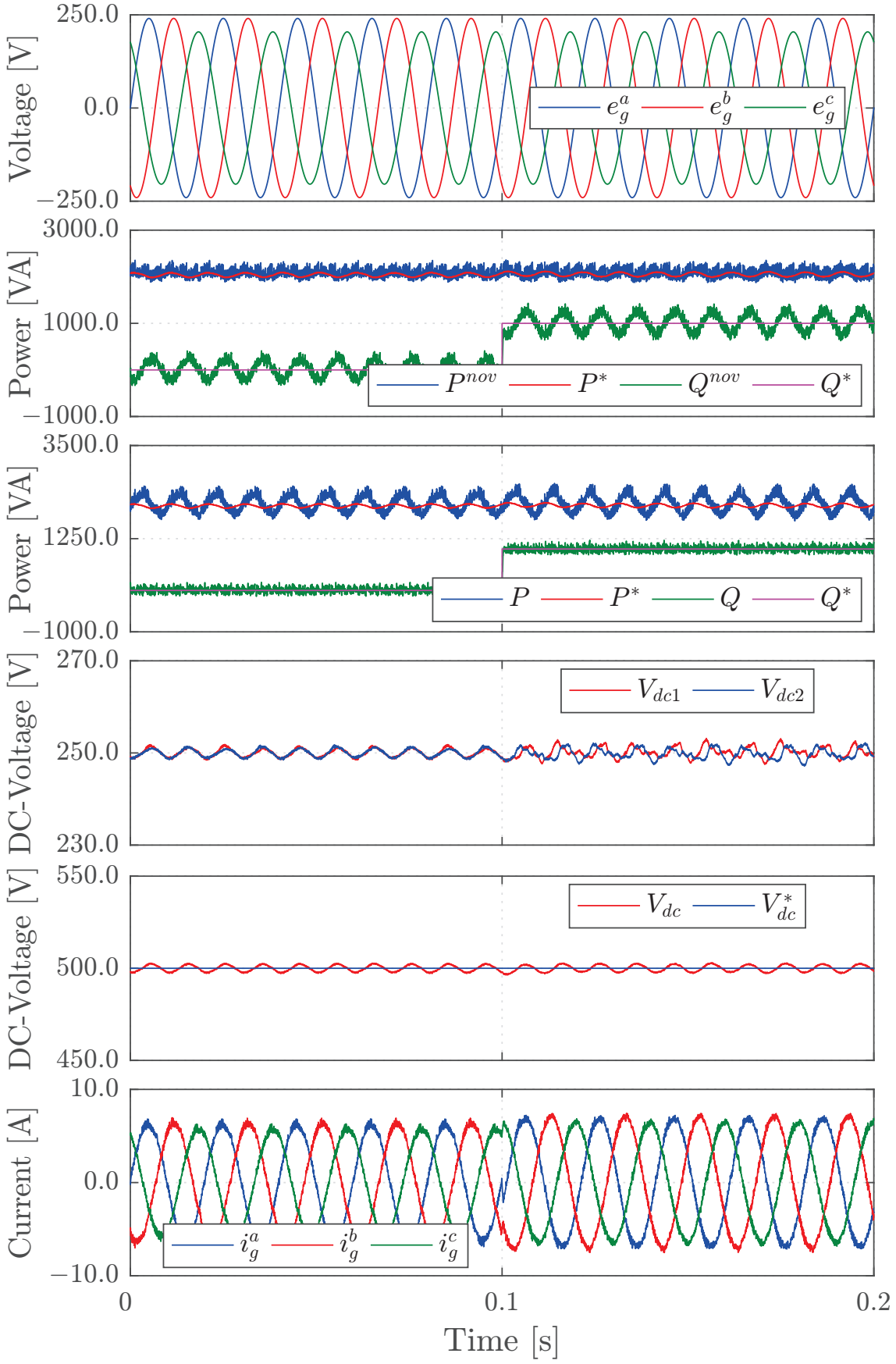

Figure 4.18: Simulation results of the DPC-NP strategy under step change in the reactive power reference

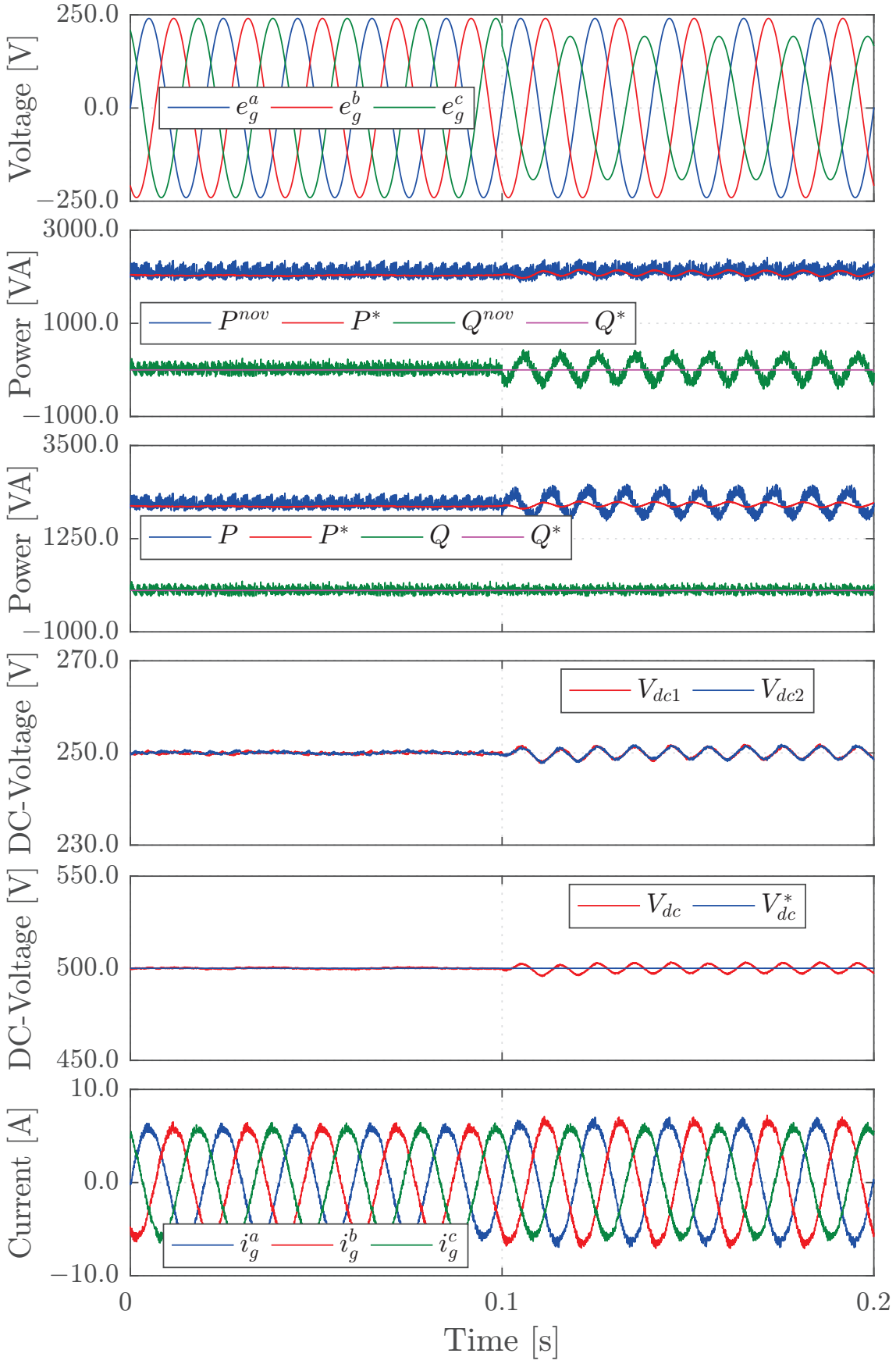

Figure 4.19: Simulation results of the DPC-NP strategy under step change in the value of grid unbalanced

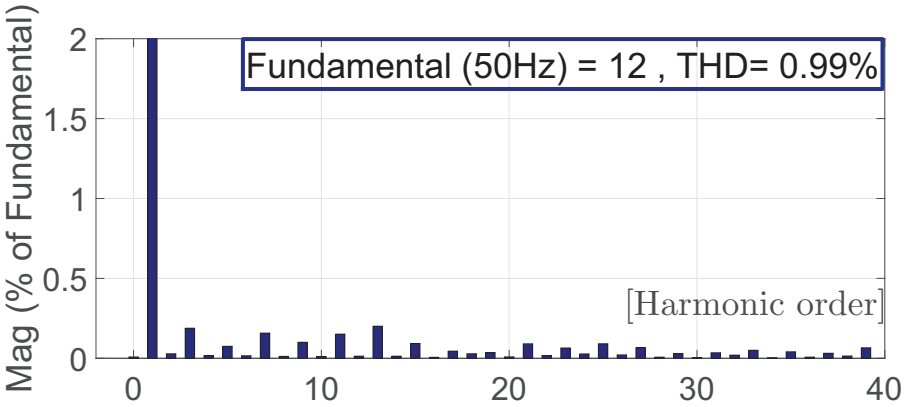

(a) DPC-NP under step change in the DC load R_L.

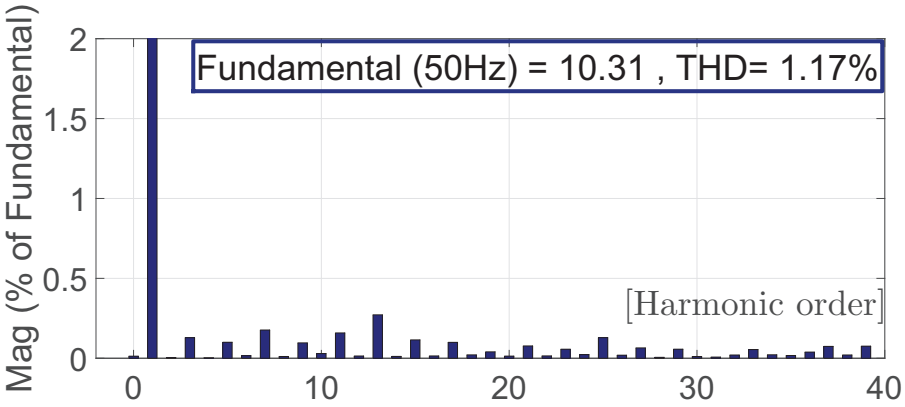

(b) DPC-NP under step change in the reactive power reference.

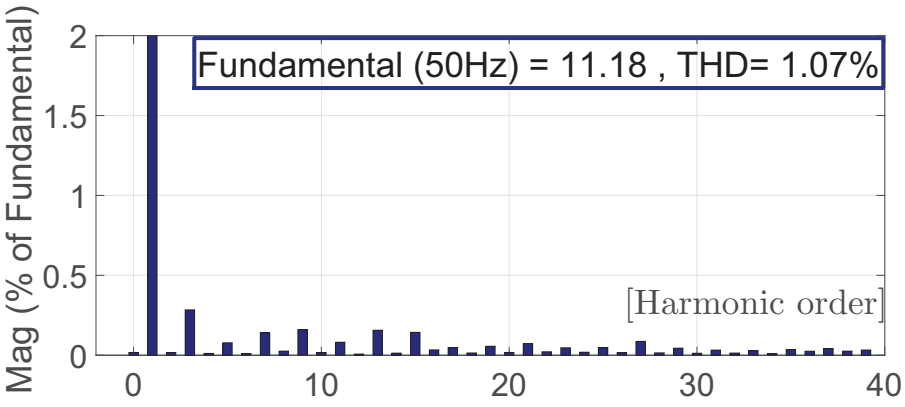

(c) DPC-NP under step change in the value of unbalanced grid

Figure 4.20: Harmonic spectrum and THD of input currents for three-level NPC rectifier, with the aforementioned control methods.

CHAPTER 5

Advanced Model Predictive Direct Power Control

With the evolution of DSPs, the application of predictive control in power electronics increases significantly in the last years. One of the model-based predictive control strategies is finte control-set model predictive control (FCS-MPC) or named also direct model predictive control (DMPC), which is analyzed and formulated in this chapter. In section 5.1, the overview of predictive control methods for power converters is summarized. Then, the operation principle and design procedure of MPC is explained. After that, a new section 5.3 about FCS-MPC is presented, including the explication of its operation principle and design procedure 5.3.1. Finally, the performance evaluation of FCS-MPC in implementation are formulated and discussed in section 5.4.

5.1 Overview of Predictive Control Methods for Power Converters

In rather recent application of control strategy in power converters, the predictive control has attracted wide attention. Many different predictive control techniques are excited in the literature and can be classified as shown in Figure 5.1, see [34].
The principle of model predictive control is based on using the system model to predict the future behavior of the controlled variables, and the controller uses this information to obtain the optimal action, according to a predefined optimization criterion.
Hysteresis based predictive control keeps the controlled variables within the boundaries of a hysteresis area [69]. In the trajectory-based control, the aims

is to force the controlled variables to follow a predefined trajectory [70]. With the deadbeat control, the predictive controllers are used instead of the PI regulators in aim to force the tracking error equal to zero in the next sampling instant by the optimal actuation [71,72]. The model predictive control (MPC) has a more flexible criterion, which is expressed in a cost function and try to make its value smaller [73].
The system operates under constant switching frequency with deadbeat control and MPC with continuous control set, which are using a modulator to generate the required voltage, and under variable switching frequency with the other controller, which are generating directly the switching signals for the converter.
Simple concepts and intuitive is the basic feature of model predictive control (MPC). Simple implementation is possible with some predictive control type (i.e., deadbeat control (just with its standard basic) and finite control set MPC for two level converter with horizon N=1), and its more complex with continuous control set. Very fast transient response can be assured by predictive control in a linear control scheme, due to no required of the cascaded structure in this case.
Including nonlinearities and restrictions on varying the design of the controllers by add some restrictions are possible. Notes that the nonlinearities lead to improve the operation of the system for all conditions. Finally, in Figure 5.1, the advantages and disadvantages of each predictive control methods are included.

5.2 Overview of operation principle and design procedure of MPC

In order to make the technique easy to understand and to implement, a step-by-step implementation is summarized as follow:

❣ Generations of the references and Measurement of the signals

All the signals required by the predictive model should be measured, included the references that should be generated depending on the application.

❣ Extrapolation of references

The main principle of FCS-MPC is selecting the best switching state, which is able to minimize the reference tracking error in the future instant and applied directly to the power converter. The extrapolation is required when the sampling time T_s is big or equal to 20 μs, that means that the fundamental frequency of the variables to be controlled is much high than the sampling frequency. To assure an effectively minimization of the tracking error, the references should be extrapolated to one or two steps time in the future (i.e, k+1 or k+2, respectively). As an exception case, no extrapolation in steady-state

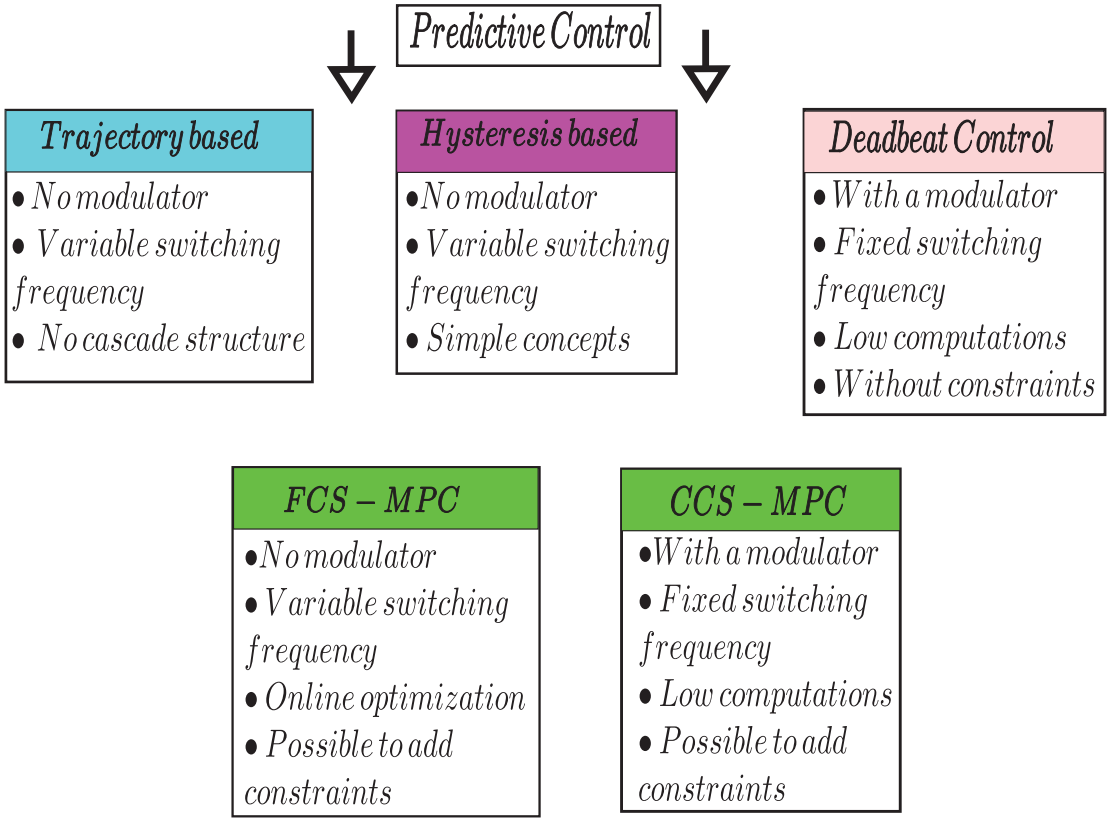

Figure 5.1: Classification of Model Predictive Control (MPC)

operation with dq frame, because the variable in dq frame are dc in nature. Another reason of using the extrapolation is the existence of a delay between the reference and variables to be controlled in the transient operation.
Several methods of extrapolation are excited in the literature [27,72]. A third-order Lagrange method uses present and two past sample values of the variable to be extrapolated [27,72,74–77]. A higher-order extrapolation method is used to increase the performance of FCS-MPC strategy [74–77]. The vector angle method is another approach for the extrapolation [27], the principle of this method is based on consideration of the change in vector angle of the three-phase variables as the basis for extrapolation, this method is suitable for the stationary frame ($\alpha\beta$) variables [78], and cannot be used in single-phase systems [27].

❣ Continuous and discrete-Time models' development

First of all, the power converter continuous-time is assumed in nature of first-order. That means,

$$\frac{dx}{dt} = Ax + Bu \tag{5.1}$$

where x denotes the controlled variables, which can be current, voltage, power, torque, flux, losses, common-mode voltage, total harmonic distortion (THD), etc. A and B represent the parameters of the systems, which can be dc-link capacitance, inductance of the filter, load resistance, etc, and u denotes the input variable (grid voltage, grid currents, dc-voltage, etc.).
After that, some predictive control methods are similar to an optimization algorithm, and the discrete-time models of continuous-time models are necessary to implement the strategy in digital control platforms. Many discretization methods excite in the literature, these methods are, impulse-invariant, zero-order hold, backward difference, forward difference, bi-linear transformations, which is combination between two methods: forward and backward difference [79]. The forward or backward Euler methods are the suitable method and can provide a first-order approximation for the derivation, due to first-order nature of the model equation in 2.10. In this work, Euler-forward method is choose to be used, due to its simplicity, accurate approximations and can be used for a small sampling interval ($T_s \leq 100\ \mu s$). The comparison between advantages and disadvantages of backward and forward Euler method can be found in [8]. The forward Euler method can be described in this equation as follow,

$$\frac{dx}{dt} = \frac{x_{[k+1]} - x_{[k]}}{T_s} \tag{5.2}$$

where x(k+1) and x(k) represent the future values of variable x at the future sample (k+1) and present sample (k), respectively.

❣ Prediction of variables

Based on the equation 5.2 of forward Euler method, the future behavior of the control variables can be predicted. A one-step prediction horizon [8] is used in the principle of the predictive control. The number of predictions for the controlled variables is equal to the number of possible switching states. The advantage of observing the future of variable is exist only in MPC, compared to classical control techniques.

❣ Cost function minimization

The cost function represents the control objectives which forces the variables to follow the references. Absolute or quadratic value of the error is commonly employed in oder to obtain the minimum value of the cost function. Depending on the required tracking error, the selecting between quadratic or absolute method can be done. The quadratic function is better when a close tracking is required. The use of constrains in MPC is very intuitive, and is applied by comparing the variable with the limit value using a logic function, and the result is multiplied by a very high weighting factor. Thus, this term has a zero value, if the variable is inside the allowed region, and it has a very high value in the opposite case [3]. The calculation of weighting

factor still one of the challenges of model predictive control, no analytical or numerical formulas are available for the calculation of weighting factor values in the literature. However, the guidelines given in [80] can be used. Two or more objectives can be achieved simultaneously by combined in a sum of error terms. When the variables have the same nature, a normalization is not required in the combination of these variables, the variables in this case can be active and reactive power, and current. In the case of variable with different nature, a normalization is required, the variables in this case can be magnetic flux and torque, or voltages and currents. To give relative importance to one term or another, a weighting factor is multiplied by this term.

$$g_k = x^*_{[k+1]} - x^p_{[k+1]} \tag{5.3}$$

where $x_{[k+1]}{}^p$ and $x^*_{[k+1]}$ are the predictive value and predictive reference value of controlled variables at the sample time (k+1), respectively.
The switching state which minimizes the cost function is chosen and then applied at the next sampling instant.

5.3 Finite-set model predictive control

One of the model predictive control (MPC) that has been applied to power converter and has attracted wide attention is finite control-set model predictive control (FCS-MPC), due to its features compared to the classical control strategies. These features [8, 27] are summarized as follow
• Its concepts is simple and easy to understand
• The inherent discrete nature of the power converter is used
• Treats the power converter as a discontinuous and nonlinear model which is the closest approximation to real-time scenario
• Possible to be applied in a wide variety of systems
• The finite number of switching state makes the optimization greatly simplified
• Possibility to compensate the dead times and system perturbations
• Able to handle multivariable control programs in a decoupled manner
• The fulfillment of many technical and control requirement at the same time is possible
• This methodology opens the door to include modifications and extensions according to specific applications
• System nonlinearities and limitations can be incorporated in a straight forward manner in the model
• Constraint handling is naturally accommodated by the method
• An intuitive approach for real-time implementation

The controller is designed to control a desired plant. Thus, it is very important to know the nature and behavior of the plant to be controlled, that makes the design of the controller easy. In this work, the plant to be controlled is

a power electronic converter, and its properties, constraints and requirements are [8, 27, 73]:
• Nonlinear nature (specifically during low switching frequency)
• Finite number of switching states (27 switching states with 3L NPC-AFE)
• Safe and reliable operation required restrictions on maximum current, switching frequency, and THD, etc
• Electric control variables should have faster response
• Favors discrete-time implementation using the industry standard digital control platforms
• Forbidden switching states, voltage balance issues, and mitigation of resonances, etc, are other restrictions and constraints for some converter topology

The operating principle and design procedure of FCS-MPC are discussed in the following step. After that, the evaluation performance of this technique in implementation is included in section 5.4.

5.3.1 Operating principle and design procedure of FCS-MPC

The problem of power converter control can be defined in the term of determination of the gate signals that will drive a generic system variable x(t) as close as possible to a desired reference value $x^*(t)$ [80]. With a finite number of control actions n and over a sample period T_s, and consider the actions of measurements, computations and control are performed in ideal case (no dealy). Thus, the evaluation of the measured value $x(t_k)$ is possible together, based on a prediction function f_p, to predict all the possible system transitions $x_{pi}(t_{k+1})$=$f_p x(t_k); S_i$, where $i = 1, ..., n$ and S_i is the control action. The cost function is formulated from variables to be controlled and the reference values at the sample instant (k+1), but due to small value of T_s, the reference value is considered to be constant over T_s. The evaluation of the cost function with the n predictions (27 with 3L NPC-AFE) lead to n different costs, and the switching vector leading to the minimum cost function ($min\{g_i\}$, for $i = 1, ..., n$) is selected as suitable gate signal of the converter.
The control targets for FCS-MPC in this work are active power, reactive power and DC-link voltage. The continuous and discrete-time model of active and reactive power are already determined in equations 2.19 and 2.22, respectively. Also, the predictive values of active and reactive power at the time sample (k+1) are formulated in equations 2.23. The continuous model of DC-link voltage can be written as

$$\frac{dV_0}{dt} = \frac{1}{C} (i_g^{abc})^T |u^{abc}| \tag{5.4}$$

With the utilization of a discrete first-order approximation of (5.4), the discrete model of the DC-link voltage is obtained as

$$\frac{V_{0[k+1]} - V_{0[k]}}{T_s} = \frac{1}{C} \left(i_{g[k]}^{abc}\right)^T \left|u_g[k]^{abc}\right| \tag{5.5}$$

Based on equation 5.5, the predictive value of DC-link voltage at the sample instant (k+1) can be written as

$$V_{0[k+1]} = V_{0[k]} + \frac{T_s}{C} \left(i_{g[k]}^{abc}\right)^T \left|u_g[k]^{abc}\right| \tag{5.6}$$

In this way, to assure that the predicted values of each of active power ($P_{[k+1]}$), reactive power ($Q_{[k+1]}$) and DC-link voltage difference ($V_{o[k+1]}$) keep tracking of their reference values (i.e., active power, reactive power and DC-link voltage difference, respectively). The cost function is formulated to achieve these control targets as [8]:

$$g(\vec{u_g})_{PDPC} = \overbrace{\gamma_P \left|P^* - P(\vec{u_g})_{[k+1]}\right|}^{\text{For controlling the active power}} + \overbrace{\gamma_Q \left|Q^* - Q(\vec{u_g})_{[k+1]}\right|}^{\text{For controlling the reactive power}} + \underbrace{\gamma_{V_o} \left|V_o^* - V_o(\vec{u_g})_{[k+1]}\right|}_{\text{For controlling the neutral point voltage}} \tag{5.7}$$

Where γ_P, γ_Q and γ_{V_o} are the weight factors of active power, reactive power and DC-link voltage difference, respectively.
Figure 5.2 shows the scheme of Finite-Set Control Model Predictive Control for the 3L NPC-AFE.

5.4 Performance evaluation of FCS-MPC

The performance of finite-control set direct power control (FCS-DPC) for 3L NPC-AFE and finite-control set direct torque control (FCS-DTC) for PMSM are evaluated experimentally by using the mentioned test-bench in 2.4. The experimental results are provided, no-comment about FCS-DTC will be provided in this part (this dissertation is focused on different control strategies of 3L-NPC rectifer). Some LabVIEW schemes of our global system are included (see Figure 5.5-5.7). The DC-link voltage reference fixed at 300 [V], the reactive power reference is set at 0 [Var] for unity power factor, 20 KHz is the value of the sampling frequency f_s. The DC-link capacitor C=1000.e^{-6}F, the load-side resistor R_L=10 Ohm, grid-side phase voltage $\vec{e}_g^{abc}$=120 V, Grid-side Reactor Resistor $R_g = 1.56\, e^{-3}\, Ohm$, Grid-side Reactor Inductance $L_g = 16\, e^{-3}\, H$.

The implementation results represent the overall and steady-state operation of FCS-DPC strategy, included the measured and reference values of active power, reactive power, DC-voltage of upper and lower capacitors, and grid current.

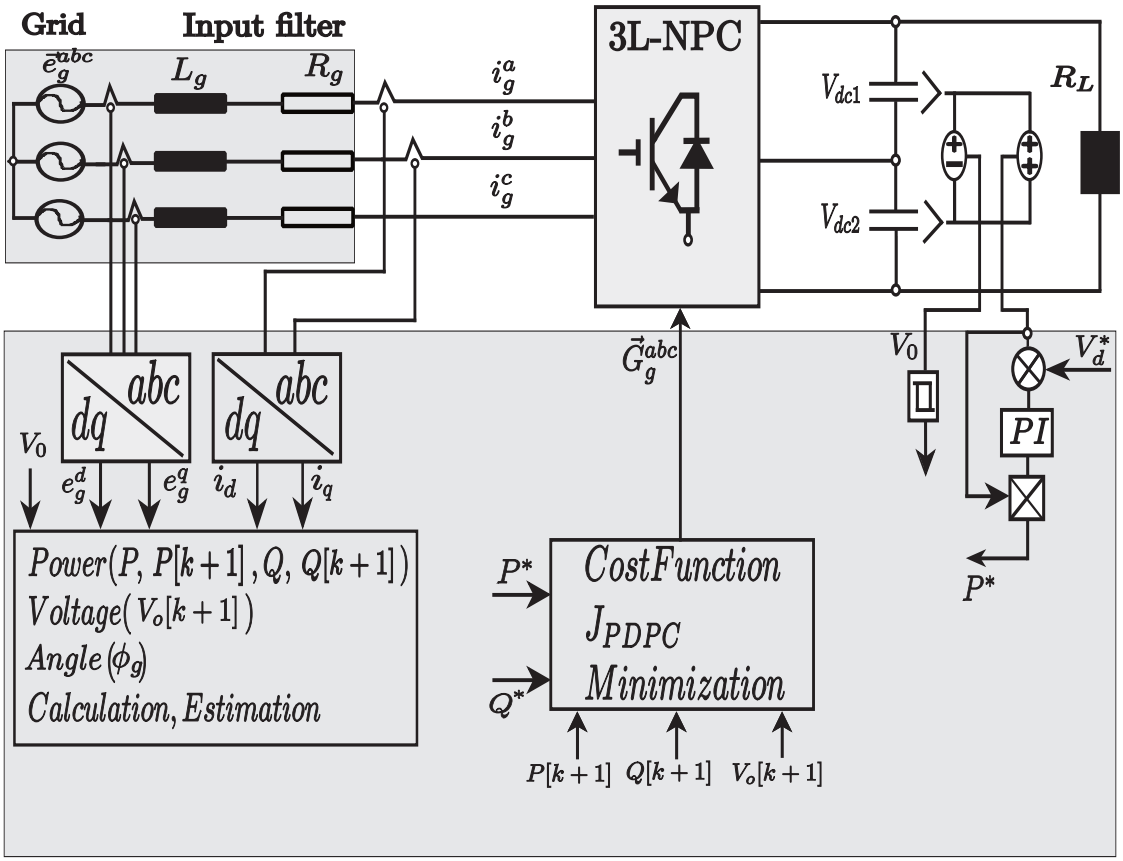

Figure 5.2: Scheme of Finite-Set Control Model Predictive Control for the 3L NPC-AFE.

❣ **Steady steady performance**

As shown in Figure 5.8, the active and reactive power track to their references with less steady steady-state error. The DC-link capacitor voltages V_{dc1}, V_{dc2} are perfectly balanced, and DC-link voltage is follow to its reference with small error. The grid current is closer to sinusoidal wave with THD=3.73 %, see Figure 5.10.

❣ **Transient-Steady Performance**

The experimental results under different step changes in load are presented in Figure 5.9. The active and reactive power track to the references with fast rise time, the DC-link capacitors are perfectly balanced during all the operating conditions, and grid currents are closer to sinusoidal wave with low THD. This operating conditions prove that the FCS-MPC is robust and handles the DC-load variations, and the control objectives of FCS-MPC technique are achieved, regarding the obtained minimum value of cost function.

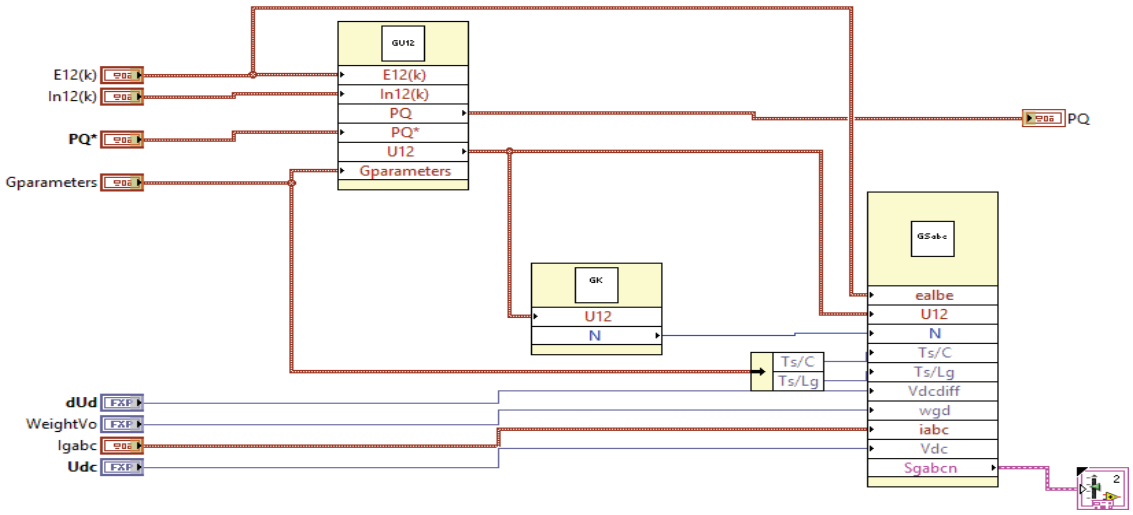

Figure 5.3: Scheme of direct model predictive control- Grid side- LabVIEW environment

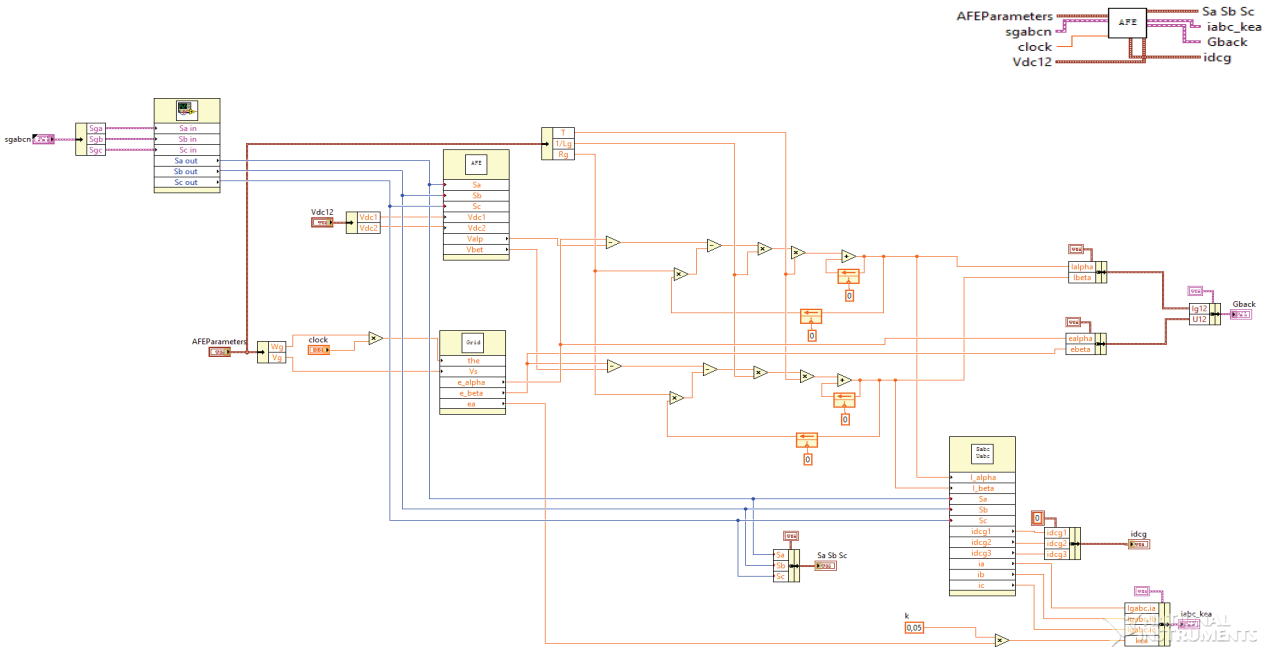

Figure 5.4: Scheme of 3L-NPC rectifier and three phase grid voltage- Grid side- LabVIEW environment

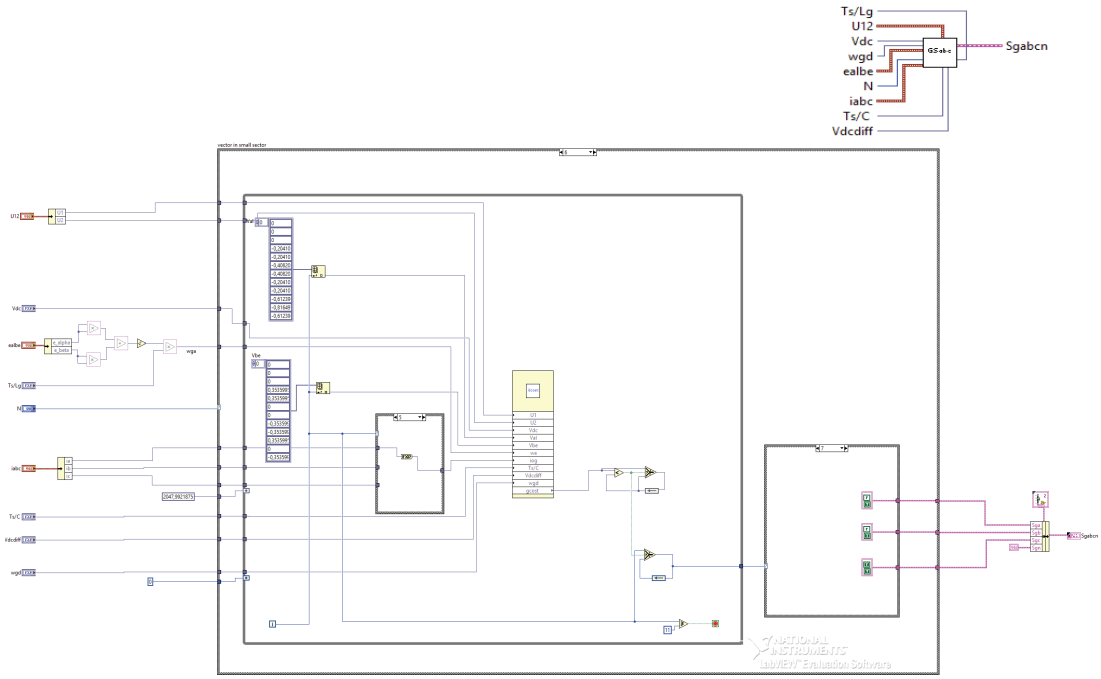

Figure 5.5: Scheme of direct model predictive control- Grid side- LabVIEW environment

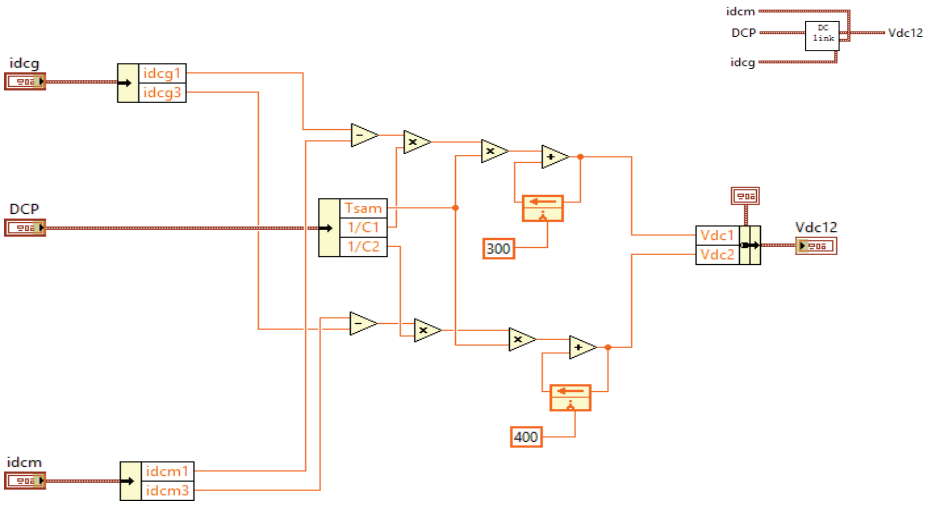

Figure 5.6: Scheme of DC-Link side - LabVIEW environment

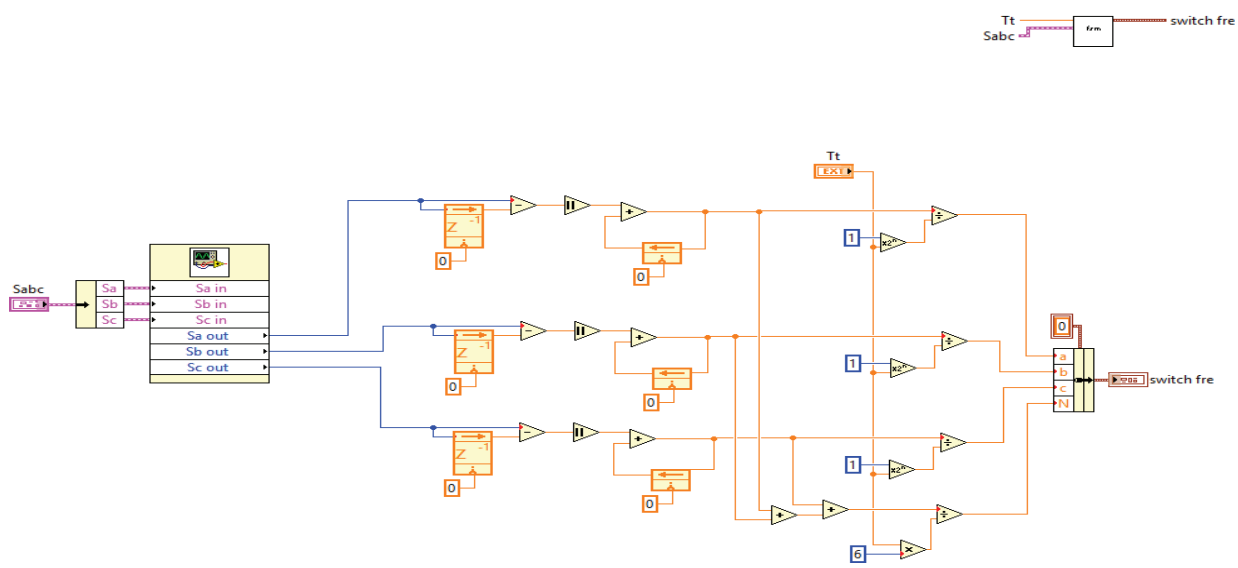

Figure 5.7: Scheme of switching frequency calculation block- LabVIEW environment

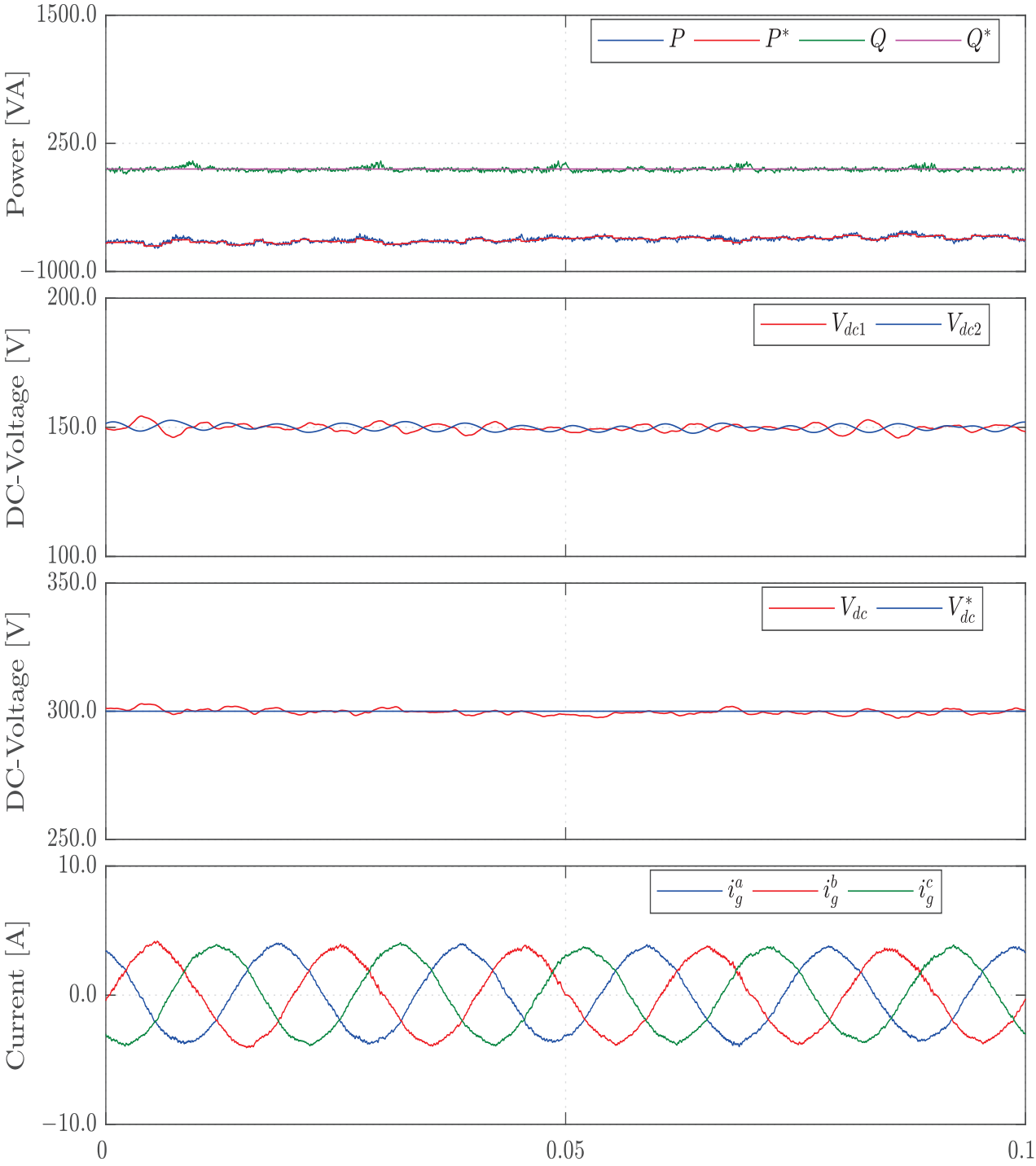

Figure 5.8: -Experimental results- Steady-state results of MPC-FCS for 3L NPC-AFE

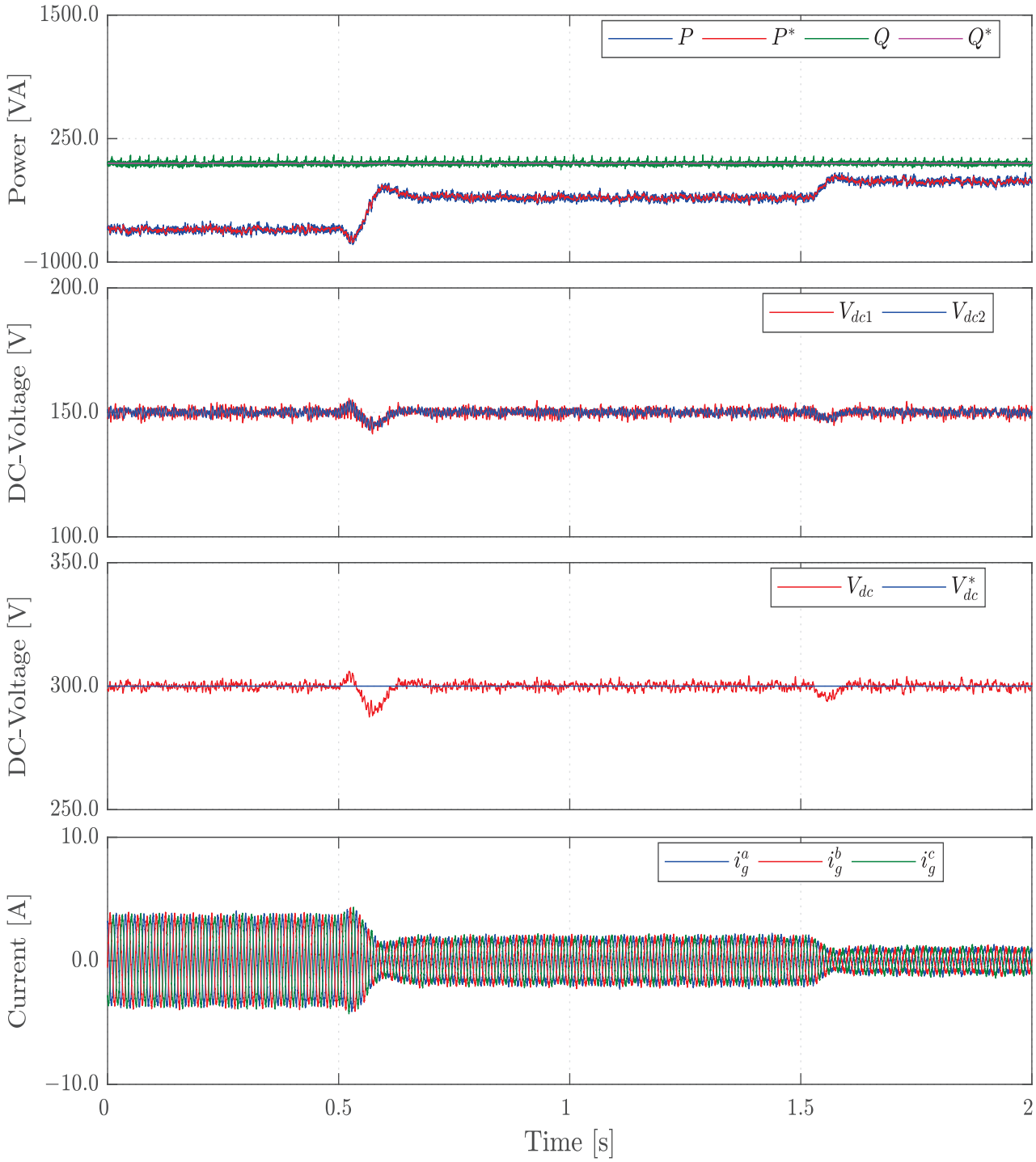

Figure 5.9: -Experimental results-Overall results of FCS-MPC for 3L NPC-AFE

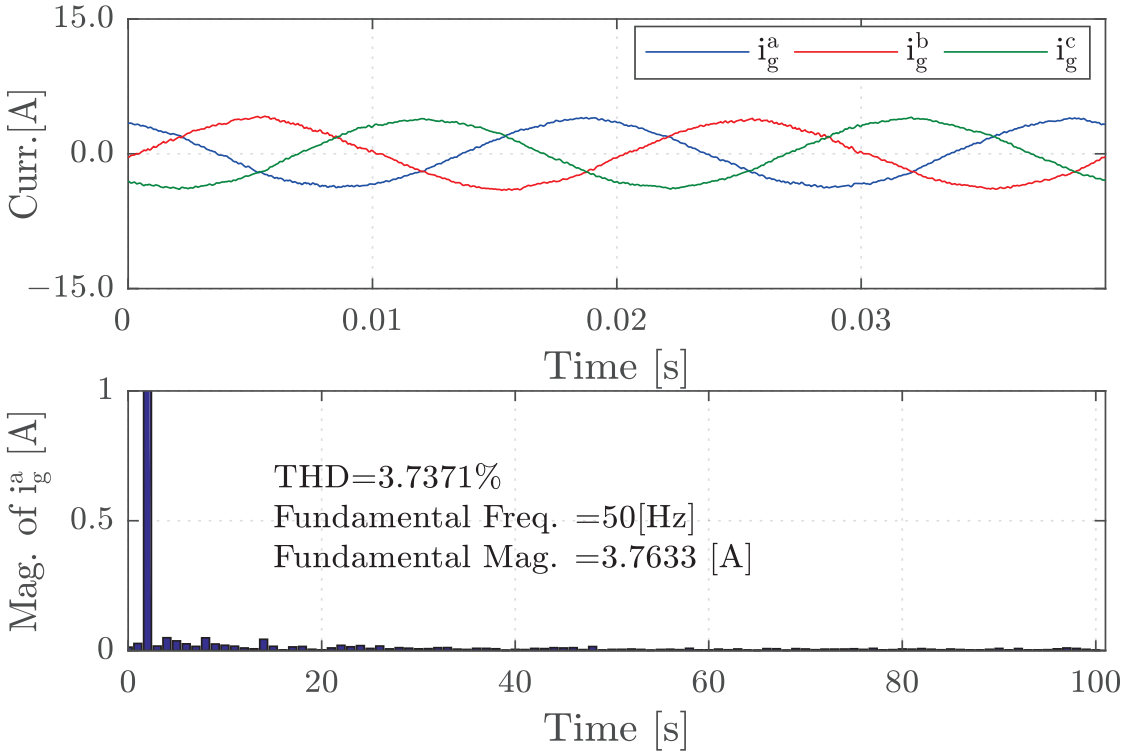

Figure 5.10: -Experimental results- Input currents with Harmonic spectrum and THD for 3L NPC-AFE

CHAPTER 6

Conclusion

6.1 Work's Goal

At the end of this Dissertation, the main goals of these works can be summarized as yielding,

Applying a different control strategies to control the selected power converter -3L NPC-AFE-, taking into consideration the weakness of the utilized control strategies, and try to solve that. Therefore, the following points summarize the focus of our works:

1. To reduce the power ripples provided by applying conventional LUT-DPC technique.
2. To fix the variable switching frequency of LUT-DPC technique.
3. Conserving the sample structure and rapid dynamic response of LUT-DPC technique.
4. Improve the performance of LUT-DPC technique under unbalanced grid voltage.
5. Implementing the advanced control technique -FCS-MPC-.

The items mentioned above are solved within our research work. The simulation results prove the good performance of the proposed control techniques. Some of these control strategies were proven experimentally and will be published in different article papers in the future.
The proposed control techniques offer several advantages over conventional LUT-DPC technique, these advantages can be mentioned in follow:

1. The simple structure and rapid dynamic response of conventional LUT-DPC technique are conserved by the most of the proposed control techniques.

2. The switching frequency is fixed by combination of the DPC technique with SVM technique.

3. The unity power factor, good quality of currents and accuracy regulation of power and DC-voltages are achieved.

4. The performance of LUT-DPC technique under unbalanced grid voltage is improved by employing a new definition of active power.

5. The performance of finite-control set direct power control (FCS-DPC) for 3L NPC rectifier is evaluated experimentally.

6.2 General Conclusion

Electricity has become a part of modern life, it has many uses in our daily life and one cannot think the world without it. The first one (i.e., information transmission) is based on using the fossil to produce the electricity. Unfortunately, due to the limited fossil fuel resources and environmental concerns, the using of this source becomes very limited, which causes a widely increased of using the second source of the electricity (i.e., energy conversion). In the energy conversion group, a hydro, wind, solar, geothermal, etc., are used as a source to produce the electricity instead of fossil. Recently, researchers have shown an increased interest in using AC adjustable speed drives and power converters in a wide range of applications (i.e., industry, transportation, renewable energies and so on). Unfortunately, using the line-side diode rectifiers in the AC adjustable speed drives provoke harmonic pollution, which required to use the active and passive filters, or PWM rectifiers. PWM rectifiers is the best one.

Our research project is based on assuring a good performance of the 3L NPC-AFE, its input and output are respectively related to three phases grid voltage with R-L filter, and load resistance. The 3L NPC-AFE has many features compared to conventional 2L converter, which are, high power application, sinusoidal input current with low THD, low voltage stress at the power semi-conductor, and less switches compared to multilevel power converter. Several classical and advanced control strategies have been proposed and applied to achieve the aim of the project. Due to the advantages of classical control strategies such as: a simple algorithm, good dynamics and so on, many works based on the classical techniques have been proposed and applied to the three level NPC rectifier. Firstly, under ideal grid voltage condition, a proposed LUT-DPC strategy for three level NPC rectifier is proposed, the conventional switching table and two-level hysteresis comparators are replaced respectively by a new switching table and three level hysteresis comparators. The new switching table is constructed by determining the influence of each switching voltage vector on the active and reactive power. With the proposed LUT-DPC strategy, the abnormal fluctuations on the reactive power waveform

are eliminated, sinusoidal input currents with accuracy regulating of powers and DC-voltages are achieved. Another improved LUT-DPC strategy is proposed, three vectors are applied equally during each odd sector instead of one vector in the case of the active power needs to be increased and reactive power needs to be decreased. The objective of this work is to deal successfully with the weakness of the conventional LUT-DPC strategy and its conventional switching table. Following, DPC-SVM strategy under balanced grid voltage is proposed. Also, due to the advantages of advanced control techniques such as: a simple concept, easy to understand, a possibility to apply it to a wide variety of systems, and to compensate the system perturbations and dead times, etc. A predictive direct power control (P-DPC) strategy is applied to control the 3L NPC-AFE, a good performance of the system is achieved. Following, the non-ideal three-phase load, asymmetry faults and power transmission system, etc., cause an unbalanced grid voltage. A new LUT-DPC strategy under unbalanced grid voltage is proposed. In this work, a new definition of active power is proposed and used instead of the conventional definition of active power. With this proposed study, nor compensation block neither calculations of the current references are required. As a result, accuracy regulation of active power, reactive power, DC-bus voltage and sinusoidal input currents are achieved.

6.3 Outlook

The most high performance strategies in the classic and advanced groups will be used to control the power converters, which are: direct power control (DPC), direct torque control (DTC), fuzzy logic control (FLC), space voltage modulation (SVM), and sliding mode control (SMC) for the classical strategy group. And predictive direct power control (P-DPC), predictive current control (PCC), and long-horizon model predictive (LHMP), with possibility to apply another kind of predictive control strategy, with taking into consideration the unbalanced and distorted of the grid voltages, the resistance and inductance parameters mismatch. For the experimental setup, a dSPACE controller/ LabVIEW for FPGA-Hardware will be used.

There are several possibilities to extend and to modify the strategies which were presented in this work: One promising extension could be a method to calculate not only one but two or even more VSPs. If e.g. only one IGBT is allowed to switch at a time and if two VSPs are calculated within one sample, “online optimized” pulse patterns and a constant switching frequency could be obtained. Such an FS-MPC method would then be fully comparable to PWM in terms of ripples on the controlled variables. Another possibility would also be to increase the prediction horizon for VSP methods.

Another very promising application for (FCS-MPC) is to perform direct speed or even position control for electrical drives. In this way all disadvantages which result from cascaded control loops could be overcome. Furthermore, it

would then also be possible to operate the drive at its physical limits while still keeping all controlled variables within their allowed range.

APPENDIX A

List of Publication

• **B. Kahia**, A. Bouafia, and A. Chaoui, "Direct power control of three-level pwm rectifier under unbalanced and harmonically distorted grid voltage conditions," in Electrical Engineering (ICEE), 2015 4th International Conference on. IEEE, 2015, pp. 1–4.

• **B. Kahia**, A. Bouafia, M. Abdelrahem, Z. Zhang, A. Chaoui, A. Krama, and R. Kennel, "Multi level hysteresis direct power control strategy for three-level npc rectifier," in 2017 5th International Conference on Electrical Engineering - Boumerdes (ICEE- B), Oct 2017, pp. 1–6.

• **B. Kahia**, A. Bouafia, and A. Chaoui, "Improved direct power control of three-level pwm rectifier under unbalanced grid conditions," 2th CIEEAM 2015 ENP of Oran, 2015.

• **B. Kahia**, A. Bouafia, M. Abdelrahem, Z. Zhang, A. Chaoui, A. Krama, and R. Kennel, "A predictive direct power control strategy for three-level npc rectifier," in Electri- cal Engineering-Boumerdes (ICEE-B), 2017 5th International Conference on. IEEE, 2017, pp. 1–5.

• **B. Kahia**, A. Bouafia, A. Chaoui, Improved direct power control of three-level PWM rectifier under unbalanced grid conditions, in: 2th CIEEAM ENP of Oran, 24–25 November, 2015.

• M. Abdelrahem, **B, Kahia**, R. Kennel, C. Hackl. M. Predictive Direct Torque Control Strategy for Surface-Mounted Permanent-Magnet Synchronous Generators. in Conference on sustainable energy supply and energy storage systems (NEIS), Hamburg, Germany, pp. 1-6, 2017.

• **Kahia, B**., Bouafia, A., Chaoui, A., Abdelrahem, M., Kennel, R. (2017). A new Look-up Table-Direct Power Control Strategy for Three-Level NPC Rectifier Using Predictive DPC. Sustainable energy supply and energy storage systems (NEIS 2017), Hamburg, Germany.

• **B. Kahia**, A. Bouafia, A. Chaoui, Z. Zhang, M. Abdelrahem, R. Kennel. (2018). A direct power control strategy for three level neutral-point-clamped rectifier under unbalanced grid voltage. Electric Power Systems Research, 161, 103-113.

• **B. Kahia**, A. Bouafia, M. Abdelrahem, Z. Zhang, A. Chaoui, A. Krama, and R. Kennel, "An Improved Look-up Table-Direct Power Control strategy for Three-Level NPC Rectifier," in Conference: The 2snd International Conference on Applied Automation and Industrial Diagnostics (ICAAID 2017) - University of Djelfa , Algeria.

Bibliography

[1] Z. Zhang, "On control of grid-tied back-to-back power converters and permanent magnet synchronous generator wind turbine systems," Ph.D. dissertation, Technische Universität München, 2016.

[2] Y. Demirel, *Energy: production, conversion, storage, conservation, and coupling*. Springer Science & Business Media, 2012.

[3] S. Kouro, M. A. Perez, J. Rodriguez, A. M. Llor, and H. A. Young, "Model predictive control: Mpc's role in the evolution of power electronics," *IEEE Industrial Electronics Magazine*, vol. 9, no. 4, pp. 8–21, 2015.

[4] F. Filsecker, R. Alvarez, and S. Bernet, "Comparison of 4.5-kv press-pack igbts and igcts for medium-voltage converters," *IEEE Transactions on Industrial Electronics*, vol. 60, no. 2, pp. 440–449, 2013.

[5] R. Ottersten, *On control of back-to-back converters and sensorless induction machine drives*. Chalmers University of Technology, 2003.

[6] T. Burton, N. Jenkins, D. Sharpe, and E. Bossanyi, *Wind energy handbook*. John Wiley & Sons, 2011.

[7] Z. Chen, J. M. Guerrero, and F. Blaabjerg, "A review of the state of the art of power electronics for wind turbines," *IEEE Transactions on power electronics*, vol. 24, no. 8, pp. 1859–1875, 2009.

[8] V. Yaramasu, "Predictive control of multilevel converters for megawatt wind energy conversion systems," Ph.D. dissertation, Ph. D. dissertation, Ryerson Univ., Toronto, ON, Canada, 2014.

[9] A. Faulstich, J. Stinke, and F. Wittwer, "Medium voltage converter for permanent magnet wind power generators up to 5 mw," in *Power Electronics and Applications, 2005 European Conference on*. IEEE, 2005, pp. 9–pp.

[10] P. Qian and L. Li, "Neutral-point voltage balancing in wind power npc three-level converter," *Electronics Letters*, vol. 53, no. 6, pp. 424–426, 2017.

[11] K.-H. Kim, Y.-C. Jeung, D.-C. Lee, and H.-G. Kim, "Lvrt scheme of pmsg wind power systems based on feedback linearization," *IEEE transactions on power electronics*, vol. 27, no. 5, pp. 2376–2384, 2012.

[12] T. Noguchi, H. Tomiki, S. Kondo, and I. Takahashi, "Direct power control of pwm converter without power-source voltage sensors," *IEEE Transactions on Industry Applications*, vol. 34, no. 3, pp. 473–479, 1998.

[13] K. Bimal, *Modern power electronics and AC drives*. Prentice-Hall, 2001.

[14] J. Pou, J. Zaragoza, S. Ceballos, M. Saeedifard, and D. Boroyevich, "A carrier-based pwm strategy with zero-sequence voltage injection for a three-level neutral-point-clamped converter," *IEEE Transactions on Power Electronics*, vol. 27, no. 2, pp. 642–651, 2012.

[15] N. Celanovic and D. Boroyevich, "A fast space vector modulation algorithm for multilevel three-phase converters," in *Conference Record of the 1999 IEEE Industry Applications Conference. Thirty-Forth IAS Annual Meeting (Cat. No. 99CH36370)*, vol. 2. IEEE, 1999, pp. 1173–1177.

[16] J. F. Silva, N. Rodrigues, and J. Costa, "Space vector alpha-beta sliding mode current controllers for three-phase multilevel inverters," in *2000 IEEE 31st Annual Power Electronics Specialists Conference. Conference Proceedings (Cat. No. 00CH37018)*, vol. 1. IEEE, 2000, pp. 133–138.

[17] R. Kanchan, K. Gopakumar, and R. Kennel, "Synchronised carrier-based svpwm signal generation scheme for the entire modulation range extending up to six-step mode using the sampled amplitudes of reference phase voltages," *IET Electric Power Applications*, vol. 1, no. 3, pp. 407–415, 2007.

[18] S. Mekhilef and M. N. A. Kadir, "Voltage control of three-stage hybrid multilevel inverter using vector transformation," *IEEE Transactions on Power Electronics*, vol. 25, no. 10, pp. 2599–2606, 2010.

[19] M. Malinowski, M. Jasinski, and M. P. Kazmierkowski, "Simple direct power control of three-phase pwm rectifier using space-vector modulation (dpc-svm)," *IEEE Transactions on Industrial Electronics*, vol. 51, no. 2, pp. 447–454, 2004.

[20] A. Bouafia, J.-P. Gaubert, and F. Krim, "Predictive direct power control of three-phase pulsewidth modulation (pwm) rectifier using space-vector modulation (svm)," *IEEE Transactions on Power Electronics*, vol. 25, no. 1, pp. 228–236, 2010.

[21] B. Kahia, "Commande mli vectorielle d'un redresseur triphasé à trois niveaux," 2013.

[22] J. Y. Hung, W. Gao, and J. C. Hung, "Variable structure control: A survey," *IEEE transactions on industrial electronics*, vol. 40, no. 1, pp. 2–22, 1993.

[23] K. Tsang and W. Chan, "Adaptive control of power factor correction converter using nonlinear system identification," *IEE Proceedings-Electric Power Applications*, vol. 152, no. 3, pp. 627–633, 2005.

[24] J. R. Massing, M. Stefanello, H. A. Grundling, and H. Pinheiro, "Adaptive current control for grid-connected converters with lcl filter," *IEEE Transactions on Industrial Electronics*, vol. 59, no. 12, pp. 4681–4693, 2012.

[25] M. A. Herran, J. R. Fischer, S. A. González, M. G. Judewicz, and D. O. Carrica, "Adaptive dead-time compensation for grid-connected pwm inverters of single-stage pv systems," *IEEE transactions on power electronics*, vol. 28, no. 6, pp. 2816–2825, 2013.

[26] B. K. Bose *et al.*, *Modern power electronics and AC drives*. Prentice hall Upper Saddle River, NJ, 2002, vol. 123.

[27] J. Rodriguez and P. Cortes, *Predictive control of power converters and electrical drives*. John Wiley & Sons, 2012, vol. 40.

[28] J. Li, S. Bhattacharya, and A. Q. Huang, "A new nine-level active npc (anpc) converter for grid connection of large wind turbines for distributed generation," *IEEE transactions on Power Electronics*, vol. 26, no. 3, pp. 961–972, 2011.

[29] J. Rodriguez, S. Bernet, P. K. Steimer, and I. E. Lizama, "A survey on neutral-point-clamped inverters," *IEEE transactions on Industrial Electronics*, vol. 57, no. 7, pp. 2219–2230, 2010.

[30] B. Wu and M. Narimani, *High-power converters and AC drives*. John Wiley & Sons, 2017, vol. 59.

[31] M. Depenbrock, "Direct self-control (dsc) of inverter fed induktion machine," in *Power Electronics Specialists Conference, 1987 IEEE*. IEEE, 1987, pp. 632–641.

[32] G. C. Sousa and B. K. Bose, "A fuzzy set theory based control of a phase-controlled converter dc machine drive," *IEEE Transactions on industry Applications*, vol. 30, no. 1, pp. 34–44, 1994.

[33] A. Savanovic, R. Benitez, H. Hashimoto, and F. Harashima, "Vss approach to dc drives control," in *Power Electronics Specialists Conference, 1988. PESC'88 Record., 19th Annual IEEE*. IEEE, 1988, pp. 235–242.

[34] P. Cortés, M. P. Kazmierkowski, R. Kennel, D. E. Quevedo, and J. R. Rodriguez, "Predictive control in power electronics and drives." *IEEE Trans. Industrial Electronics*, vol. 55, no. 12, pp. 4312–4324, 2008.

[35] Y. Shen and H. Nian, "Improved dpc strategy of grid-connected inverters under unbalanced and harmonic grid conditions," in *Electrical Machines and Systems (ICEMS), 2013 International Conference on*. IEEE, 2013, pp. 1566–1570.

[36] R. Zaimeddine and T. Undeland, "Direct power control strategies of a grid-connected three-level voltage source converter vsi-npc," in *Power Electronics and Applications (EPE 2011), Proceedings of the 2011-14th European Conference on*. IEEE, 2011, pp. 1–7.

[37] D. Zhi, L. Xu, and B. W. Williams, "Improved direct power control of grid-connected dc/ac converters," *IEEE Transactions on Power Electronics*, vol. 24, no. 5, pp. 1280–1292, 2009.

[38] L. Ning, H. Jingjing, Z. Hui, W. Yue, and W. Zhao'an, "A novel direct power control strategy of three-level npc rectifier without abnormal instantaneous reactive power fluctuation," *ICPE (ISPE)* , pp. 2764–2769, 2015.

[39] B. Kahia, A. Bouafia, and A. Chaoui, "Direct power control of three-level pwm rectifier under unbalanced and harmonically distorted grid voltage conditions," in *Electrical Engineering (ICEE), 2015 4th International Conference on*. IEEE, 2015, pp. 1–4.

[40] S. Rivera, S. Kouro, B. Wu, S. Alepuz, M. Malinowski, P. Cortes, and J. Rodriguez, "Multilevel direct power control—a generalized approach for grid-tied multilevel converter applications," *IEEE Transactions on Power Electronics*, vol. 29, no. 10, pp. 5592–5604, 2014.

[41] K. Kulikowski and A. Sikorski, "New dpc look-up table methods for three-level ac/dc converter," *IEEE Transactions on Industrial Electronics*, vol. 63, no. 12, pp. 7930–7938, 2016.

[42] K. Djazia, F. Krim, A. Chaoui, and M. Sarra, "Active power filtering using the zdpc method under unbalanced and distorted grid voltage conditions," *Energies*, vol. 8, no. 3, pp. 1584–1605, 2015.

[43] H. Yin and S. Dieckerhoff, "Experimental comparison of dpc and voc control of a three-level npc grid connected converter," in *Power Electronics for Distributed Generation Systems (PEDG), 2015 IEEE 6th International Symposium on*. IEEE, 2015, pp. 1–7.

[44] F. A. Ramírez, M. A. Arjona, and C. Hernández, "A novel parameter-independent fictive-axis approach for the voltage oriented control of single-phase inverters," *Journal of Power Electronics*, vol. 17, no. 2, pp. 533–541, 2017.

[45] N. E. A. M. Hassanain, A. Y. Abbas, and M. H. Ahmed, "Performance analysis of hybrid electric vehicle battery charger using voltage oriented control," *International Journal of Scientific & Engineering Research*, vol. 5, pp. 2229–5518, 2015.

[46] C. Ortega, A. Arias, C. Caruana, J. Balcells, and G. M. Asher, "Improved waveform quality in the direct torque control of matrix-converter-fed pmsm drives," *IEEE Transactions on Industrial Electronics*, vol. 57, no. 6, pp. 2101–2110, 2010.

[47] P. Rioual, H. Pouliquen, and J.-P. Louis, "Regulation of a pwm rectifier in the unbalanced network state using a generalized model," *IEEE Transactions on Power Electronics*, vol. 11, no. 3, pp. 495–502, 1996.

[48] H.-s. Song and K. Nam, "Dual current control scheme for pwm converter under unbalanced input voltage conditions," *IEEE transactions on industrial electronics*, vol. 46, no. 5, pp. 953–959, 1999.

[49] M. Reyes, P. Rodriguez, S. Vazquez, A. Luna, R. Teodorescu, and J. M. Carrasco, "Enhanced decoupled double synchronous reference frame current controller for unbalanced grid-voltage conditions," *IEEE Transactions on power electronics*, vol. 27, no. 9, pp. 3934–3943, 2012.

[50] P. Peltoniemi, P. Nuutinen, M. Niemela, and J. Pyrhonen, "Voltage oriented control of a single-phase lvdc distribution network inverter," in *Applied Power Electronics Conference and Exposition, 2009. APEC 2009. Twenty-Fourth Annual IEEE*. IEEE, 2009, pp. 1589–1595.

[51] H. Nian, P. Cheng, and Z. Zhu, "Coordinated direct power control of dfig system without phase-locked loop under unbalanced grid voltage conditions," *IEEE Transactions on Power Electronics*, vol. 31, no. 4, pp. 2905–2918, 2016.

[52] H. Nian, Y. Shen, H. Yang, and Y. Quan, "Flexible grid connection technique of voltage-source inverter under unbalanced grid conditions based on direct power control," *IEEE Trans. Ind. Appl.*, vol. 51, no. 5, pp. 4041–4050, 2015.

[53] H. Nian and Y.-p. Song, "Multiple target implementation for a doubly fed induction generator based on direct power control under unbalanced and distorted grid voltage," *Frontiers of Information Technology & Electronic Engineering*, vol. 16, no. 4, pp. 321–334, 2015.

[54] Y. Suh and T. A. Lipo, "Modeling and analysis of instantaneous active and reactive power for pwm ac/dc converter under generalized unbalanced network," *IEEE Transactions on Power Delivery*, vol. 21, no. 3, pp. 1530–1540, 2006.

[55] Y. Komatsu and T. Kawabata, "A control method of active power filter where system voltage contains negative-phase-sequence component or zero-phase-sequence component," in *Power Electronics and Drive Systems, 1995., Proceedings of 1995 International Conference on.* IEEE, 1995, pp. 583–586.

[56] Y. Zhang, J. Long, Y. Zhang, T. Lu, Z. Zhao, and L. Jin, "Table-based direct power control for three-level neutral point-clamped pulse-width modulated rectifier," *IET Power Electronics*, vol. 6, no. 8, pp. 1555–1562, 2013.

[57] B. Liu, Y. Zha, T. Zhang, and S. Chen, "Triple-state hysteresis direct power control for three phase pwm rectifier," in *Mechatronics and Automation (ICMA), 2015 IEEE International Conference on.* IEEE, 2015, pp. 783–789.

[58] B. Kahia, A. Bouafia, M. Abdelrahem, Z. Zhang, A. Chaoui, A. Krama, and R. Kennel, "Multi level hysteresis direct power control strategy for three-level npc rectifier," in *2017 5th International Conference on Electrical Engineering - Boumerdes (ICEE-B)*, Oct 2017, pp. 1–6.

[59] L. Serpa, P. Barbosa, P. K. Steimer, and J. W. Kolar, "Five-level virtual-flux direct power control for the active neutral-point clamped multilevel inverter," in *Power Electronics Specialists Conference, 2008. PESC 2008. IEEE*. IEEE, 2008, pp. 1668–1674.

[60] B. Kahia, A. Bouafia, and A. Chaoui, "Improved direct power control of three-level pwm rectifier under unbalanced grid conditions," *2th CIEEAM 2015 ENP of Oran*, 2015.

[61] S. Kwak, U.-C. Moon, and J.-C. Park, "Predictive-control-based direct power control with an adaptive parameter identification technique for improved afe performance," *IEEE Trans. Power Electron*, vol. 29, no. 11, pp. 6178–6187, 2014.

[62] B. Kahia, A. Bouafia, M. Abdelrahem, Z. Zhang, A. Chaoui, A. Krama, and R. Kennel, "A predictive direct power control strategy for three-level npc rectifier," in *Electrical Engineering-Boumerdes (ICEE-B), 2017 5th International Conference on*. IEEE, 2017, pp. 1–5.

[63] J. Rodriguez, M. P. Kazmierkowski, J. R. Espinoza, P. Zanchetta, H. Abu-Rub, H. A. Young, and C. A. Rojas, "State of the art of finite control set model predictive control in power electronics," *IEEE Transactions on Industrial Informatics*, vol. 9, no. 2, pp. 1003–1016, 2013.

[64] J. Eloy-Garcia, S. Arnaltes, and J. Rodriguez-Amenedo, "Direct power control of voltage source inverters with unbalanced grid voltages," *IET Power Electronics*, vol. 1, no. 3, pp. 395–407, 2008.

[65] L. Shang, D. Sun, and J. Hu, "Sliding-mode-based direct power control of grid-connected voltage-sourced inverters under unbalanced network conditions," *IET power electronics*, vol. 4, no. 5, pp. 570–579, 2011.

[66] Y. Zhang and C. Qu, "Table-based direct power control for three-phase ac/dc converters under unbalanced grid voltages," *IEEE Transactions on Power Electronics*, vol. 30, no. 12, pp. 7090–7099, 2015.

[67] Y. Zhang, J. Gao, and C. Qu, "Relationship between two direct power control methods for pwm rectifiers under unbalanced network," *IEEE Transactions on Power Electronics*, vol. 32, no. 5, pp. 4084–4094, 2017.

[68] H. Akagi, Y. Kanazawa, and A. Nabae, "Instantaneous reactive power compensators comprising switching devices without energy storage components," *IEEE Transactions on industry applications*, no. 3, pp. 625–630, 1984.

[69] J. Holtz, "A predictive controller for the stator current vector of ac machines fed from a switched voltage source," *Proc. of IEE of Japan IPEC-Tokyo'83*, pp. 1665–1675, 1983.

[70] P. Mutschler, "A new speed-control method for induction motors," in *Proc. Conf. Rec. PCIM*, 1998, pp. 131–136.

[71] T. Kawabata, T. Miyashita, and Y. Yamamoto, "Dead beat control of three phase pwm inverter," *IEEE Transactions on Power Electronics*, vol. 5, no. 1, pp. 21–28, 1990.

[72] O. Kukrer, "Discrete-time current control of voltage-fed three-phase pwm inverters," *IEEE Transactions on Power Electronics*, vol. 11, no. 2, pp. 260–269, 1996.

[73] S. Kouro, P. Cortés, R. Vargas, U. Ammann, and J. Rodríguez, "Model predictive control—a simple and powerful method to control power converters," *IEEE Transactions on industrial electronics*, vol. 56, no. 6, pp. 1826–1838, 2009.

[74] M. Rivera, V. Yaramasu, A. Llor, J. Rodriguez, B. Wu, and M. Fadel, "Digital predictive current control of a three-phase four-leg inverter," *IEEE transactions on industrial electronics*, vol. 60, no. 11, pp. 4903–4912, 2013.

[75] V. Yaramasu, M. Rivera, B. Wu, and J. Rodriguez, "Model predictive current control of two-level four-leg inverters-part i: concept, algorithm, and simulation analysis," *IEEE Transactions on Power Electronics*, vol. 28, no. 7, pp. 3459–3468, 2013.

[76] M. Rivera, V. Yaramasu, J. Rodriguez, and B. Wu, "Model predictive current control of two-level four-leg inverters—part ii: Experimental implementation and validation," *IEEE Transactions on Power Electronics*, vol. 28, no. 7, pp. 3469–3478, 2013.

[77] M. Odavic, V. Biagini, P. Zanchetta, M. Sumner, and M. Degano, "One-sample-period-ahead predictive current control for high-performance active shunt power filters," *IET Power Electronics*, vol. 4, no. 4, pp. 414–423, 2011.

[78] P. Cortes, F. Quiroz, and J. Rodriguez, "Predictive control of a grid-connected cascaded h-bridge multilevel converter," in *Power Electronics and Applications (EPE 2011), Proceedings of the 2011-14th European Conference on*. IEEE, 2011, pp. 1–7.

[79] J. Jiang, "Preservations of positive realness under discretizations," in *PROCEEDINGS OF THE AMERICAN CONTROL CONFERENCE*, vol. 1. AMERICAN AUTOMATIC CONTROL COUNCIL, 1993, pp. 443–443.

[80] P. Cortés, S. Kouro, B. L. Rocca, R. Vargas, J. Rodríguez, J. I. León Galván, S. Vázquez Pérez, and L. García Franquelo, "Guidelines for weighting factors design in model predictive control of power converters and drives," in *International Conference On Industrial Technology (ICIT), 1-7. Gippsland, Australia: IEEE*. IEEE, 2009.

Abstract

Recently, researchers have shown an increased interest in using of multilevel converters in wide range of application such as: AC adjustable speed drives, industry, transportation, renewable energies and so on. Unfortunately, using the line-side diode rectifiers in such application as, AC adjustable speed drives, provoke harmonic pollution of electrical energy distribution networks. As curative solution of this problem, active and passive filters are used to reduce input current distortion of diode rectifiers. On the other hand, the preventive solution consists the substitution of the conventional diode rectifiers with new structures of AC / DC non-polluting converters, which have resistive behaviour towards the network. This research work deals with modeling and control of the three-level active-front end neutral-point-clamped PWM converter (3L AFE-NPC) to achieve nearly sinusoidal grid currents and unity power factor operation. Compared to the useful conventional two level converter, several features in high applications can be provided by 3L AFE-NPC, as, low total harmonic distortion (THD) of grid currents, low switching voltages stress and so on. Regrettably, this converter has some inherent problems, which are, voltage drifts and voltage ripples of the neutral-point. Therefore, many scientific researchers proposed several software and hardware methods to solve these problems. The control algorithm plays a decisive role in maintaining the stability of the whole system under normal operation and fault conditions.

Within this dissertation, improved and proposed control techniques are developed and discussed in details. These new strategies are based on improvement of direct power control with look-up-table under the case of balanced and unbalanced grid voltage, and apply one of the advanced control techniques, which is, finite-control set model predictive control (FCS-MPC). The aims of these proposed works are to solve the drawbacks of utilized conventional control strategies under ideal/non-ideal grid voltage conditions and load variation, with keeping the algorithm simple and be easy to implement. Finally, the Matlab-Simulink environment is utilized to confirm the performance of the proposed schemes. The performances of some control techniques are experimentally assessed at hardware-in-the loop test-bench, which has labVIEW for FPGA-hardware technology.
Key words: PWM rectifier, direct power control (DPC), Model predictive control, SVM, THD, Unbalanced grid voltage.

Résumé

Récemment, les chercheurs ont montré un intérêt accru pour l'utilisation de convertisseurs multiniveaux dans une large gamme d'applications telles que: les entraînements à vitesse variable, l'industrie, les transports, les énergies renouvelables, etc. Malheureusement, l'utilisation des redresseurs à diode côté réseau électrique dans ces applications, telles que les variateurs de vitesse alternatifs, provoque une pollution harmonique des réseaux de distribution d'énergie électrique. Comme solution curative de ce problème, les filtres actifs et passifs sont utilisés pour réduire la distorsion du courant d'entrée des redresseurs à diode. D'autre part, la solution préventive consiste à remplacer les redresseurs à diodes classiques par de nouvelles structures de convertisseurs AC / DC non polluants, qui ont un comportement résistif vis-à-vis le réseau électrique. Ce travail de recherche porte sur la modélisation et le contrôle du convertisseur AC/DC à 3 niveaux AFE-NPC (3L AFE-NPC) afin d'absorber des courants de réseau quasi sinusoïdaux avec un facteur de puissance unitaire. Comparé au convertisseur conventionnel à deux niveaux, 3L AFE-NPC peut offrir plusieurs fonctionnalités dans les applications de hautes performances, telles que la distorsion harmonique totale (THD) faible des courants du réseau, les contraintes de tension de commutation faibles, etc. Malheureusement, ce convertisseur présente des problèmes inhérents, à savoir des dérives de tension et des ondulations de tension du point neutre. Par conséquent, de nombreux chercheurs scientifiques ont proposé plusieurs méthodes pour résoudre ces problèmes. L'algorithme de contrôle joue un rôle décisif dans le maintien de la stabilité du système dans des conditions de fonctionnement et de défaillance normales.

Dans cette thèse, des techniques de contrôle améliorées et proposées sont développées et discutées en détail. Ces nouvelles stratégies sont basées sur l'amélioration du contrôle direct de la puissance avec une table de commutation dans le cas d'une tension de réseau équilibrée et non équilibrée, et appliquent l'une des techniques de contrôle avancées, à savoir le contrôle prédictif par modèle à contrôle fini (FCS-MPC). Les travaux proposés ont pour objectif de résoudre les inconvénients des stratégies de contrôle conventionnelles utilisées dans des conditions de tension de réseau idéales/non idéales et de variations de la charge, tout on maintien l'algorithme simple et facile à mettre en œuvre. Enfin, l'environnement Matlab-Simulink est utilisé pour confirmer la performance des stratégies de contrôle proposées. Les performances de certaines techniques de contrôle sont évaluées de manière expérimentale sur un banc de test hardware-in-the-loop, doté de labVIEW pour la technologie matérielle FPGA.
Mots clés: PWM rectifier, Control direct de puissance (DPC), Contrôle prédictif à modèle, SVM, THD, Réseau déséquilibré.

ملخص

في الآونة الأخيرة ، أظهر الباحثون اهتمامًا متزايدًا باستخدام المحولات متعددة المستويات في مجموعة واسعة من التطبيقات مثل: محركات السرعة المتغيرة ، والصناعة ، والنقل ، والطاقة المتجددة ، إلخ. لسوء الحظ ، فإن استخدام مقومات الصمام الثنائي من جهة الشبكة الكهربائية في هذه التطبيقات يسبب تلوثًا لشبكات توزيع الطاقة. كحل علاجي لهذه المشكلة ، يتم استخدام المرشحات الفعالة وغير الفعالة للحد من تشويه التيارات المغذية لمقومات الصمام الثنائي. من ناحية أخرى ، يتمثل الحل الوقائي في استبدال مقومات الصمام الثنائي التقليدية بهياكل جديدة من محولات AC / DC غير الملوثة ، والتي تعتبر كمقاومة بالنسبة للشبكة الكهربائية.

يركز هذا البحث على النمذجة والتحكم في محول PWM AC/DC ذو المستوى 3 (3L AFE-NPC) لإقتطاع تيارات من الشبكة الكهربائية شبه جيبية مع معامل استطاعة يساوي الوحدة. مقارنةً بالمحول التقليدي ذي المستويين ، يمكن أن يقدم 3 L AFE-NPC العديد من الميزات في التطبيقات عالية الأداء ، مثل التشوه التوافقي الكلي المنخفض لتيارات الشبكة ، وقيود الجهد المنخفض للتبديل ، وما إلى ذلك. لسوء الحظ ، هذا المحول لديه مشاكل متأصلة ، وهي عدم توازن التوتر وتموجات الجهد المحايدة. نتيجة لذلك ، اقترح العديد من الباحثين العلميين عدة طرق لحل هذه المشكلات. تلعب خوارزمية التحكم دورًا حاسمًا في الحفاظ على استقرار النظام بأكمله في ظل ظروف التشغيل والفشل العادية.

في هذه الأطروحة ، تم تطوير تقنيات التحكم المحسنة والمقترحة ومناقشتها بالتفصيل. تعتمد هذه الاستراتيجيات الجديدة على تحسين التحكم المباشر في الإستطاعة من خلال طاولة تبديل في حالة توتر شبكة متوازن وغير متوازن ، وتطبيق إحدى تقنيات التحكم المتقدمة ، وهي التحكم التنبئي بواسطة نموذج التحكم المحدود (FCS-MPC). يهدف العمل المقترح إلى حل عيوب استراتيجيات التحكم التقليدية المستخدمة في ظروف توتر الشبكة المثالية / غير المثالية وتغيرات الحمولة، مع إبقاء الخوارزمية بسيطة وسهلة التنفيذ. أخيرًا ، يتم استخدام نظام Matlab-Simulink لتأكيد أداء استراتيجيات التحكم المقترحة. يتم تقييم أداء بعض تقنيات التحكم بشكل تجريبي على منصة اختبار للأجهزة في حلقة مع labVIEW لتكنولوجيا الأجهزة FPGA.
كلمات مفتاحية: مقوم PWM ، التحكم المباشر في الطاقة ، نموذج التحكم التنبئي ، SVM، THD ، شبكة غير متوازنة.